REPUBLIQUE ALGERIENNE DEMOCRATIQUE ET POPULAIRE

Ministère de l'Enseignement Supérieur et de la Recherche scientifique

Université El-Hadj Lakhdar-BATNA 1

Faculté des Sciences de la Matière

Département de Physique

THÈSE

En vue de l'obtention du
Diplôme de Doctorat en Sciences

Présenté par:

Benmachiche. samira

Thème :

Simulation et optimisation des cellules solaires des structures Metal-isolant-semiconducteur MIS a differents materiaux semiconducteurs en couche mince

Spécialité : Sciences des Matériaux

Soutenue le …18…/ 12…/ 2023

Devant le jury:

Président :	**Belbacha Eldjemai**	**Professeur**	**Université de Batna 1**
Rapporteur :	**Dehimi Lakhdar**	**Professeur**	**Université de Batna 1**
Examinateurs :	**Saadoune Achour**	**Professeur**	**Université Biskra**
Examinateurs	**Terghini.Ouarda**	**M.C.A**	**Université Biskra**
Invité	**Bencherif Hicham**	**M.C.B**	**Ecole Supérieur des Energies Batna(HNSREESD)**

Ministry of Higher Education and Scientific Research
University of Batna1- Hadj Lakhdar
Faculty of Science
Department of Physics

DOCTORAL THESIS

Field: **of Material Sciences Physics**
Option:Physics

Specialty:**materials sciences**

Theme

Simulation and optimization of solar cells of Metal-Insulator-Semiconductor structures (MIS) with different thin-film semiconductor materials

Presented by**:**

Samira Benmachiche

Supervising Committee

BelbachaEldjemai	**Prof**	**University Batna 1**	**President**
Dehimi Lakhdar	**Prof**	**University Hadj Lakhdar – Batna1**	**Supervisor**
Terghini Warda	**MCA**	**University Biskra**	**Examiner**
Saadoune Achour	**Prof**	**University Biskra**	**Examiner**
Bencherif Hicham	**MCB**	**Higher School of Energies Batna(HNSREESD)**	**Guest**

Academic year2023/2024

Dedication

To my late father Hocine Allah yerrahmou

To my mother for all the sacrifices and for these years of help and support

To the person, who without her this work would never have seen the light of day: My husband Fouad, your devotion, your help, your support and your encouragement have allowed me to never deviate from my objective, to my reason for living, to my children, to my brothers

And finally, to all the people I love.

Acknowledgements

In the Name of Allah, the Beneficent, the Merciful

I am profoundly thankful to Allah, the Almighty, upon whom we rely for sustenance and guidance. I thank Him for providing me with the strength and capability to successfully complete this study.

Additionally, I extend my sincere appreciation to my advisor, Pr. Dehimi Lakhder, for his invaluable guidance.

I also would like to thank the committee members, Pr. Belbacha Eldjemai for having done me the honor of presiding over the jury. From Batna1 University, Terghini Warda from University of Biskra, and Pr. Saadoune Achour, from Biskra University.

It is imperative that we convey our sincere gratitude to each and every teacher who imparted knowledge to us, starting from the basics and continuing to guide us to this present moment. I extend my appreciation to all those who, from near or far, contributed to the completion of this endeavor

Finally, I would like to thank all my family; I thank those who stayed behind so that they would be happy and all my friends. In order not to forget anyone, my sincere thanks go to all those who helped me in the realization of this modest thesis.

Abstract

At present, silicon-based solar cells hold a dominant position in the solar cell market due to silicon's appropriate band gap matching the solar spectrum and its abundance on Earth. However, the efficiency of silicon-based solar cells has limitations, leading researchers and developers to focus on alternative approaches for further advancements in solar cell technology.

Advancements in technology pave the way for cutting-edge research in the development of highly efficient and cost-effective MIS solar cells, offering promising prospects for diverse and widespread applications. The device was subjected to precise analyses using the Silvaco Atlas software, enabling a comprehensive numerical investigation into the correlation between various effects and the device's performance and reliability.

In this thesis, the electrical performance of a metal-insulator-semiconductor (MIS) solar cell is evaluated. The focus is on its design with various high-k dielectrics, the objective of the study is to optimize the device's geometrical dimensions while enhancing quantum mechanical tunneling mechanisms, The thesis also provides a comprehensive comparison between the suggested solar cell structures using crystalline silicon (c-Si) and thin film silicon (hydrogenated amorphous silicon, a-Si:H).It explains the physics underlying both thin-film silicon solar cells and c-Si, emphasizing the use of diverse material selections involving high-k insulator layers. These layers play a pivotal role in overcoming the limitations of conventional SiO_2, such as Al_2O_3, HfO_2, Si_3N_4, TiO_2, and Ta_2O_5. The evaluation focuses on comparing performance parameters, with a primary emphasis on conversion efficiency. Additionally, the study assesses the impact of interface state density, doping density, oxide thickness, and oxide fixed charge on the electrical outputs of the proposed MIS solar cell.

As observed from the responses of the devices, MIS diodes utilizing HfO_2 and Ta_2O_5 as the insulating layers exhibit the highest efficiency under visible light. This is attributed to the fact that these diodes enable more efficient tunneling of hot electrons due to the asymmetry of the thin energy barrier. Consequently, the insulating layer plays a crucial role in determining the tunneling probability of electrons and optimizing the conversion efficiency, as evidenced by the findings of this study.

Keywords: MIS solar cell; Silicon, Silvaco-Atlas; tunneling current, high-k

Résumé

Actuellement, le marché des cellules solaires est dominé par les cellules solaires à base de silicium, car la bande interdite du silicium correspond de manière appropriée au spectre solaire et le silicium est le matériau le plus abondant sur la terre. Cependant, l'efficacité des cellules solaires à base de silicium est limitée, c'est pourquoi la recherche et le développement se concentrent sur des méthodes alternatives.

Les avancées technologiques ouvrent la voie à des recherches de pointe dans le développement de cellules solaires MIS hautement efficaces et rentables, offrant des perspectives prometteuses pour des applications diverses et étendues. L'appareil a été soumis à des analyses précises à l'aide du logiciel Silvaco Atlas, permettant une investigation numérique approfondie de la corrélation entre divers effets et les performances et la fiabilité de la cellule.

Cette thèse évalue les performances électriques d'une cellule solaire métal-isolant-semi-conducteur (MIS) conçue en utilisant différents diélectriques à constante diélectrique élevée (k élevé). L'étude vise à optimiser les dimensions géométriques du dispositif tout en améliorant les mécanismes de tunnel mécanique quantique. En outre, une comparaison globale entre les structures de cellules solaires proposées en silicium cristallin (c-Si) ou en film mince (silicium amorphe hydrogéné (a-Si:H)) est présentée, décrivant la physique des cellules solaires en silicium à couches minces et c-Si avec différentes sélections de matériaux basées sur des couches d'isolants à constante diélectrique élevée (k élevé).

Les matériaux spécifiques (Al_2O_3, HfO_2, Si_3N_4, TiO_2 et Ta_2O_5) sont évalués pour comparer les paramètres de performance, en mettant l'accent sur l'efficacité de conversion. De plus, l'effet de la densité des états d'interface, de la densité de dopage et de la charge fixe d'oxyde sur les sorties de courant électrique de la cellule solaire MIS proposée est évalué.

À la fin de cette étude, les diodes MIS à base de HfO_2 et Ta_2O_5 ont obtenu le rendement le plus élevé sous la lumière visible. Cette performance supérieure est due à la présence d'une barrière d'énergie plus fine et plus asymétrique que dans les autres diodes MIS. Cette barrière plus fine permet à un plus grand nombre d'électrons de tunneler à travers la couche isolante. L'épaisseur de la couche isolante est donc un paramètre critique pour la probabilité de l'effet tunnel des électrons et l'optimisation du rendement de conversion

ملخص.

في الوقت الحالي ، تحتل خلايا الطاقة الشمسية القائمة على السيليكون موقعًا مهيمنًا في سوق الخلايا الشمسية نظرًا لتوافق فجوة طاقة السيليكون المناسبة مع الطيف الشمسي ووفرتها على الأرض. ومع ذلك، تواجه خلايا الطاقة الشمسية القائمة على السيليكون تحديات في كفاءتها ، مما يدفع الباحثين والمطورين إلى التركيز على أساليب بديلة لتحسين التكنولوجيا الشمسية.

التطورات التكنولوجية تمهد الطريق لأبحاث متطورة في مجال تطوير خلايا الطاقة الشمسية MIS عالية الكفاءة والفعالية من حيث التكلفة، والتي تقدم آفاقًا واعدة لتطبيقات متنوعة وواسعة النطاق. تم إجراء تحليلات دقيقة للخلية باستخدام برنامج Silvaco Atlas، مما سمح باجراء تحقيق رقمي شامل في العلاقة بين التأثيرات المختلفة وأداء الخلية وموثوقيته.

محور هذه الأطروحة هو تقييم الأداء الكهربائي لخلية شمسية من نوع معدن-عازل-شبه موصل(MIS) . يركز البحث على تصميمها باستخدام عوازل كهربائية عالية الثابت k .(high-k) ، ويهدف إلى تحسين الأبعاد الهندسية للجهاز مع تعزيز آليات النفوذ الكمومي. توفر الأطروحة أيضًا مقارنة شاملة بين هياكل الخلايا الشمسية المقترحة باستخدام السيليكون البلوري (c-Si) والسيليكون الرقيق (السيليكون غير المتبلور المهدرج، .(a-Si:H) تشرح الفيزياء الكامنة وراء كل من خلايا الطاقة الشمسية الرقيقة السيليكونية والسيليكون البلوري، مع التركيز على استخدام تشكيلات متنوعة للمواد تشمل طبقات عازلة عالية الثابت .k تلعب هذه الطبقات دورًا محوريًا في التغلب على قيود أكسيد السيليكون SiO_2 التقليدي، مثل Al_2O_3و HfO_2 و Si_3N_4 و TiO_2 و .Ta_2O_5 يركز التقييم على مقارنة معلمات الأداء، مع التركيز الأساسي على كفاءة التحويل. بالإضافة إلى ذلك، تقييم الدراسة تأثير كثافة حالة الواجهة، وكثافة الإشابة، وسماكة الأكاسيد، وشحنة الأكاسيد الثابتة على المخرجات الكهربائية لخلية MIS الشمسية المقترحة

كما لوحظ من استجابات الأجهزة، فإن الثنائيات المعدنية العازلة - شبه الموصلة (MIS) التي تستخدم HfO_2 و Ta_2O_5 كطبقات عازلة تحقق أعلى كفاءة تحت الضوء المرئي. ويعزى ذلك إلى حقيقة أن هذه الثنائيات تسمح بنفوذ أكثر كفاءة للإلكترونات الساخنة بسبب عدم تناسق حاجز الطاقة الرقيق. وبالتالي، تلعب الطبقة العازلة دورًا حاسمًا في تحديد احتمال نفوذ الإلكترونات وتحسين كفاءة التحويل، كما يتضح من نتائج هذه الدراسة..

Table of Contents

DEDICATION I

ACKNOWLEDGEMENTS II

ABSTRACT IV

RÉSUMÉ V

ملخص VI

TABLE OF CONTENTS VI

LIST OF FIGURES X

LIST OF TABLES XIII

LIST OF ABBREVIATIONS .... ERROR! BOOKMARK NOT DEFINED.

GENERAL INTRODUCTION 1

CHAPTER IGENERAL INFORMATION ON MS AND MIS STRUCTURES 7

1. INTRODUCTION 8
2. METAL-SEMICONDUCTOR CONTACTS (MS) 8
   - 2.1 N-type semiconductor with Φm> ΦS 10
   - 2.2. P-type semiconductor with $\Phi_M < \Phi_S$ 11
3. THE METAL / OXIDE / MIS SEMICONDUCTOR STRUCTURE: 12
   - 3.1 General Description: 12
   - 3.2. Device Structure 12
4. CLASSIFICATION OF MIS TUNNEL DIODES 13
   - 4.1. Band diagram: 16

5- THE INFLUENCE OF INSULATORS ON ENERGY BAND DIAGRAMS. 19
   - 5.1-Charge Carrier Fluxes: 19
   - 5.2. Variations in Barrier Height: 20
   - 5.3. Surface State Treatment 20

6. THEORY OF MIS SOLAR CELLS: 21
7. TRANSPORT MODELS: 23
   - 7.1. Characterization of the semiconductor region. 24

7.2. Characterization of tunneling through the insulator: 25
7.3. Interface States 27
8. CONCLUSION 28
REFERENCES 29
CHAPTER II THE PROPERTIES OF THE MAIN MATERIALS 32
1. INTRODUCTION 33
2. MATERIAL PROPERTIES 33
2.1. Crystalline silicon (c-Si): 34
2.2. Thin-film solar cells: 35
2.2.1. Hydrogenated amorphous silicon: 36
2.2.2. Thin layers of dielectric materials 37
3. THE DIFFERENT CATEGORIES OF DIELECTRICS: 38
3.1. High-k 39
4. PROPERTIES OF AVAILABLE DIELECTRICS (OXIDES USED IN THE SIMULATION) OXIDES USED IN THE SIMULATION: 42
4.1. Silicon Oxide: 42
4.1. Silicon nitride Si3N4: 42
4.2. Tantalum oxide (Ta_2O_5): 42
4.3. Aluminum oxide or alumina Al_2O_3: 43
4.4. Hafniumb oxide HfO_2: 44
4.5. Titanium oxideTiO_2: 44
5. THE OPTICAL PROPERTIES OF OXIDES USED 44
6. OXIDE CHARGES IN SILICON DIOXIDE THIN FILMS 48
6.1. Fixed oxide charge (Q_f): 48
6.2. Interface trapped charge (Q_i): 48
6.3. Ionic mobile charges: 49
6.4. Oxide trapped charge (Qt): 49
7. DIFFERENT TYPES OF CONDUCTION IN THE OXIDE 49
7.1. Thermionic conduction 50
7.2. Conduction by direct tunnel effect 50
7.3. Fowler-Nordheim type tunneling conduction 50
7.4. Hopping Conduction: 50
7.5. Poole-Frenkel effect conduction 50

8.Conclusion……………………………………………………………………………51

REFERENCES 52

CHAPTER III PHYSICS MODEL AND METHOD 56

1. INTRODUCTION: 57

2. DEVICE SIMULATOR: ATLAS MODULE.. 57

2-1.Structure of the reference cell used 58

2.2 Structure and Mesh Editor: 58

2.3. Numerical Methods: 59

4. THE PHYSICAL MODELS USED FOR THE SIMULATION UNDER ATLAS/SILVACO.............. 61

4.1. Mobility models 62

4.2. Recombination models used for simulation under ATLAS/SILVACO 63

4.2.1. Shockley-Read-Hall (SRH) recombination.. 63

4.2.2. Auger recombination 64

4.2.3. Langevin recombination 66

4.3. The tunnel effect 67

4.4 - Models of the Density of States (DOS) used in simulation 68

5. OVERVIEW OF THE INVESTIGATED MIS SILICON SOLAR CELL... 71

5.1. Model for Silicon based MIS junction Diode 71

5.2-Input parameters:.. 73

6. CONCLUSION... 74

REFERENCES 75

CHAPTER IV RESULTS AND INTERPRETATIONS 76

1. INTRODUCTION: 78

2. DEVICE STRUCTURE: 79

3. SIMULATION MODELS AND PARAMETERS 82

4. RESULTS AND DISCUSSION 83

4.1 Effect of the Insulator Thickness 83

4.2 Effect of the Base Thickness:.. 87

4.3. Influence of Doping Concentration 91

4.4 Interface States Effects 97

4.5. Impact of Fixed Oxide Charges 100

4.6 Effect of Metal Work Function 103

5. SOLAR CELLS SPECTRAL RESPONSE 106
CONCLUSION 109
REFERENCES 110
GENERAL CONCLUSION 113
APPENDIX 116

LIST OF FIGURES

Figure I. 1: Band diagrams of (a) a metal and (b) a semiconductor without any interaction ... 9
Figure I. 2: Schottky barrier between a metal and an n-type semiconductor with $\Phi_m>\Phi_s$; (a) band diagrams before contact; (b) equivalent band diagram after the contact ... 10
Figure I. 3: Schottky barrier between a metal and a p-type semiconductor with $\Phi_m<\Phi_S$; (a) band diagrams before contact; (b) equivalent band diagram after the contact ... 11
Figure I. 4: Illustration of a Metal-Insulator-Semiconductor (MIS) Diode Schematic Diagram ... 13
Figure I. 5: Energy Band Diagrams of n-Type and p-Type Si MIS Structures with Schottky Barrier at Oxide/Semiconductor Interface in Thermal Equilibrium of the Depletion Regime. ... 15
Figure I. 6: Simple equilibrium energy-band diagram of the p-type MIS solar cell. ... 17
Figure I. 7: Illustration of Energy Band Diagram for MIS solar cells System with P-Type Semiconductor Region. V_a applied Under zero illuminations. ... 18
Figure I. 8: Possible charge transport mechanisms for a MIS tunnel diode under forward bias ... 19
Figure I. 9: Voltage and current output from an illuminated Solar cell ... 22
Figure II. 1: a) Si atomic configuration, b) position in periodic table and c) physical structure ... 35
Figure II. 2: Spatial Configuration of Hydrogenated Undoped Amorphous Silicon (a-Si:H) Illustrated with Atom Arrangement and Chemical Bonds. Blue and black dots correspond to silicon and hydrogen atoms, respectively. Chemical bonds are shown as black lines, open ends correspond to dangling bonds ... 37
Figure II. 3: Classification of dielectric materials according to their permittivity, the evolution of the dielectric losses is also represented. ... 38
Figure II. 4: band diagramSiO_2 (a) is substituted by a high-k dielectric with a same capacitance using a larger thickness which leads to a reduction to a leakage current ... 3
Figure II. 5: [36] Refractive indices of oxides as a function of wavelength (a) SiO_2 (b): Al_2O_3 (c): HfO_2 (d): TiO_2 (e):Ta_2O_5 (f):Si_3N_4 ... 45
Figure II. 6: Reflected, transmitted and absorbed radiation ... 46
Figure II. 7: Law of reflection ... 47
Figure II. 8: Various charge varieties within the oxide ... 49

Figure II. 9: Schematic representation of the different types of conduction in the oxide. 51
Figure III. 1: Device simulator's low-level simulation and scheme for sub-modules 58
Figure III. 2: Metal- Insulator- Semiconductor (MIS) cell two-dimensional structure. 58
Figure III. 3: Definition of regions. 60
Figure III. 4: Transitions through a level inside the band gap of a semiconductor. 64
Figure III. 5: Diagram illustrating Auger recombination 65
Figure III. 6: DOS du silicium amorphe hydrogéné dopé p 70
Figure IV. 1: Cross-Sectional Illustration of a 2D MIS Solar Cell Structure 79
Figure IV. 2Optical parameters of (c-Si), (a-Si:H), SiO_2, HfO_2 and Al_2O_3 (a) refractive index n(b) 81
Figure IV. 3: Variation of (J-V) Characteristics with Al-SiO2-p Oxide Thickness in c-Si and a-Si:H-Based MIS Solar Cell Structures 83
Figure IV. 4: Observable Variations in J-V Characteristics with Different Oxide Materials in(c-Si) and (a-Si:H)-Based MIS Solar Cell Structures... 84
Figure IV. 5: Performance Analysis: Conversion Efficiency, Fill Factor, Short-Circuit Current Density, and Open-Circuit Voltage Behavior in Various Designs of c-Si-Based MIS Solar Cell 85
Figure IV. 6: Performance Analysis: Conversion Efficiency, Fill Factor, Short-Circuit Current Density, and Open-Circuit Voltage Behavior in Various Designs of (a-Si:H)-Based MIS Solar Cells 86
Figure IV. 7: Variations in (J-V) Characteristics of Different MIS Solar Cell Designs with Changing Cell Thickness; (a) Al-SiO2/c-Si structure, (b) Al-SiO2-a-Si:H structure...... 88
Figure IV. 8: Performance Analyses of c-Si-Based MIS Solar Cell Designs: Conversion Efficiency, Fill Factor, J_{sc}, and Voc Behavior across Varied Base Thicknesses..................... 89
Figure IV. 9: Performance Analysis of (a-Si:H)-Based MIS Solar Cell Designs: Conversion.. 90
Figure IV. 10: J-V characteristics of theSiO2-based MIS solar cell as a function of the substrate doping. a)- Al-SiO_2-p(c-Si), b)- Al-SiO_2-p (a-Si: H). 92
Figure IV. 11: the output characteristics of the suggested MIS solar cell, utilizing various high-k materials, in relation to the substrate doping levelsfor $(c-Si)$. 93
Figure IV. 12: the output characteristics of the suggested MIS solar cell, utilizing various high-k materials, in relation to the substrate doping levelsfor (a-Si: H).................... 94

Figure IV. 13: demonstrates the distribution of electric fields within the device for various materials. $(c-Si)$ 95
Figure IV. 14: demonstrates the distribution of electric fields within the device for various materials. (a-Si: H) 96
Figure IV. 15: J-V characteristics of the SiO2-based MIS solar cell for different interface state densities. a)- Al-SiO_2-p(c-Si), b)- Al-SiO_2-p (a-Si: H). 97
Figure IV. 16: the output characteristics of the suggested MIS solar cell, utilizing various high-k materials, in relation to the interface state density for (c-Si). 98
Figure IV. 17: the output characteristics of the suggested MIS solar cell, utilizing various high-k materials, in relation to the interface state density for (a-Si:H). 99
Figure IV. 18: J-V characteristics of the conventional MIS solar cells: for different fixed oxide charge a- Al-SiO_2-p(c-Si), b- Al-SiO_2-p(a-Si:H) 100
Figure IV. 19: Effect of Oxide Fixed Traps Density on the Output Characteristics of MIS Solar Cells Utilizing Different High-k Materials Compared to c-Si -Based MIS Solar Cell 101
Figure IV. 20: J-V characteristics of the conventional MIS solar cells: a- Al-SiO_2-p(c-Si), b- Al-SiO_2-p(a-Si:H) 102
Figure IV. 21: I-V Characteristics of SiO_2-Based MIS Solar Cell Across Various Work Functions 103
Figure IV. 22: Comparison of Output Characteristics of MIS Solar Cells Utilizing Different High-k Materials with the Metal Work Function Value of (c-Si) -Based MIS Solar Cell 104
Figure IV. 23: Comparison of Output Characteristics of MIS Solar Cells Utilizing Different High-k Materials with the Metal Work Function Value of a-Si:H-Based MIS Solar Cell 105
Figure IV. 24: Spectral Response of MIS Solar Cell as a Function of Wavelength 107

LIST OF TABLES

Table II. 1: Comparison of relevant properties of high-K dielectrics. 40

Table II. 2: Main electrical properties of dielectric materials 41

Table III. 1: Some of Atlas's mobility models.. 63

Table III. 2: The default values used for the simulation of Auger recombination. 65

Table IV. 1: MIS references parameters 79

Table IV. 2: Defects parameters for (a-Si:H) 79

Table IV. 3: Input data of the proposed dielectrics materials 80

List of symbols

A	Richardson constant
χ_s	Electron affinity of silicon
D_{it}	Interface state density
D_n	Diffusion constant for electrons
D_p	Diffusion constant for holes
E	Electric field or Energy
E_C	Conduction band energy level
E_{fn}	Quasi-Fermi level for electrons
E_{fp}	Quasi-Fermi level for holes
E_G	Band gap Energy
$\mathbf{E_{gi}}$	band gaps o f the insulator
E_{gs}	band gap of semiconductor
E_i	The intrinsic fermi level
f_m	The probability of occupancy of states of energyin the metal
f_s	The probability of occupancy of states of energy in the semiconductor
η	Efficiency
I	Current
I_o	Reverse saturation current
I_{sc}	Short circuit current
J	Current density
Jn	Electron current density
J_p	Hole current density
J_r	Recombination current density
J_{RC}	Generation/recombination current density between conduction band and surface states
J_{Rg}	Generation/recombination current density between valence band and surface states
J_{th}	The thermionic emission of electrons into the metal
J_{CT}	Conduction band tunneling current density
J_{ST}	Tunneling current density between metal and surface states

J_d	The diffusion currentdensity
J_{VT}	Valence band tunneling current density
μ_n	Electron mobility
μ_p	Hole mobility
N_A	Acceptor doping density
N_D	Donor doping density
ni	Intrinsic carrier density
N_n	Density of state for electrons
N_p	Density of state for holes
N_{ss}	Surface state density
P	Hole concentration
ϕ_B	Potential barrier of a Schottky diode
ϕ_M	Metal work function
ϕ_S	Surface potential
q	Electronic charge
FF	Fill factor
G	Generation rate
R_C	Contact resistance
RS	Series resistance
$R(\lambda)$	the reflection coefficient
T	Temperature
d	Oxide thickness
U	Recombination rate
(J-V)	Characteristic (voltage –current)
J_{sc}	Short circuit current
V_{oc}	Open circuit voltage
V_m	The maximum power point voltage
$\alpha(\lambda)$	absorption coefficient
$\phi_{CB}(x)$	represents the energy of the insulator conduction band edge.

GENERAL INTRODUCTION

Among the most promising and rapidly advancing methods for harnessing non-conventional energy resources are those that utilize the photovoltaic (PV) effect. This phenomenon directly converts sunlight into electricity, which can be seamlessly integrated into the power grid through the use of solar panels [1-2-3]. Crystalline silicon (c-Si) wafer-based PV has held the leading position as the dominant solar cell technology, contributing to around 90% of the total solar cell production. The advantage of using Si over other semiconductor materials stems from its ready availability in highly purified form and its simple solar cell structure, which facilitates cost-effective production and material costs. Furthermore, the presence of a well-established microelectronics industry adds to its favorable position [4-5-6] in the early 1950s, Bell Laboratories pioneered the development of the first solar cell utilizing a diffused p-n junction. However, its sunlight energy conversion efficiency was merely approximately 6% during that era, and the production costs were very high [7].One promising alternative technique for fabricating solar cells is to replace the diffused p-n junction with a metal-semiconductor junction, also known as a Schottky barrier. [8] When a metal interfaces with a semiconductor, it forms a Schottky junction that selectively allows carriers to pass through. The electronics field commonly manufactures Schottky diodes by applying metal onto clean silicon surfaces in high vacuum environments [9]. The work function mismatch between the metal and semiconductor determines the type of conduction inversion that takes place in the semiconductor [10].

Minimizing the rate of minority carrier recombination at the interface between the metal and semiconductor is a major challenge to increasing conversion efficiency [11]. A thin insulating layer, such as SiO_2, placed between the metal and semiconductor converts the MS structure into a MIS type structure. This approach is considered an intriguing one that has the potential to significantly increase the open-circuit voltage [13]. The ability to facilitate selective charge carrier transport while significantly minimizing minority carrier recombination rate is one of the most advantageous methods for improving solar cell efficiency [12].

The best solution to improve the current flow in a solar cell using quantum mechanical tunneling techniques is to utilize a dielectric material characterized by a high dielectric constant (high-k). SiO_2 is a suitable option, but other high-k materials, such as Al_2O_3, HfO_2, Si_3N_4, TiO_2, and Ta_2O_5, can offer even better performance. These materials have a higher capacitance than SiO_2, which means that they can store more charge. They also have a lower leakage current, which means that less charge is lost through the dielectric layer. The

utilization of high-k materials is crucial for various applications, including solar cells, transistors, and capacitors [14-15-16].

The aim of this thesis is to develop innovative material systems and structures, particularly thin films of amorphous silicon (Si-a: H) and crystalline silicon (c-Si), to improve the selective contact between high-k dioxide-based minority charge carriers and silicon (p-type). This enhanced selective contact has been engineered to serve as a highly efficient electron contact in a MIS solar cell [17- 18].

High-k dioxide-based contacts are crucial for improving the performance of next-generation electronic devices. The high dielectric constant of high-k dioxides allows them to create a strong electric field at the interface with silicon, which helps separate minority carriers from majority carriers. This separation of carriers can lead to an increase in the open-circuit voltage of the solar cell. High-k dioxides are also relatively stable and can withstand the harsh conditions inside a solar cell. These contacts integrate the extraction and separation of minority carriers from the p-type silicon absorber inside a single contact junction, using the aforementioned high-k dielectrics [19- 20]. Therefore, studying the I-V characteristics of MIS diodes with these high-k dielectric materials could lead to the development of new and more efficient electrical devices.

To improve the performance of the studied solar cells, they are subjected to the AM1.5 standard spectrum at room temperature (300 K). The research will be conducted with the assistance of numerical simulation software SILVACO-ATLAS, which facilitates the calculation of all internal solar cell parameters [21]. The software also calculates external factors like current-density voltage (I-V) behavior. These can be used to extract the output photovoltaic parameters of the solar cell, such as the short circuit current density (J_{sc}), open circuit voltage (V_{oc}), fill factor (FF), maximum power (P_{max}) generated by the cell, and the photovoltaic conversion efficiency.

The key elements influencing the conversion efficiency of MIS solar cells include the thickness of the insulator, the metal's work function, surface state properties, oxide charge, substrate thickness, and various high-k oxides. This study aims to determine the optimal design for contacts in solar cells. The thesis will be organized as follows, excluding the general introduction and conclusion section:

- The first chapter of this thesis outlines the fundamental principles, key concepts, electrical properties, and general operation of MS and MIS solar cells. We have examined the background information on the electrical properties, the phenomenological model for solar cells, and the methodology employed to assess the theoretical performance of MIS solar cells.

- The second chapter discusses the motivation for material selection in high-k oxide MIS solar cells. The chapter includes definitions of several high-k oxides as solar cell materials and an overview of the research on various oxides used in MIS solar cells.

- Chapter III of the thesis provides a comprehensive overview of the Silvaco TCAD simulation, including a glossary of terms and an outline of all the simulation procedures used for our particular solar cell. Furthermore, it offers a detailed description of the two-dimensional solar cell simulation and the characteristics of the materials used in the simulation.

- Chapter IV of the thesis presents simulations of the photovoltaic behavior of MIS solar cells to identify the criteria that enable these cells to operate at their highest capacity. This study aims to clarify the effectiveness of amorphous silicon as an active region in MIS solar cells. Detailed investigations were conducted into the optical and electrical performance of MIS structures. The study focused on using c-Si and a-Si:H substrates, along with various high-k oxides, to improve carrier tunneling mechanisms in solar cells. Several important simulations were carried out, with SiO_2 used as a reference. The effects of various parameters on the performance of MIS solar cells were examined, and the findings from our simulations will be discussed.

References

[1]-ManjotKaur, Harjit Singh, Comparison of Silicon Solar Cells and Thin Film Solar Cells Volume 3, Issue 2, May (2016)

[2]- Christoph Alexander Meßmer, Numerical Simulation and Analysis of Metal Oxide Contact Properties for Silicon Heterojunction Solar Cells DOI:10.13140/RG.2.2.19788.10886/1 Master of Science Physics Freiburg im Breisgau (2017).

[3]-Y. Ren, N. M. Nursam, D. Wang, K. J. Weber, "Charge storage stability in silicon nitride for surface passivation", the 25th European Photovoltaic Solar Energy Conference, Valencia, Spain, September 06-10,(2010).

[4]- Daniel Vossing, M.Sc, Titanium Dioxide as Minority Charge Carrier Separating Contact to Crystalline P-Type Silicon Albert-Ludwigs-University Freiburg Freiburgim Breisgau Deutschland, (2018)

[5]-Paul Procela,∗,Philipp Löperb, Felice Crupia, Christophe Ballifb, Andrea Ingenitob Numerical simulations of hole carrier selective contacts in p-type c-Si solar cells© 2019 Elsevier.

[6]-Sebastian Z. Oener, Jorik van de Groep, Bart Macco, Paula C.P. Bronsveld, Wilhelmus (Erwin) M.M Kessels, Albert Polman, and Erik C. Garnet Metal-Insulator-Semiconductor Nanowire Network Solar Cells • Publication Date (Web): 12 May (2016)

[7]- Renaud Varache, Développement, caractérisation et modélisation d’interfaces pour cellules solaires à haut rendement à base d’hétérojonctions de silicium, Université Paris-Sud (2012)

[8]-Rhoderick,E. H;Williams, R.H. Metal-Semiconductor Contacts; 2nded;Oxford University Press: New York, (1988).

[9]- Öner, S.Z. Metal-insulator-semiconductor nanowire network solar cells Metal-insulator-semiconductor (MIS) University of Amsterdam (2020).

[10]-Sze, S. M.; Ng, K. K. Physics of Semiconductor Devices, 3rd ed.; Wiley: New Jersey, (2007).

[11]-Godfrey, R. B.; Green, M. A. 655 mV open-circuit voltage, 17.6% efficient silicon MIS solar cells, Volume34, 790–793.(1979)

[12]- Hezel, R. Prog. Photovoltaics, Research and Applications. Recent Progress in MIS Solar Cells, 5, 109–120. (1997)

[13]-Green, M. A.; King, F. D.; Shewchun, Minority carrier MIS tunnel diodes and their application to electron- and photo-voltaic energy conversion—I. Theory J. Solid. State.Electron.Volume 17, Issue 6, 551–561.(1974)

[14]-Shewchun, J.; Green, M. A.; King, F. D.Minority carrier MIS tunnel diodes and their application to electron- and photo-voltaic energy conversion II Experiment Solid State Electron, Volume 17, 563–572.(1974)

[15]-Hsin-Yu Lee Research on MIS Stacked Solar Cells National Chiao Tung University (2009)

[16]- John Robertson, High dielectric constant gate oxides for metal oxide Si, Cambridge University transistors October (2005)

[17]-D. Misra, H. Iwai, and H. Wong, High-k Gate Dielectrics, the Electrochemical Society Interface. 14(2), 30-35 (2005).

[18]-Güllü Ö,Türüt A."Electrical analysis of organic dye-based MIS Schottky contacts". Microelectronic Engineering, 87(12), 2482-2487, (2010)

[19- Karataş Ş, YildirimN, Türüt A."Electrical properties and interface state energy distributions of Cr/n-Si Schottky barrier diode". Superlattices and Microstructures, 64, 483-494, (2013)

[20] -A. P. Huang, Z. C. Yang, and Paul K. Chu, Hafnium-based High-K Gate Dielectrics, Advances in Solid State Circuits Technologies., 16(1), 334-350 (2010).

[21]-SILVACO-TCAD. ATLAS user's manual: device simulation software. California: SILVACO International.

Chapter I

GENERAL INFORMATION ON MS AND MIS STRUCTURES

1. Introduction

Modern semiconductor devices rely on the precise manipulation of the electronic characteristics of metal-semiconductor (MS) contacts. The direct metal-semiconductor contact can cause increased surface recombination due to the presence of metal-induced band gap states and dangling bonds [1- 2- 3- 4]. Leading solar cell designs that tackle this issue include the metal-insulator-semiconductor (MIS) solar cell. These structures offer the charge-separation capabilities observed in Schottky junctions, while avoiding the adverse effects of direct metal-semiconductor contact.

Theoretical analyses and real-world experiments have shown that this structure simultaneously addresses the main shortcoming of Schottky barrier solar cells such as the limited open-circuit photo voltage, should be addressed while maintaining their desirable properties, such as their high efficiency and fast response time, which make them a potential replacement for p-n junctions in large-scale terrestrial solar cell applications [5- 6], these junctions have two key benefits over traditional p-n junction solar cells: a greatly streamlined manufacturing process and exceptional passivation capabilities, resulting in high open-circuit voltages [7- 8]. This research conducts a thorough investigation of ideas developed from these models with an emphasis on their application and importance in the setting of practical solar cells.

2. Metal-Semiconductor Contacts (MS)

The metal-semiconductor (MS) interface exerts a pivotal influence on shaping the performance of semiconductor devices. The quality of the contact between the metal and semiconductor can have a substantial impact on the device's efficiency, stability, and dependability.

When two materials make contact, electron flow occurs from the material with the higher Fermi level to the material with the lower Fermi level until the Fermi levels are aligned. This creates a potential barrier at the interface, called the barrier height. The barrier height determines the amount of current that can flow through the contact. A high barrier height can lead to low efficiency and poor device performance. Therefore, it holds significance to optimize the metal-semiconductor contact in order to achieve high device performance. You can determine the barrier height by using the equation provided below:

$$q\phi_b = q(\phi_m - \chi_S) \text{ .... (N-type)} \tag{I.1}$$

$$q\phi_b = E_G - (\phi_m - \chi_S) \text{...... (P-type)} \tag{I.2}$$

The Schottky barrier height, Φ_B, is the energy difference between the metal work function, Φ_m, and the electron affinity of the semiconductor, χ. In a semiconductor with a band gap Eg between the conduction band minimum (E_{CB}) and valence band minimum (E_{VB}), the majority of the metal-induced gap states are located near the E_{CB} minimum [9].

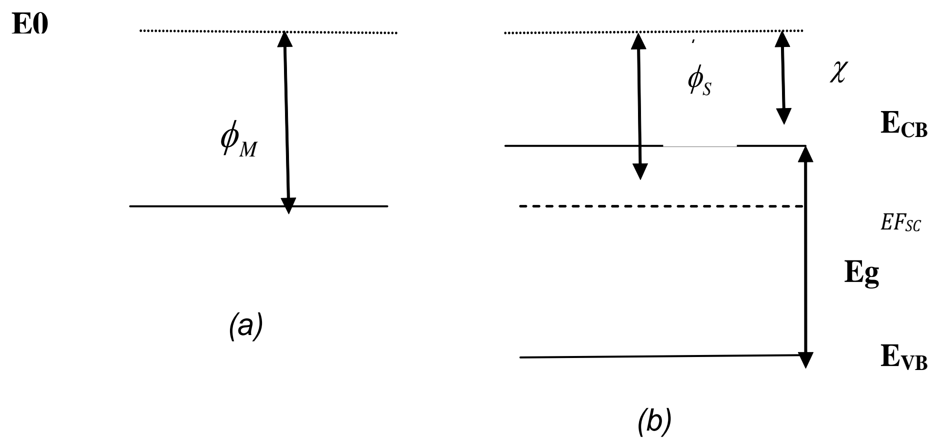

Figure I. 1: Band diagrams of (a) a metal and (b) a semiconductor without any interaction

The quality of the metal-semiconductor (MS) interface notably impacts the performance of solar cells. Considerable scientific and technological research has been conducted on metal-semiconductor (MS) contacts, due to their desirable properties and extensive use in electrical applications, optoelectronic, and electrochemical devices. The majority of carriers are hindered by the existence of a barrier in MS contacts, which essentially behave as rectifying Schottky contacts or non-rectifying ohmic contacts. A carrier-selective interface is considered efficient if it has a low resistance for majority carriers and a high barrier for minority carriers. One example is the use of an ohmic contact, in which majority carriers do not experience any difficulty. If the work function of a metal is lower than that of an n-type semiconductor, an ohmic contact can be established between them. ohmic contacts are difficult to fabricate due to Fermi level pinning (FLP), which prevents the Fermi level from aligning with the work function of the metal. This forces us to deal with Schottky barriers, which hinder majority carriers and provide recombination centers for minority carriers, reducing the open-circuit voltage of the solar cell.

2.1. N-type semiconductor with Φm>ΦS

As seen in the figure, when $\Phi_m > \Phi_S$, the Fermi level of the n-type semiconductor is already higher than that of the metal before they come into contact, the Fermi levels of both sides align, resulting in the semiconductor's Fermi level decreasing by an amount equal to the disparity in their work function concerning the Fermi level of the metal . However, To achieve Fermi level alignment and establish equilibrium, the electrostatic potential of the semiconductor must be elevated relative to that of the metal, which means that the electrostatic potential of the semiconductor must increase.

As shown in Figure (I. 2), when a contact is made in the presence of both an n-type semiconductor and a metal, the depletion region is a region of space charge that forms at the interface between a semiconductor and a metal, the formation of this depletion region results from the movement of electrons from the semiconductor to the metal, which leaves behind positively charged donor ions.

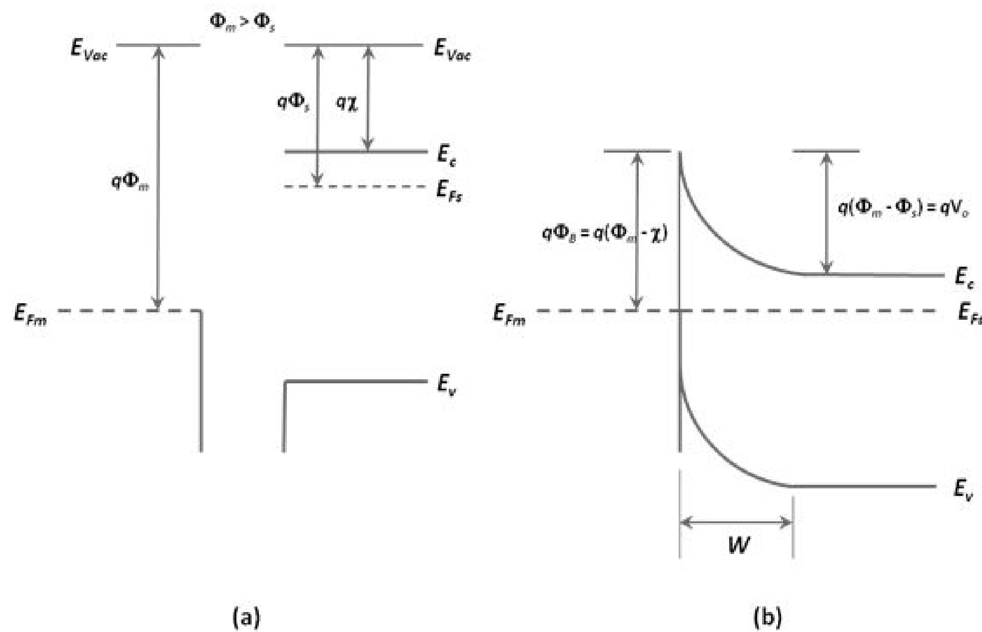

Figure I. 2: Schottky barrier between a metal and an n-type semiconductor with Φ_m>Φ_s; (a) band diagrams before contact; (b) equivalent band diagram after the contact [12].

The contact potential, V_O, is the voltage that develops across the depletion region to prevent Additional electron transport occurs from the semiconductor to the metal. The contact

potential equals the potential barrier height divided by the difference between the work function potentials of the metal and semiconductor (Φ_m - Φ_s) [12].

2.2. P-type semiconductor with Φ_M<Φ_S

In the energy band diagram illustrating a Schottky barrier between a metal and a p-type semiconductor, shown in Figure (2-2), where Φ_m< Φ_S, the metal's Fermi level is initially above that of the p-type semiconductor before contact. When contact is made, a depletion region W develops near the junction within the p-type semiconductor. This phenomenon occurs because, in order to achieve Fermi level alignment at equilibrium, a positive charge on the metal side and a negative charge on the p-type semiconductor side of the junction are essential.

The positive charge on the metal side is counterbalanced by the negative charge stemming from ionized acceptors within the depletion region W. This results in the creation of a potential barrier, V_O whose height mirrors the disparity in work functions between the semiconductor and metal (Φ_S – Φ_m). This barrier effectively halts as an blockage to prevent further hole migration from the semiconductor into the metal. Adjusting the potential can be accomplished by applying a voltage across the junction, enabling similar adjustments as in the metal-n-type semiconductor junction [12].

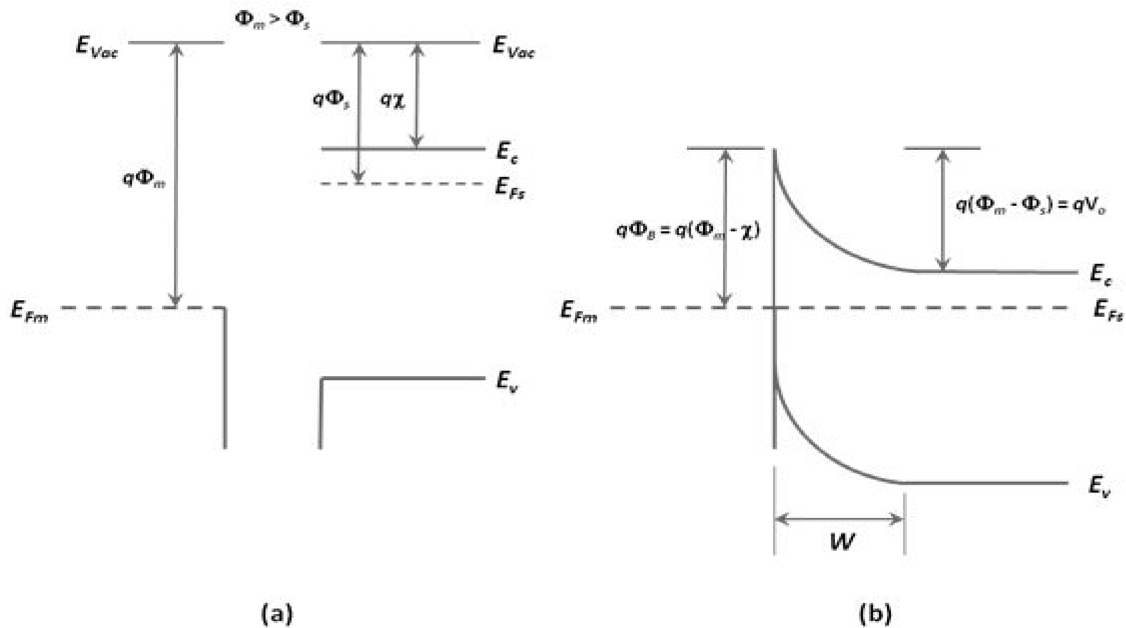

Figure I. 3: Schottky barrier between a metal and a p-type semiconductor with Φ_m<Φ_S; (a) band diagrams before contact; (b) equivalent band diagram after the contact [12].

3. Metal / Oxide / MIS Semiconductor structure:

3.1 General Description:

The (MIS) device structure is a Schottky junction with an added insulator layer that modifies the interface. The depletion region forms due to the variation in the Fermi levels between the metal and semiconductor. The insulating layer enables the diode to function as a minority carrier device by effectively reducing the quantity of majority carriers passing through the semiconductor-to-metal contact. This reduction in the reverse saturation current density (J_0) enhances the potential for higher conversion efficiency, A rise in the open-circuit voltage (V_{oc}) occurs, and an absence of noticeably smaller reductions in the short-circuit current density (J_{sc}) and fill factor (FF) [19- 20- 21].

The oxide layer must also have dielectric properties that support the variance in work function between the metal and semiconductor enabling considerable photovoltage production across the MIS junction. Silicon dioxide (SiO_2) is the material of choice for improving current conduction via quantum mechanical tunneling methods [22- 23- 24].

Silicon dioxide (SiO_2) has established itself as an efficient surface passivation material in both photovoltaic research and industry. However, reduced mobility reduces efficiency when the oxide layer is scaled down. Securing the dependability and enduring stability of high-k/Si structures is imperative necessitates addressing technical challenges like interfacial traps, fixed oxide traps, doping, and the impact of metal work functions.

3.2. Device Structure

Figure (I-4). Illustrates a diagrammatic representation of the semiconductor (MIS) solar cell being studied in this research, this device has a distinctive construction with a number of essential characteristics. Notably, the insulating layer has a thickness specified as "d", which ranges between 10 and 30 Å. The absorber side is mostly controlled by a p-type semiconductor. This layer increases the Schottky barriers. Experiments suggest that silicon oxide (SiO2), which was produced by thermally oxidizing silicon, was the first oxide used as an insulator in the interfacial layer, which is described as a broad band-gap material or insulator. The letter "L" stands for the semiconductor substrate's thickness.

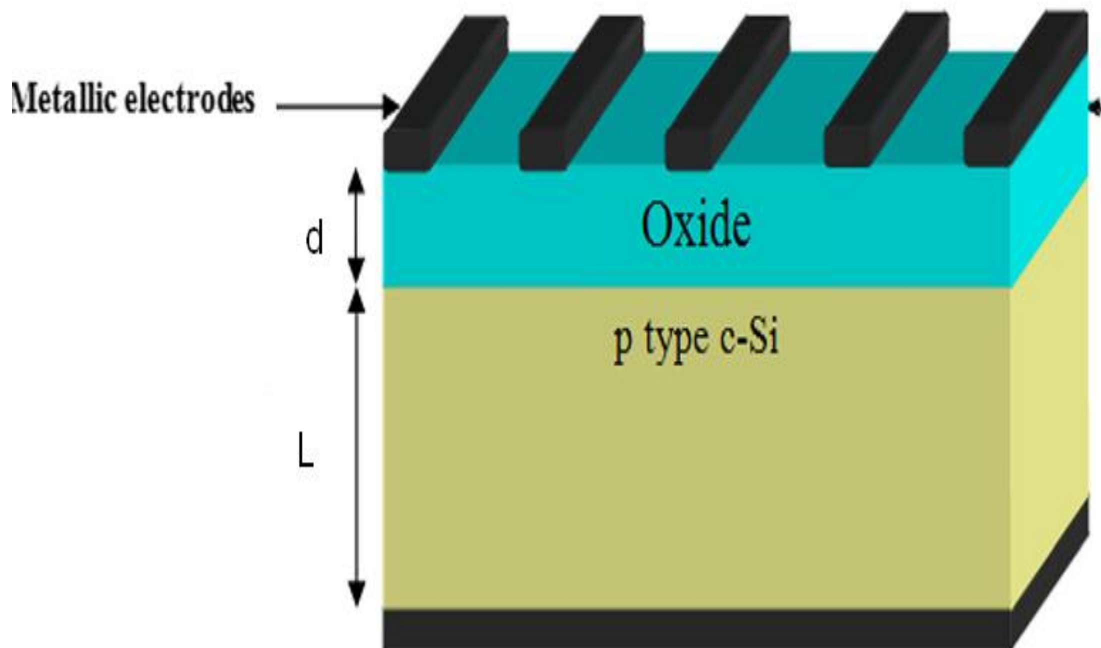

Figure I. 4: Illustration of a Metal-Insulator-Semiconductor (MIS) Diode Schematic Diagram

4. Classification of MIS Tunnel Diodes

As mentioned earlier, the functionality of MIS devices is significantly impacted by both the work function Φ_m of the metal and the insulator's thickness [25]. The thickness of the insulating layer has significant ramifications for many system features, emphasizing the importance of gaining a thorough comprehension of these effects for the development of advanced MIS structure cleaving.

Whether a device qualifies as a Schottky contact is contingent on the thickness of the insulator layer, MIS capacitor, or MIS tunnel diode. A Schottky contact forms when the insulator is thinner than 10 Å, making the layer permeable to carriers, allowing them to tunnel easily. The system exhibits the properties of a MIS capacitor when there is a thick insulating layer (> 50 Å), as the insulator blocks all charge carrier passage. Therefore, the tunnel current is what limits the performance of these equilibrium devices. In these cases, the modest tunneling current does not significantly affect the diode's electrostatic potential. Due to their similarity to MOS capacitors with leakage issues are ill-suited for use in solar applications.

However, an alternative device type known as a MIS tunnel diode arises with insulator thicknesses ranging from 10 Å to 50 Å.

These devices are therefore very promising for solar applications since they exhibit operating characteristics that closely mimic a p-n junction [26]. Although the MIS tunnel diode is sometimes referred to as a Schottky barrier diode, complete barrier traversal via direct tunneling is governed by a tunneling probability that is primarily determined by the insulator thickness. The significant band gap difference between insulators and semiconductors a barrier is established that hinders the movement of both electrons and holes, at the semiconductor-metal junction

. By allowing direct tunneling through an insulator layer, an electron and hole "tunneling probability" is created, facilitating their movement from the semiconductor to the metal. To amplify these effects and consequently boost the solar cell's efficiency, the insulator's thickness should be adequate to elevate the effective potential barrier, leading to a decrease in reverse saturation current and an elevation in open circuit voltage. On the other hand, the insulator must also possess a thinness that permits an adequate flow of tunneling current. The resultant current flow can be characterized as [25].

$$J(V) = A^{*}T^{2}\exp\left(-\alpha_{T} d_{ox}\sqrt{q\Phi_{T}}\right)\exp\left(\frac{-q\Phi_{b}}{k_{b}T}\right)\left[\exp\left(\frac{qV}{nk_{b}T}\right)-1\right]$$

$$\alpha_{T} = \frac{4\pi\sqrt{2qm^{*}}}{h} \quad .. \quad (I.3)$$

Where Φ_T is the effective barrier height, d_{ox} the insulator thickness and the first exponential term represents the tunneling probability.

The ability of a MIS diode device to perform metal work determines whether it operates as a majority carrier diode or a minority carrier diode. Figure (I.-5) depicts this [25-26]. By choosing metals with a low work function, it's possible to establish a minority carrier diode on p-type silicon substrates. Conversely, when dealing with n-type silicon, employing metals with a high work function enables the creation of a majority-carrier diode. To ensure optimal performance, the insulator's thickness should be kept sufficiently thin to prevent tunnel-limiting the minority carrier current at different biases and facilitate accumulation for higher value. The oxide thermal equilibrium must also have a lower value in order to achieve

surface inversion [27]. When the surface potential ϕ_s, surpasses the potential difference between the intrinsic and doped Fermi levels in the semiconductor bulk, ϕ_B as described by equation (I.4) and illustrated in Figure (I.6), the condition for weak inversion in a semiconductor is established.

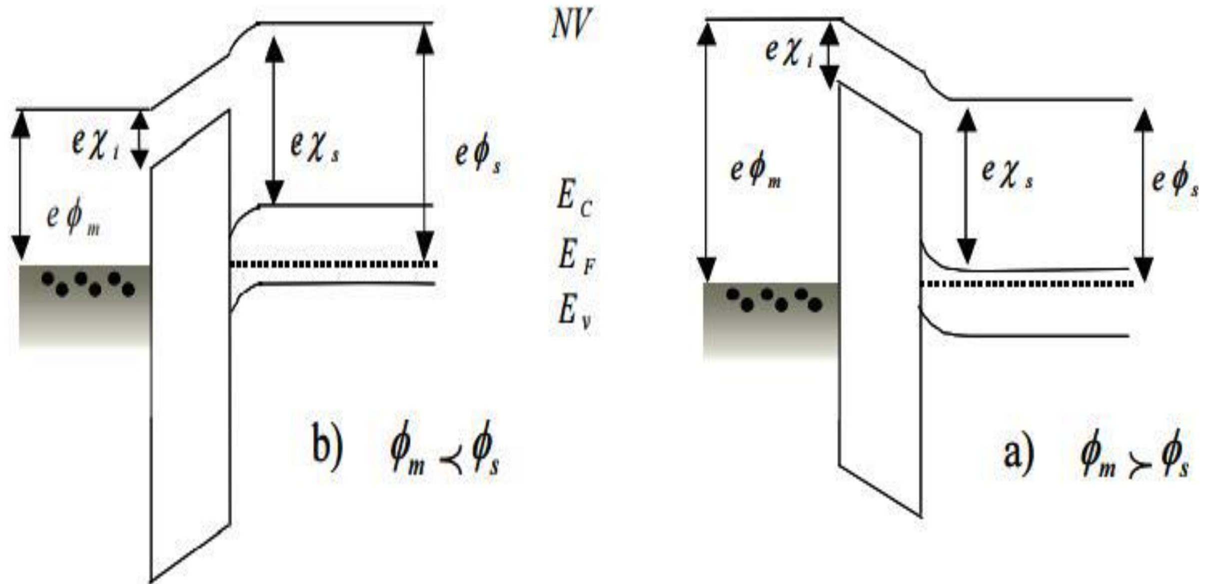

Figure I. 5: Energy Band Diagrams of n-Type and p-Type Si MIS Structures with Schottky Barrier at Oxide/Semiconductor Interface in Thermal Equilibrium of the Depletion Regime.

$$\phi_B = \frac{k_B T}{q} \ln\left(\frac{N_D}{n_i}\right) \quad \text{(I-4)}$$

Where k_B is the Boltzmann constant, T is the temperature of the semiconductor, q is the electronic change, N_D is the doping density of the semiconductor, and n_i is the intrinsic carrier density.

The specific barrier height at the metal-insulator, as depicted in the diagram below, plays a crucial role. Two different conditions can be seen under zero bias:

-Low barrier height: The semiconductor surface undergoes inversion, the deviation from the characteristics of an ideal diode when subjected to reverse bias causes the J-V characteristics to deviate. This is because the majority-carrier current becomes more dominant in influencing the structure.

-High barrier height: The semiconductor surface enters an accumulation state. This leads to a J-V curve resembling that of an ideal diode, where the structure is primarily influenced by the minority-carrier current. This case is harnessed in the creation of solar cells.

The role is reversed for n-type semiconductors.

4.1. Band diagram:

In Figure I.6, The band diagram can be used to understand how voltage U controls the flow of current in a p-type semiconductor device, relative to the top metal contact. The band gap of an insulator is denoted by E_{gi} , and the band gap of a semiconductor is denoted by E_{gs} . The energy difference between the conduction bands of a semiconductor and an insulator is called ΔE_{cs} . This energy difference is also equal to the height of the metal-to-insulator barrier, which is affected by the metal's vacuum work function.

Incorporating an insulator layer within the thickness range of 10 to 50 angstroms allows the device to function as a minority carrier metal-insulator-semiconductor (MIS) tunnel diode, as shown in Figure (I.7).This design modification effectively reduces the dark current (J_{Dark}) in the discussed solar cell, while also effectively minimizing recombination current at the interface between the oxide and silicon (Si) layers at the front surface. The solar cell's overall current when illuminated is stated as follows:

$$J_{tot} = J_{Dark} - J_{ph} \quad (I.5)$$

Photocurrent J_{ph} and dark current J_{Dark}, denoted by, display unique traits in MIS solar cells. The oxide's high transparency and wide band gap predominantly generate photocurrent within the neutral and depletion regions of the silicon. These two photocurrent components are notably affected by the incident photon wavelength

$$J_{ph} = J_{depletion} + J_{neural} \quad \text{(I.6)}$$

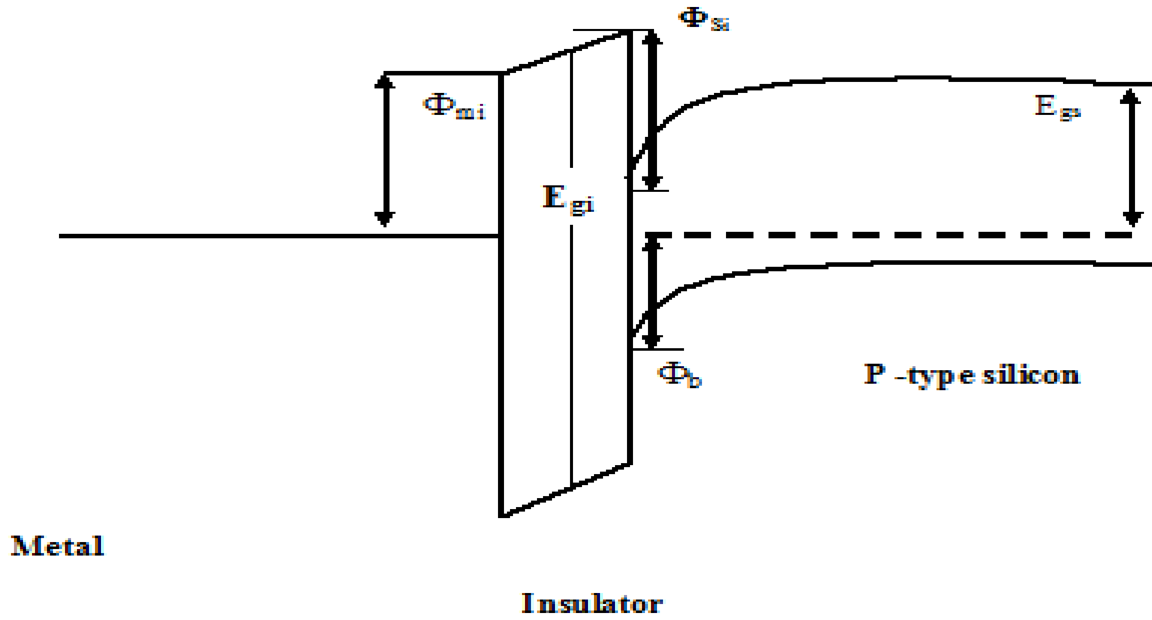

Figure I. 6: Simple equilibrium energy-band diagram of the p-type MIS solar cell.

The photocurrent in MIS solar cells is augmented by the migration of minority carriers as they tunnel across the oxide potential barrier, in addition to the previously mentioned currents. This illustrates the involvement of surface minority carriers in photocurrent generation. Consequently, the short-circuit current (I_{sc}) in MIS cells is similar to that in p-n junction cells. However, the fill factor (FF) and open-circuit voltage (V_{oc}) are greatly influenced by the saturation current density, denoted as J_0 [29], and the total dark current is defined as such.

$$J_{Dark} = J_{th} + J_{rg} + J_d + J_{ST} \quad \text{(I. 7)}$$

Where J_{th} varies from the thermionic emission of electrons into the metal, J_{rg} is the depletion layer recombination-generation current density, J_d and signifies the injection-diffusion current density, J_{ST} a net current flow towards the metal from surface states localized at the interface between the semiconductor and insulator.

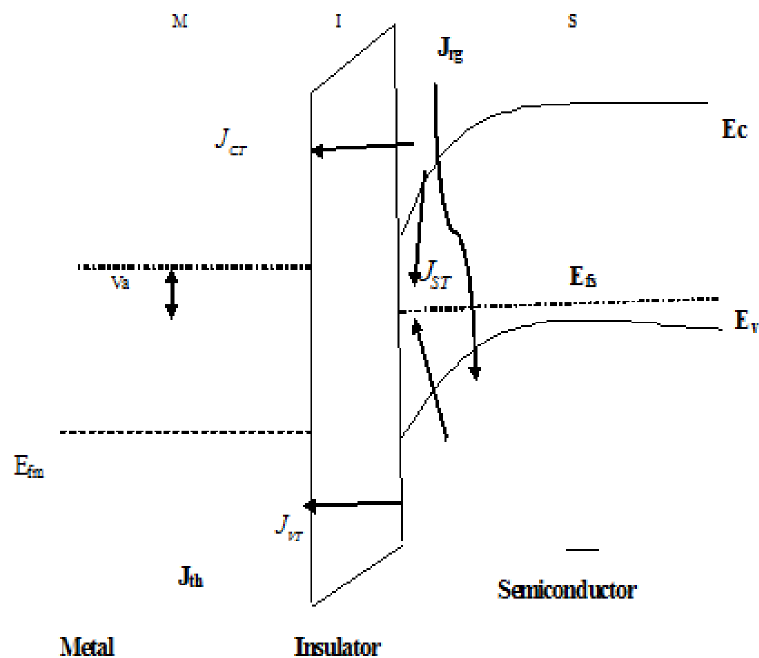

Figure I. 7: Possible charge transport mechanisms for a MIS tunnel diode under forward bias

When a device is biased, two types of tunneling currents can flow from the semiconductor to the metal: conduction band tunneling current and valence band tunneling current. These currents are caused by electrons tunneling from the conduction band or valence band of the semiconductor to states in the metal [28].These currents represent the effective movement of charges between the semiconductor's conduction and valence bands, resulting from recombination-generation processes in the corresponding states [21].

In conclusion, the thermionic emission current is minimal based on the temperature dependency of the current in minority carrier MIS devices. Thermionic emission, depletion layer recombination-generation, injection-diffusion, net current from surface states, and tunneling currents are only a few of the mechanisms that can affect the current density in MIS devices. Depending on the operating circumstances, temperature, and other contributing variables, these processes' contributions vary in magnitude.

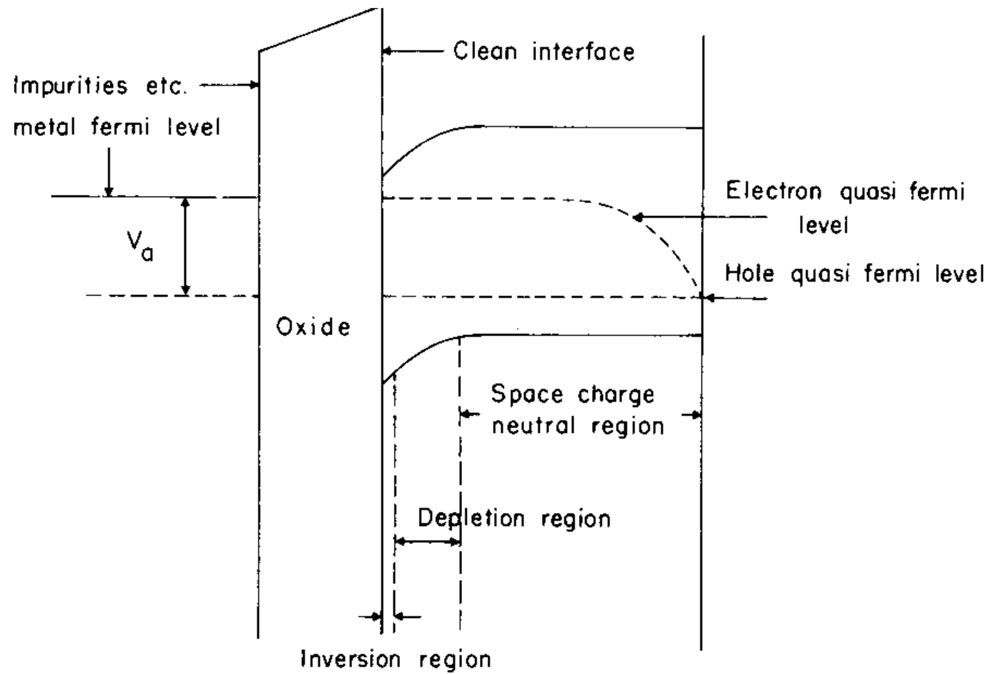

Figure I. 8: Illustration of Energy Band Diagram for MIS solar cells System with P-Type Semiconductor Region. V_a applied Under zero illuminations [14].

5- The Influence of Insulators on Energy Band Diagrams.

A comprehensive grasp of how insulators impact (MIS) structures is paramount for the progression of MIS diode technology, as it significantly shapes numerous system attributes. Therefore, a profound comprehension of these phenomena imperative for the successful advancement of MIS diodes

5.1. Charge Carrier Fluxes:

Because insulators possess significantly wider band gaps compared to semiconductors, this leads to the formation of a barrier that restricts the movement of electrons and holes between the semiconductor and the metal. Consequently, Charge carriers frequently rely on tunneling events to facilitate their passage. The subsequent equations are applicable for estimating the probability of both electrons and holes undergoing this tunneling transition.

$$T_n \approx \exp(-\alpha_t d \sqrt{\phi_n}) \tag{I-8}$$

$$T_p \approx \exp(-\alpha_t d \sqrt{\phi_p}) \quad \text{(I-9)}$$

The tunneling probability for electrons and holes denoted as T_n and T_p respectively, can be described using the given equations. Here, $\propto_t$represents a constant that relies on the effective mass of electrons in the insulator, d represents the thickness of the insulator, and ϕ_n and ϕ_p correspond to the energetic barriers encountered by electrons and holes respectively during tunneling, the tunneling probability is exponentially influenced by the thickness of the insulator, leading to significant variations in the flux of charge carriers across the interface between the semiconductor and metal.

5.2. Variations in Barrier Height:

The effect is caused by the presence of electronic states within the insulator; several semiconductor-insulator-metal systems have Demonstrated alterations in the barrier height, as opposed to the metal. Layer atop the insulating material in these systems, the junction barrier height is determined by the presence of mid-gap states in the material. The type of insulator used and the precise processing parameters used during deposition both factors will contribute to determining the extent to which the insulator impacts the barrier height. It is noteworthy that even little adjustments to the deposition procedure made by various research teams have resulted in significant variations in the characteristics of the material that has been created through synthesis.

5.3. Surface State Treatment

Apart from changing the flow of charge carriers and the barrier height, insulators have the capacity to passivate surface states that are present on the semiconductor surface, avoiding Fermi level pinning. Improvements in efficiency have been seen when insulating materials are utilized for surface state passivation.

6. Theory of MIS solar cells:

Based on the electrical behavior displayed by a sizable diode, the metal-insulator-semiconductor solar cell theory describes solar cells with these three components. A photovoltaic cell may produce electricity when it is illuminated, which causes the current-

voltage (I-V) curve to shift towards the fourth quadrant. Figure (I.9) in the referenced document shows how the size of this shift directly relates to how much light is incident on the solar cell's performance is frequently assessed by analyzing its current-voltage (I-V) curve, both under illumination and in the absence of light in order to determine important characteristics such as open circuit voltage (V_{oc}), short circuit current density (I_{SC}), and fill factor. The ratio of the maximum to the fill factor is used to calculate power output to the product of V_{oc} and I_{SC}, with V_m and I_m representing the voltage and current, respectively, at the point of maximum power output [30-31].

Analyzing these important parameters, such as the fill factor, along with studying the illuminated and dark current-voltage (I-V) curves, offers valuable insights into the behavior of solar cells. These examinations provide crucial information about the efficiency and performance of MIS solar cells, as well as aid in identifying the primary loss mechanisms within the solar cell.

$$FF = \frac{I_m V_m}{I_{sc} V_{oc}} = \frac{P_m}{I_{sc} V_{oc}} \quad \text{(I. 10)}$$

The fundamental theory governing the performance of commercially accessible silicon p-n junction solar cells should be mentioned for future reference. The current-voltage (I-V) relationship may be used to characterize these cells' properties, which can be summed up as follows.

$$I = I_0 \left(e^{\frac{qv}{nk_B T}} - 1 \right) - I_{sc} \quad \text{(I-11)}$$

In the provided equation, where I_0 represents the diode's leakage current in the absence of light or dark saturation current, V stands for the applied voltage across the diode's terminals, q denotes the elementary charge, k_B represents Boltzmann's constant, n signifies the ideality factor, and T indicates the temperature.

The I_{sc} value, representing the short-circuit current density, is determined by analyzing the I-V curve at zero voltage. Its magnitude is predominantly influenced by factors like the quantity of incident photons, spectral characteristics, solar cell area, optical traits, and the efficiency of collecting light-generated carriers.

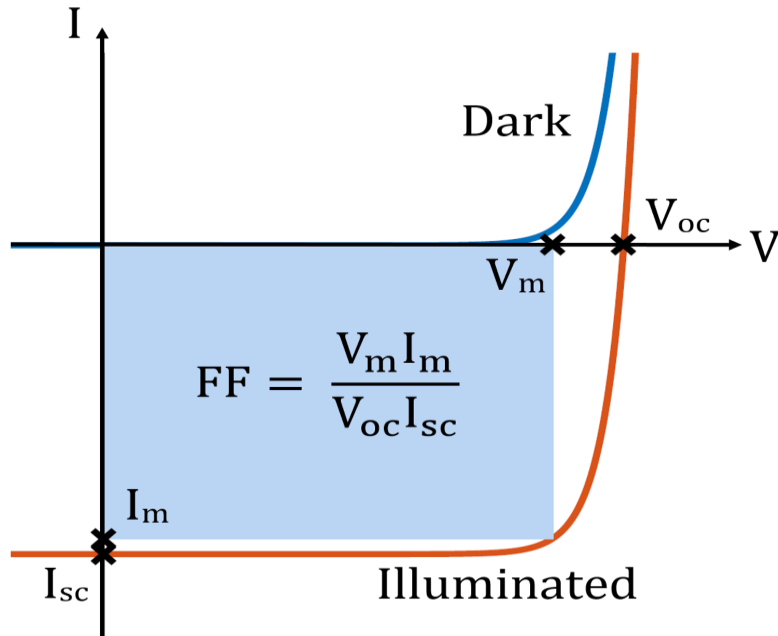

Figure I. 7: Voltage and current output from an illuminated Solar cell

Conversely, the V_{oc}, denoting the open circuit voltage, can be derived from equation (I.12) by equating I to zero, as determined from the I-V curve analysis.

$$V_{OC} = n\frac{kT}{I_0}\ln\left(\frac{I_{SC}}{I_0}+1\right) \tag{I. 12}$$

In the scenario where n equals 1, the saturation current I can be formulated in the following manner.

$$I_0 = Aqn_i^2\left[\frac{1}{N_A}\left(\frac{D_n}{\tau_n}\right)^{\frac{1}{2}}+\frac{1}{N_D}\left(\frac{D_p}{\tau_p}\right)^{\frac{1}{2}}\right] \tag{I. 13}$$

In an ideal junction with n equal to 1, the open circuit voltage (V_{oc}) achieves its peak value. Nevertheless, as n increases, the reverse saturation current (I_o) increase, leading to a decrease in V_{oc} Due to the logarithmic nature of the relationship described in equation (I.12),

V_{oc} exhibits effective saturation with respect to light intensity. The value of V_{oc} is directly linked to the semiconductor's band gap, while the dark current (I_o) The electrical properties of the material are primarily influenced by the band gap and temperature. i.e.

$$n_i^2 = N_C N_V \exp\left[-\frac{E_g}{KT}\right] \tag{I.14}$$

With a wider band gap or lower temperature, I_o decreases, and V_{oc} increases. In both short and open circuit states, power generation ceases, and the power output becomes zero if either or both conditions are met [32]. The device achieves maximum power output when both the voltage and current reach their respective maximum values.

$$P_{max} = I_{max} V_{max} \tag{I. 15}$$

A solar cell's power conversion efficiency (η) is determined by the ratio of the power output of the cell to the power input from the sun.

$$\eta = \frac{P_{max}}{P_{in}} \tag{I.16}$$

$$P_{max} = I_{sc} V_{oc} FF \tag{I.17}$$

7. Transport Models:

Three main regions must be taken into account when assessing carrier transport in a metal-insulator-semiconductor (MIS) device: the silicon semiconductor, the insulator, and the conductor. Each of these regions significantly contributes to facilitating the flow of carriers within the device.

Below are included the pertinent equations explaining the behavior of a minority carrier metal-insulator-semiconductor (MIS) tunnel diode, as well as the necessary changes made to the original program. For reference, Figure (I-8) also includes a copy of the band diagram showing the current components for the minority carrier MIS diode.

Diode current in the MIS tunnel is enabled by the process of tunneling through the dielectric barrier, leading to conduction and valence bands. The current is then carried farther in the silicon region by drift diffusion. It is noteworthy that the carriers that first tunnel into

the surface states in the silicon band gap gradually mixes back with the silicon bands before actively taking part in the drift-diffusion process.

7.1. Characterization of the semiconductor region.

Drift and diffusion processes, which may be efficiently represented by a set of five linked non-linear equations, control how carrier transport behaves inside the semiconductor area. Poisson's equation is employed to calculate the electrical potential, which is represented in these equations by the typical symbols for various physical variables.

$$\frac{dF}{dX} = \frac{q}{\varepsilon_S}\left(P - n + N_D^+ - N_A^-\right) \quad) \qquad \text{(I.8)}$$

here is a direct relationship between the electric field and the electrostatic potential.;

$$F = \frac{d\psi}{dX} \qquad \text{(I.19)}$$

The variables ND and NA represent the concentrations of donor and acceptor dopants, respectively, while n and p indicate the densities of electron and hole carriers. Additionally, q represents the charge of an electron.

$$\frac{1}{q}\left(\frac{dJ_n}{dX}\right) + G = U \qquad \text{(I.20)}$$

$$\frac{1}{q}\left(\frac{dJ_p}{dX}\right) - G = -U \qquad \text{(I.21)}$$

.

In this context, G represents the carrier generation rate, R signifies the recombination rate, and J_p and J_n stand for the current densities of holes and electrons, respectively.
In the case of a static problem, the continuity equations (I.20) and (I.21) can be simplified

$$J_n = q\mu_n nF + qD_n \frac{dn}{dX} \tag{I.22}$$

$$J_n = q\mu_p PF - qD_p \frac{dP}{dX} \tag{I.23}$$

The parameters μ_n and μ_p represent the mobility of electrons and holes, respectively, while D_n and D_p denote the diffusion coefficients of electrons and holes. Furthermore, U_n and Up stand for the recombination rates of electrons and holes. In the context of carrier generation, G is a function that describes the electron-hole generation rate, which includes both the external generation rate due to incident light and additional factors

$$G = \int_0^{\lambda_C} [1 - R(\lambda)]\alpha(\lambda)N(\lambda)\exp[-\alpha(\lambda)x]d\lambda \tag{I.24}$$

Here $R(\lambda)$represents the reflection coefficient, $\alpha(\lambda)$signifies the absorption coefficient, $N(\lambda)$represents the number of photons per second per unit area, and, λ_C is the cutoff wavelength corresponding to the semiconductor's band gap energy.

7.2. Characterization of tunneling through the insulator:

MIS structures with ultrathin insulating layers exhibit intriguing properties due to direct tunneling currents between the metal and semiconductor. By taking into account the preservation of both energy and transverse momentum during tunneling transitions between these two materials, the equations governing the current flow between them can be defined as follows.

$$J = \frac{q}{2\pi^2 h} \int_{-\infty}^{\infty} dE(f_m - f_s) \int dse^{-n} \tag{I.25}$$

Where

$$n = \frac{2}{h}\int_{xa}^{xb}\left(p_{T_i}{}^2 - p_i{}^2\right)^{\frac{1}{2}} dx \qquad (I.26)$$

A two-band model was utilized to characterize the insulator, and its energy-momentum relationship is articulated as follows.

$$\frac{p_i^2}{2} m_{Ti} = [E - \phi_{CB}(x)][d + [E - \phi_{CB}(x)] / E_{gi}] \qquad (I.27)$$

Where $\phi_{CB}(x)$ the energy at the conduction band edge of the insulator is represented as Ec. Assuming a parabolic relationship between the transverse energy E_T, and the transverse momentum, P_T, for particles in all three regions of the device, the resulting expression for electron current flow between the metal and the semiconductor's conduction band is as follows

$$J_{CT} = 4\pi q \frac{m_{Ti}}{h^3} \int_0^{E_{max}} dE\left(f_m - f_s\right) \int_0^{\left(\frac{m_{Ts}}{m_{Ti}}\right)} dE_T e^{-n} \qquad (I.28)$$

Where

$$n = \frac{2}{h}(2m_{Ti})^{\frac{1}{2}} \int_{xa}^{xb} \left(E_T - (E - \phi_{CB}) \times [1 + (E - \phi_{CB}) / E_{gi}]\right)^{1/2} dx \qquad (I.29)$$

If we take the semiconductor band edge as the energy reference point, a similar relationship can be applied to the current density between the metal and the valence band of the semiconductor.

7.3. Interface States

Insulators can function as passivation layers on the semiconductor surface, Apart from altering the movement of charge carriers and the barrier height; it also helps prevent Fermi

level pinning. Current flow channels can be expanded via insulator-based surface passivation employing insulating materials. Several processes, The current flow within the metal-insulator-semiconductor (MIS) structure is influenced by various mechanisms, including generation/recombination between the conduction band and surface states (J_{RC}), tunneling between the metal and surface states (J_{TS}), and generation/recombination between the valence band and surface states (J_{RV}).. Determining the surface states' Fermi level, which in turn controls their occupancy (f_{ss}), is necessary to provide a tunneling current to the interface states, as shown in the supplied equation, a time constant indicating the rate of charge collection and release within the surface states also affects the current flow in this situation.

$$J_{TS} = \int_{E_c}^{E_v} qN_{ss}(f_{ss} - f_m)T_q \frac{1}{\tau} dE \quad \text{(I-30)}$$

The density of surface states, denoted as N_{ss}, plays a crucial role in this context. The occupancy of these surface states is determined by balancing the tunneling current into the surface states with the recombination/generation current taking place at the interface

$$J_{TS} = J_{RC} + J_{RV} . \quad \text{(I-31)}$$

.Furthermore, to accurately model the drift-diffusion current within the substrate, it's crucial to incorporate the additional recombination current components. Hence, the boundary conditions at the semiconductor/insulator interface play a vital role in addressing these effects.

$$J_n = J_{TC} + J_{RC} \quad \text{(I-32)}$$

$$J_P = J_{TV} + J_{RV} \quad \text{(I-33)}$$

8. Conclusion

This chapter delves into the significance of MIS interfaces in generating photovoltage in specific semiconductors. Metal-insulator-semiconductor (MIS) solar cells have garnered significant attention for their potential in cost-effective photovoltaic solar energy conversion, particularly when compared to p-n junction solar cells. They offer ease of fabrication and cost advantages on a larger scale. The introduction of an insulating layer between the metal and semiconductor has demonstrated improved performance for these solar cells. Over the past few decades, MIS solar cell development has seen notable advancements, including the adoption of high-k oxides as substitutes for SiO_2.

References

[1]-Hsin-Yu Lee, Yi-Shian Max Lin, Kuang-Yang Kuo, Tzu-Yueh Chang, and Po-Tsung Lee, "Post-annealing Temperature Effect on the Optical and Electrical Properties of the Nano-structured Si/SiO2 Multilayer", ISSCT'08, Taipei, Taiwan(2008)

[2]- Sebastian Z. Oener, Jorik van de Groep, Bart Macco, Paula C. P. Bronsveld, W.M. M. Kessels, Albert Polman, Erik C. Garnett' Metal-Insulator-Semiconductor Nanowire Network Solar Cells' ECN Solar Energy

[3]-Orak I, Toprak M, Türüt A,' Illumination Impact on the Electrical Characterizations of an Al/Azure A/p-Si Heterojunction' Phys. Scr. 89(115810) 1-5(2014)

[4]-Rajesh KR, Menon CS, Study on the Device Characteristics of FEPC and FEPCCl''organic thin film Schottky diodes: influence of oxygen and post deposition annealing'. Journal of Non- Crystalline Solids 353(4): 398-404. (2007)

[5]- Öner, S.Z. Metal-insulator-semiconductor nanowire network solar cells Metal-insulator-semiconductor (MIS) University of Amsterdam (2020).

[6]-E. H. Rhoderick and A. Rothwarf, "Metal–Semiconductor Contacts," Physics Today, vol. 32, no. 5, pp. 66–71, (1979)

[7]-RH Cox and H Strack. Ohmic contacts for GaAs devices. Solid-State Electronics, 10(12), pp. 1213–1218, 1967

[8]-V. Heine. "Theory of Surface States" Physical Review, 138(6A):A1689 A1696, (1965).

[9]-Rehan Younas Computational Analysis of Tunnel Oxide Passivated Contact Solar Cells (TOPCON) University of Management Sciences (LUMS) (2018)

[10]- Srikanth Yanamana gandla 'Synthesis and Characterization of Schottky Diodes on n-Type CdTe Nanowires Embedded In Porous Aluminate plates'University of Kentucky (2008).

[11]-J. Plá, E. Centurioni, C. Summonte, R. Rizzoli, A. Migliori, A. Desalvo, and F. Zignani, "Homojunction and heterojunction silicon solar cells deposited by low temperature–high frequency plasma enhanced chemical vapour deposition", Thin Solid Films, vol. 405, pp. 248, (2002)

[12]-Srikanth Yanamana gandla Synthesis and Characterization of Schottky Diode On n-Type Cadmium (CdTe) Nanowires Embedded In Porous Alumina University of Kentucky (2008)

[13]-Zhores I.Alferov, V.M.Andreev, M. B. Kagan, I. I. Protasov, and V. G. Trofim,Fiz. Tekh.Poluprovodn, Vol.4, pp 2378 (1970)

[14]- Shewchun J, Singh R, Green MA, Theory of metal-insulator-semiconductor solar cells, J Appl Phys 48(2):765–770, (1977).

[15]- VexleraMI, Tyaginova SE, Yu B, Illarionova Y, Singd YK, Shenp AD, Fedorova VV, Isakov DV Physics of Semiconductor devices 47(5):686–694 (2013).

[16] R. Singh, \Growth of thin thermal silicon dioxide _lms with low defect density," Microelectronics Journal, vol. 23, no. 4, pp. 273 281, (1992)

[17] M. Green, E. Gusev, R. Degraeve, and E. Garfunkel, \Ultrathin (< 4 nm) SiO2 and Si-O-N gate dielectric layers for silicon microelectronics: Understanding the processing, structure, and physical and electrical limits," Journal of Applied Physics, vol. 90, no. 5, pp. 2057{2121, (2001)

[18]**-** Rachmat Mulyadi, drs The Preparation And Properties Of ITO/TIN/Silicon Solar Cells 1989

[19]-Islam R, Saraswat KC (2014) In 2014 IEEE 40th photovoltaic specialist conference (PVSC)

[20]-Petrosyants KO, Popov DA (2015)2nd international conference on modeling, identification and control, Atlantis press

[21]**-**Michael Greer, A 6% Efficient MIS Particulate Silicon Solar Cell Oregon State University (1998)

[22]- R. Van Overstraeten, R. Mertens, Optimisation Of New Types Of MIS Silicon Solar Cells, EC Solar Energy R&D Program Project C - Photovoltaic Conversion, 1982, Leuven - Heverlee (Belgium).

[23]-M.A.Green, F. D. King and J. Shewchun, Minority Carrier MIS Tunnel Diode and Their Application to Electron and Photo-Voltage Energy Conversion -1 Theory(1973)1.973-State l

[24]-H.J:Hovel, "Solar Cells Semiconductors and Semimetals", Vol. 11 Academic Pres(1975)t

[25]- M. A. Green and J. Shewchun Current Multiplication In Metal –Insulator - Semiconductor (MIS) Tunnel Diodes. Solid-State Electronics, **Vol.** 17. pp. 349-365(1974)

[26]-D. L. Pulfrey, .MIS Solar Cells: A Review," IEEE Transactions on Electron Devices, vol. 25, no. 11, pp. 13081317, Nov 1978

[27]-M. Green, F. King, and J. Shewchun: Minority carrier MIS Tunnel Diodes And Their Application to Electron-And Photo-voltaic Conversion I.Theory ,"Solid-State Electronics, vol. 17, no. 6, pp. 551561, (1974)

[28]-O.M. Nielsen, Current Mechanism of Tunnel M.I.S, solar cells, IEEE.PROC, Vol. 127,Pt.I, No. 6, December (1980)

[29]- ChanchaiVithsupalert B.E., Theory Of Metal-Insulator-Semiconductor (MIS) Solar Cells, Thesis (1977), University of New South Wales.

[30]- S. M. Sze and K. K. Ng, Physics of Semiconductor Devices. John Wiley &Sons, (2006)
[31]- F.A. Lindholm, J.G. Fossum, E.L. Burgess, Application of the superposition principle to solar-cell analysis, IEEE Trans. Electron Devices. 26 (1979) 165–171.doi:10.1109/T-ED.19400
[32]-S.S. Li,' Semiconductor Physical Electronics', Springer US, Boston, MA, (1993) doi:10.1007/978-1-4613-0489-0. (1979)

[33]-H. Ullah, B. Marí, H.N. Cui,'Investigation on the Effect of Gallium on the Efficiency of CIGS Solar Cells through Dedicated Software', Appl. Mech. Mater. 448–453 1497–1501. doi:10.4028/www.scientific.net/AMM.448-453.1497. (2013)

Chapter II

THE PROPERTIES OF THE MAIN MATERIALS

1. Introduction

MIS (Metal-Insulator-Semiconductor) solar cells, which are based on c-Si wafer technology, have become an integral part of modern technology, finding diverse applications in electronics, optoelectronics, and bioelectronics. This thesis aims to develop a silicon MIS solar cell model by incorporating different materials. Crystalline silicon (c-Si) and p-type amorphous silicon (a-Si:H) can be used as absorber materials, and various high-k oxides are used in the contact zones. The research conducted in this thesis focuses on the dielectric films SiO_2, HfO_2, Si_3N_4, Al_2O_3, TiO_2, and Ta_2O_5, with particular attention given to understanding their distinctive features. The following sections provide in-depth explanations of these materials.

2. Material properties

Solar energy conversion depends heavily on photovoltaic materials; these materials are recognized for their capability to convert photons into electrons via the photovoltaic (PV) effect, with the photovoltaic material situated within the absorbing layer, where it facilitates the conversion of light into electrical energy. Although many semiconductor materials exhibit this effect, only a select few are commercially viable due to limitations such as minimizing thickness and being widely accessible [4]. There are numerous photovoltaic materials in use today, and many more are being researched and developed for future use thanks to intensive research.

The main materials used for the absorbing layer in the current standard PV solar cell technology pose a significant problem due to their highly recombinative metal contact. To enhance the performance of single-junction silicon cells, this idea suggests employing semiconductor (MIS) structures comprised of both (c-Si) and (a-Si: H) materials as selective carrier contacts. The composition of this layer, whether single or multilayered, is determined by the specific material being used and the required application requirements. New strategies have been developed that use so-called "passivating contacts."

Optimizing the functionality and stability of metal oxide semiconductor device requires adding an insulator layer between the metal and semiconductor contacts. As a result, there has been an increased interest in studying the electrical properties of metal oxides, especially high-k gate dielectric materials including Al_2O_3, HfO_2, Ta_2O_5, and TiO_2. These materials have garnered considerable attention due to their potential to replace SiO_2 in gate applications,

creating a crucial insulating layer between the metal and semiconductor interface. High-k materials are highly attractive for improving device performance and reliability because they offer advantages such as higher capacitance and lower leakage current.

2.1. Crystalline silicon (c-Si):

Currently, large wafer-fabricated crystalline silicon modules, which include both large-grain polycrystalline and single-crystalline silicon, are the mainstay of the photovoltaic (PV) module production industry. These modules have become very popular due to their improved conversion efficiency, but their large physical dimensions, expensive price, and high processing temperature remain as limitations. They are also known as conventional solar cells, and in 2009 they accounted for around 85% of the market [5]. Compared to other solar cells made of different materials, these devices have the advantage of high charge carrier mobility and a longer lifespan.

Because of its special properties, including its semiconductor nature, silicon is a preferred element for use in electrical devices crystalline silicon (c-Si) possesses a highly organized and uniform lattice structure throughout the material. Additionally, silicon, the Earth's most plentiful element in the crust, is non-toxic, which further contributes to its uniform electrical and optical properties throughout the material [6].

Silicon is not highly reactive, but it is more reactive than germanium. The band gap of crystalline silicon (c-Si) is approximately 1.12 eV at 25°C, making it more suitable for operation at higher temperatures. The electron affinity of silicon is approximately 4.05 eV. Silicon is categorized as an indirect semiconductor, featuring tetravalent silicon atoms covalently bonded in a lattice structure resembling that of a diamond. This ordered lattice structure improves the efficiency of converting light into electricity. The band gap of silicon closely matches the peak of the sun's spectral irradiance on Earth, making silicon an excellent candidate for light absorption; crystalline silicon (c-Si) typically necessitates relatively thick wafers, typically in the range of 200-300 μm. Furthermore, it can be readily doped by incorporating foreign atoms into its structure.

A major disadvantage of crystalline silicon solar cells is the fundamental instability of the crystalline structure at the surface, which causes the formation of many defects. These defects contribute to a high surface recombination rate, which results in significant charge carrier losses the manufacturing of these solar cells involves the formation of a p-n junction,

starting with a crystalline silicon wafer that has been p-doped (or n-doped), and then adding an n-doped (or p-doped) layer using high-temperature diffusion of the doping material, typically at around 1000°C. However, this time-consuming and expensive method has led to continuous research into alternative technologies. Although the exact date of silicon's discovery is unknown, it is known that pure silicon was first synthesized and described in 1823 (Seitz & Einspruch, 1998) [7].

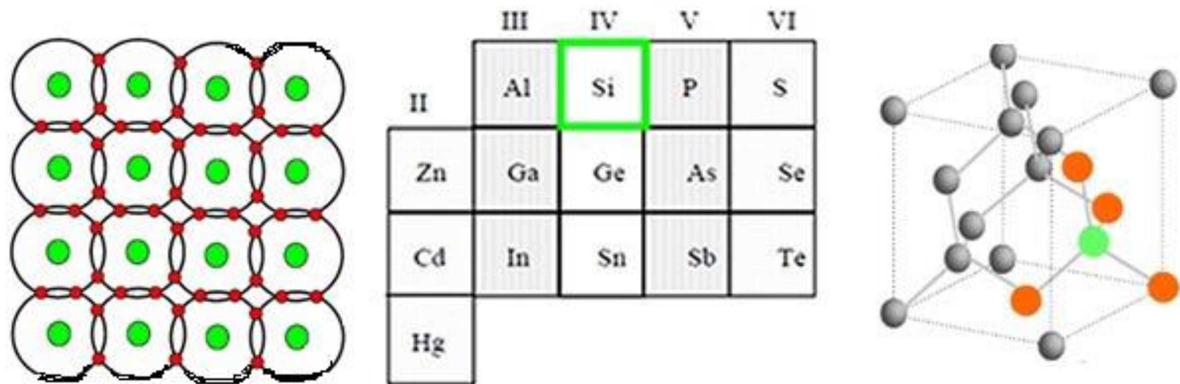

Figure II. 1: a) Si atomic configuration, b) position in periodic table and c) physical structure [12].

2.2. Thin-film solar cells:

Thin-film solar cells are commonly referred to as second-generation PV devices, constitute a smaller yet swiftly expanding sector within the PV industry. They held around 15% of the market share by 2009. Single-junction thin-film devices have the same Shockley-Queisser performance limit as traditional silicon devices; however, they can be manufactured at significantly reduced expenses [8- 9].

The primary benefit of thin-film solar cells lies in their cost-effectiveness during production. Which is achieved by using thin layers of semiconductor material instead of silicon wafers. The market is currently seeing a slow but steady influx of thin-film solar cells made of Si films, including amorphous silicon (a-Si), microcrystalline silicon (μc-Si), polycrystalline silicon, their mixtures, CdTe, and Cu(In,Ga)Se(2) (CIGS). The type of material used depends on the specific application field. The main topic of The focus of this research is on hydrogenated amorphous silicon (a-Si:H), which has become essential in thin-film solar technologies due to its cost-effectiveness resulting from minimal material usage and low-temperature production methods. This research also prioritizes the investigation of thin-layer dielectrics, particularly oxide materials.

2.2.1. Hydrogenated amorphous silicon:

In the 1970s, two scientists from Dundee University, Walter Spear and Peter Le Comber, were the first to demonstrate the semiconducting properties of amorphous silicon. They showed that amorphous silicon could be doped with a pentavalent and trivalent atom to create a p-i-n junction just like crystalline silicon. Si atom placement in amorphous silicon (a-Si) lacks long-range organization, resulting in random clumping and the absence of a clear atomic location pattern [10]. consequently, amorphous silicon (a-Si) has a high density of defects and undesired features, which makes it more difficult to determine its optical and electrical properties. However, the inclusion of hydrogen markedly improves the semiconductor's characteristics. Figure 2 shows a schematic representation of hydrogenated amorphous silicon, also known as a-Si:H, which is a material that is ideal for many different uses [11].

Amorphous silicon (a-Si) has a larger band gap than crystalline silicon (c-Si), with an EG of 1.7 eV. This has advantages for passivating contacts and produces a high absorption coefficient (>10^5 cm-^{1}) for photons with energies between 1.6 and 1.8 eV, which are above the band gap [9- 12]. In experimental conditions, hydrogenated amorphous silicon (a-Si:H) can be deposited to achieve thicknesses up to 100 times thinner than crystalline silicon for very thin films [6].

Besides its use in solar cells, a-Si finds extensive applications in thin-film transistors, color sensors, and flat-panel display scanners. Its widespread adoption in these applications is attributed to its remarkable versatility, While various high-throughput techniques allow deposition at low temperatures between 150°C to 350°C, it's important to note that hydrogenated amorphous silicon (a-Si:H), particularly in doped forms, exhibits a relatively short minority-carrier lifetime, necessitating the use of an electric field [7].

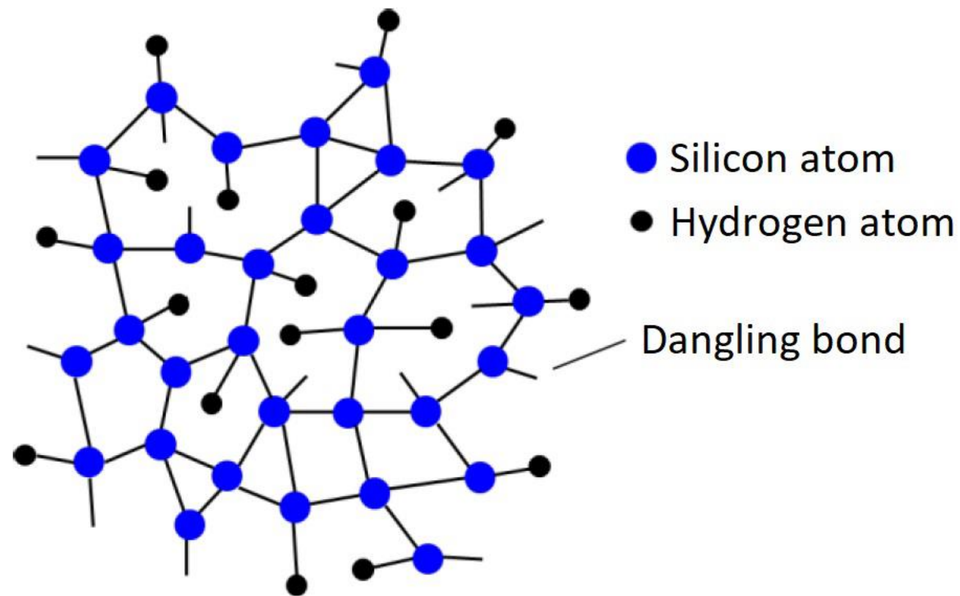

Figure II. 2: Spatial Configuration of Hydrogenated Undoped Amorphous Silicon (a-Si:H) Illustrated with Atom Arrangement and Chemical Bonds. Blue and black dots correspond to silicon and hydrogen atoms, respectively. Chemical bonds are shown as black lines, open ends correspond to dangling bonds [12]

2.2.2. Thin layers of dielectric materials

Many devices incorporate thin layers, and the materials chosen depend on the intended application. This particular work focuses on thin dielectric layers, specifically oxides [13]. In optics and optoelectronics, dielectric films are utilized to achieve a well-defined optical response, aiming for a specific reflection or transmission factor over a range of wavelengths [14]. The electrical properties of the dielectrics used in Metal/Insulation/sc (MIS) structures are critical for the targeted new applications. This section presents the dielectrics based on their permittivity range, including low-k, high-k, and very high-k, as well as the primary physical and electrical characteristics of these materials.

3. The different categories of dielectrics:

This non-exhaustive list of materials gives some examples of dielectrics used, studied, anticipated or innovative, some of which will be the subject of further studies thorough. A classification according to the permittivity range is proposed:

-« Medium-k » ($10 \leq k \leq 15$)

-«High-k » ($15 \leq k \leq 100$

-« very High-k » ($k \geq 100$)

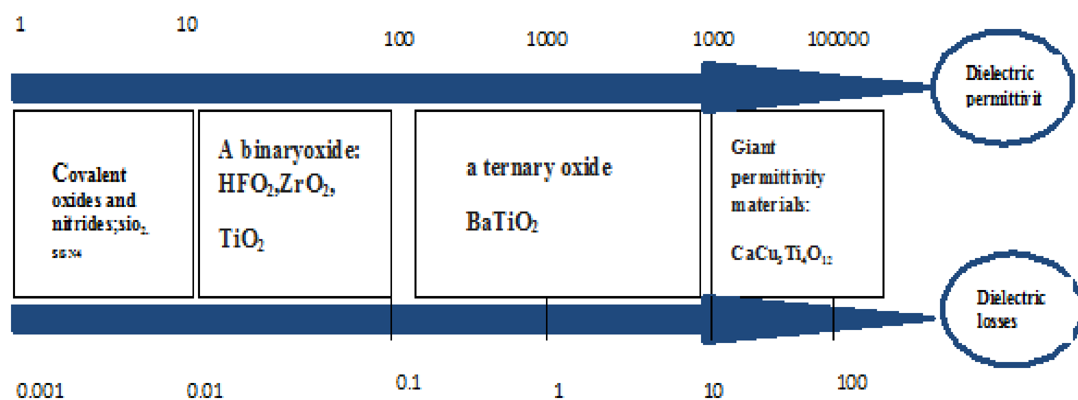

Figure II. 3: Classification of dielectric materials according to their permittivity, the evolution of the dielectric losses is also represented.

One might initially suppose that oxides with the highest possible permittivity, or "very high-k" oxides, would be the most appropriate. However, the choice of material is not that easy since the barrier height decreases as the dielectric constant increases. Thus, a balance must be struck between the dielectric constant and the band gap, which imposes constraints on the utilization of materials possessing extremely high permittivity. Barrier heights hold significant importance as they influence the effective energy levels for electrons in the conduction band and holes in the valence band, thereby guiding the selection of materials with high dielectric constants (high-k).These high-k materials provide increased capacitance and lower leakage current. However, It's worth emphasizing that in numerous high-k materials, a higher dielectric constant is accompanied by a narrower band gap, typically around 5-6 eV. As a result, a desired range for permittivity is typically between (25-30) to achieve a suitable balance of electrical properties.

3.1. High-k

In practice, materials with high permittivity, called "high-k" (in English), These materials play a pivotal role across a diverse array of applications, serving as interfaces in metal/insulator/semiconductor structures (MIS) to replace SiO2 in a variety of electronic devices, such as field-effect transistors, capacitors, and memory storage applications. [16-17-18]. the utilization of high-k materials has played a important role in advancing the development of MIS-type solar cells. The emergence of nanostructures has created further opportunities for these systems to exhibit novel physical phenomena and subsequent utilization in developing possible novel devices Advancements in high-k material development. has opened up new possibilities for the design and fabrication of electronic devices. [19] High-k dielectrics are materials with a significantly higher dielectric constant than silicon dioxide, which is commonly employed as a gate dielectric. The utilization of high-k gate dielectrics is a key strategy designed to facilitate the ongoing miniaturization of microelectronic components [20]. Figure II.4 The study illustrates how the utilization of high-k dielectrics effectively reduces leakage tunneling current in MIS structures while simultaneously preserving the same capacitance.

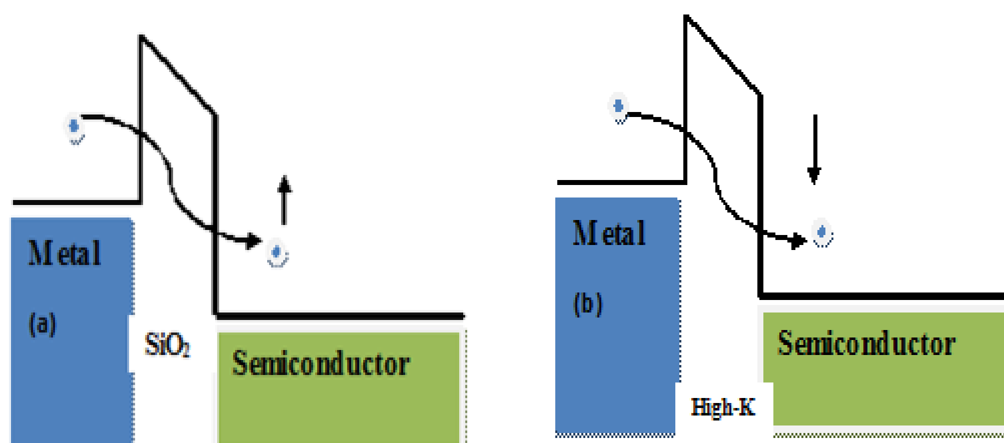

Figure II. 4: band diagramSiO$_2$ (a) is substituted by a high-k dielectric with a same capacitance using a larger thickness which leads to a reduction to a leakage current

Yet replacing SiO$_2$, which has amazing qualities including few electrical flaws, great interface characteristics, high thermal stability, and a considerable band offset, is difficult and

results in the loss of a number of useful features, as the dielectric constant increases, these properties are lost. The goal, therefore, is to find a replacement material that minimizes leakage currents, physically thicker and with a high permittivity, of type "high-k" [21].

Material	Dielectric(K)	Band Gap(EG)	(ΔEc) To Si
SiO_2	3.9	8.9	3.2
Si_3N_4	7	5.1	2
Al_2O_3	9	8.7	2.8
Y_2O_3	15	5.6	2.3
La_2O_3	30	4.3	2.3
Ta_2O_5	26	4.5	1-1.5
TiO_2	80	3.5	1.2
HfO_2	25	5.7	1.5
ZrO_2	25	7.8	1.4

Table II. 1: Comparison of relevant properties of high-K dielectrics. [25]

The following conditions must be met for a SiO_2 replacement to be effective in the semiconductor manufacturing process:

- Because of its elevated dielectric constant, (K value), it should be commercially viable at various scaling nodes.

- In case where the oxide directly interfaces with the Si channel, it must have thermodynamic stability.

-It must have band offsets with Si that are more than 1 eV to decrease the introduction of carriers. into its own energy bands, and operate as an effective insulator.

-The substance must be kinetically stable, allowing for processing at 1000 °C for 5 seconds (in a gate-first flow).

-In order to provide dependable charge transmission, it should create a strong electrical interaction with Si; the content must have at least [22-23-24].

The replacement material must meet several criteria, including a high K value for economic use, thermodynamic stability with the Si channel, this material functions as an insulator, boasting band offsets of over 1 eV when in contact with Si. It showcases kinetic stability, establishes a positive electrical interface with Si, and displays a low presence of electrically active defects. While several high-k materials, including Al_2O_3, HfO_2, Si_3N_4, Ta_2O_5, and TiO_2, are suitable for gate oxide, they each present some challenges. For example, these films, produced through Atomic Layer Deposition (ALD), exhibit dielectric constants spanning from 3.9 to 300. Table 1.2 presents an overview of the key high-k candidates and their corresponding characteristics [25].

chemical formula	SiO2	Si_3N_4	Al2O3	HfO2	Ta_2O_5	TiO_2
Molar mass	60.08g/mol	140.28g/mol	101.96g/ mol	210.49g/mol	441.893g/mol	79.866g/mol
Density	4.23g/cm3	3.17 g/cm3	3.95g/cm 3	9.68g/cm3	8.2g/cm3	79.866g/mol
Fusion point	1600^0C	1,900 °C	2072^0C	2758^0C	1,872 °C	1843^0C
Boiling point	2230^0C	1900 °C,	2977°C	5400^0C	29720C	2972^0C
Refractive index:	n=1.4655(λ=1.6.µm	*n* = 2.4631	n=1.6216 (λ=1.54µ m)	n=2.0711 (λ=1.54µm	n=2.4335 (λ=1.53.µm	2.4335 (λ=1.53.µm)
Extinction coefficient	(k=0.0001)	*k* = 0.000030	(k=0.0000	(k=0.0000)	k=0.0001	k=0.0001)
Relative dielectric constant	3.9	7	9.5	25	26	80
Gap	9eV	5.1	8.8eV	5.8eV	4.5 eV	3.5 eV

Table II. 2: Main electrical properties of dielectric materials

4. Properties of available dielectrics' Oxides used in the simulation':

4.1. Silicon Oxide:

Silicon oxide (SiO_2), with a relative permittivity of 3.9, was the first material to be integrated into silicon technologies. It has good thermal and chemical stability, and a wide forbidden band (Eg) of around 9 eV, making it a good insulator. Due to these qualities, it has been used in MIS solar cells for a long time. Later, silicon nitride (Si_3N_4) replaced SiO_2 as it made it possible to achieve higher capacitance values. This dielectric has a relative permittivity that varies between 6 and 8, depending on the deposition mode, interface with the lower electrode, and oxygen level in the film. This enables capacitance densities up to 2 nF/mm² to be achieved; its band gap of 5.1 eV, lower than that of SiO_2, still allows for reduced leakage currents [26].

4.1. Silicon nitride Si3N4:

Silicon nitride (Si_3N_4) is known for its excellent mechanical properties in both room and elevated temperatures, making it a promising material for high-temperature structural applications. A specific Si_3N_4 material designed for radome applications exhibits a higher dielectric constant of 7.9, unlike commercially available SiO_2 with an average particle size of 1-5 µm.

To address concerns about high leakage currents and boron infiltration, alternative gate dielectric configurations Examples include oxy-nitrides and stacks consisting of oxides and nitrides. have been developed as interim substitutes. These configurations have a somewhat elevated dielectric constant (K value) than SiO_2, which helps to reduce leakage due to their slightly thicker physical layers [26].

4.2. Tantalum oxide (Ta_2O_5):

Having a band gap of 4.4 eV and interesting structural and functional properties, Ta2O5 is a promising a material with a wide band gap that can be utilized. in a variety of applications. Its dielectric constant energy (DEC) values range from 1-1,5 eV, with dielectric constants between 10 and 80. Due to its well-established maturity, Ta_2O_5 has primarily been used in memory capacitor applications [27].

Amorphous Ta_2O_5 films typically have poor current leakage protection due to organic contaminants or oxygen vacancies, resulting in the Frenkel-Pool effect. As a result, crystalline films are often preferred for gate oxide applications. Despite having a wide band gap of

around 4.0 eV at ambient temperature, amorphous Ta_2O_5 can act as a photocatalyst. However, the high permittivity of Ta_2O_5 and Si is limited by interfacial interactions. Ta_2O_5 is less common for submicron MOSFET devices because of its low thermal stability with Si and short electron band offset. However, the density of fixed charges and leakage current, the density of fixed charges and leakage current, the density of fixed charges and leakage current, can be effectively reduced [27- 28].

4.3. Aluminum oxide or alumina Al_2O_3:

The incorporation of aluminum oxide (Al_2O_3) into the PV industry has been a major advancement in this field [27]. This dielectric material exhibits fundamentally different properties from conventional surface passivation materials. Notably, the Al_2O_3 the layer possesses a significant concentration of inherent negative charge [28].

In microelectronic fabrication, Al_2O_3 is one of the most common dielectrics is a popular choice for dielectrics because of its significant band gap of approximately 8.8 eV and its relatively high dielectric constant of about 9. In the photovoltaic community, Al_2O_3 has attracted significant interest for its effective surface passivation capabilities, which lead to improved efficiency. Ultra-thin layers of the deposition of Al_2O_3 on photo anodes employed in dye-sensitized solar cells efficiently inhibits rear recombination between electrons and the photo anodes, resulting in an enhanced overall cell efficiency [29]. the refractive index of Al_2O_3 thin films, approximately 1.6 at a wavelength of 630 nm, indicates its suitability for anti-reflection applications in c-Si solar cells. Alumina (Al_2O_3) has a ΔE_C range of 2.3-2.8 eV, this material, extensively researched for numerous applications, and is known for its exceptional stability and durability.

Al_2O_3 offers several advantages, as outlined in Table (II.1), notably its outstanding thermal stability and efficiency as a diffusion barrier [26]. It serves to inhibit atomic migration within stacked films, especially between semiconductor substrates and higher-k materials. Alumina (Al_2O_3) possesses advantageous traits like a high band gap, thermodynamic stability even at elevated temperatures on silicon, and amorphous properties in relevant conditions. However, it does fall within a specific range of dielectric constants despite its wide band gap.

Notably, Al_2O_3 has a refractive index close to 1.65, indicating that it does not absorb the visible spectrum, thus improving the optical qualities of both front and rear surfaces. Studies have confirmed that this dielectric is suitable for passivating both n-type and p-type silicon [32].

4.4. Hafniumb oxide HfO_2:

Hafnium oxide (HfO_2) and its silicate or aluminate derivatives have risen as prominent candidates for replacing traditional gate dielectrics in the upcoming years. Notably, HfO_2 has attracted significant attention within the photovoltaic community due to its effectiveness in surface passivation, leading to improved efficiency. Utilizing ultra-thin HfO_2 for the application layers on photo anodes in dye-sensitized solar cells effectively prevents rear recombination between electrons and the photo anodes, ultimately leading to enhanced cell efficiency.

HfO_2 stands out as a significant wide-band gap material due to its intriguing structural characteristics and a high permittivity (K = 22-25). Furthermore, when in contact with silicon, HfO_2 displays outstanding chemical and thermal stability, regarding its refractive index of HfO_2 thin films has been reported at n = 2.0711 (λ = 1.54 µm). Extensive research has been conducted on HfO_2 with a ΔEC value of 1.5 eV [33].

4.5. Titanium oxideTiO_2:

Titanium dioxide (TiO_2) has been a focal point of extensive research for its application in high-K memory capacitors and transistors. Its appeal lies in its elevated permittivity, depending on the crystal structure and deposition process employed; the value of K can range from 80 to 110. This heightened permittivity is a result of significant contributions from soft phonons linked to Ti ions, a feature distinct from other metal oxides.

Transistors utilizing (TiO_2) display nearly ideal characteristics but encounter mobility issues. The low-field effective mobility is approximately 160 cm for (TiO_2), This is significantly lower, by three orders of magnitude, compared to the mobility observed in (TiO_2)-based MOSFETs. The decrease in mobility is due to the existence of interface trap states and surface irregularities at the (TiO_2)/Si interface, with the electron traps in (TiO_2) being a result of oxygen vacancies. [34.35].

5. Optical properties of oxides used

The precise and accurate measurement of optical properties of materials, such as reflectance, transmittance, emittance, absorptance, and the index of refraction, is essential for the advancement of optical technology and its applications. Optical properties encompass

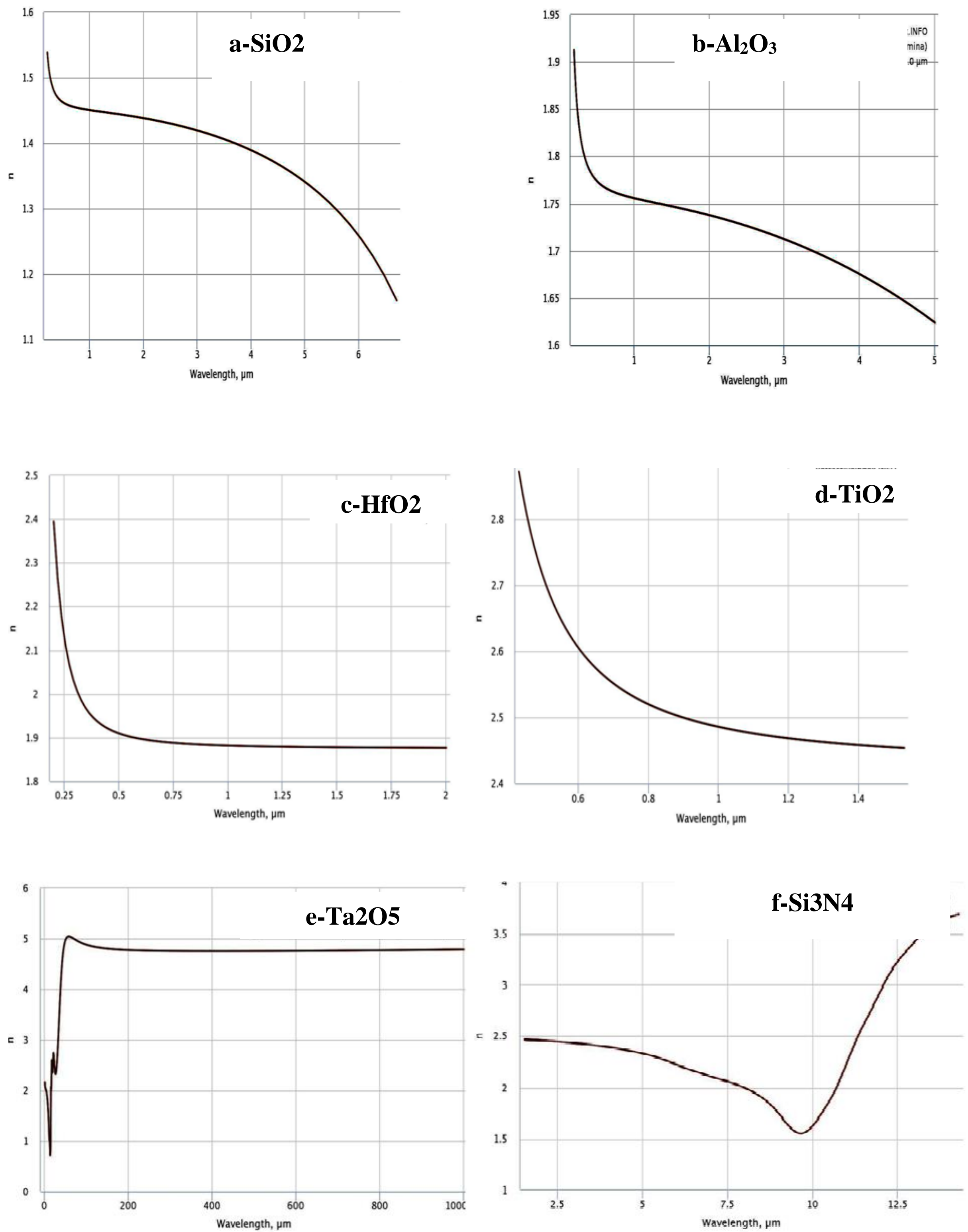

Figure II. 5: Refractive indices of oxides as a function of wavelength (a) SiO_2 (b): Al_2O_3 (c): HfO_2 (d): TiO_2 (e): Ta_2O_5 (f): Si_3N_4 [36]

-

The refractive index of a substance is determined by the ratio of the speed of light in a vacuum (C) to the speed of light in the material (V), as explained by this formula.

$$n = \frac{C}{V} \tag{II-1}$$

The speed of light within a material is not constant; it changes with wavelength. The following figure illustrates how the refractive indices of various oxides used in the simulation vary with wavelength.

The refractive index, often denoted as 'n' or 'n' in equations and texts, is a numerical value derived from the speed of light in a denser medium relative to its speed in a vacuum. This parameter plays a crucial role in calculating reflection coefficients and predicting transmission patterns through the Snell-Descartes relationship. Relation ship

$$n_1 \sin \theta_1 = n_2 \sin \theta_2 \tag{II-2}$$

When light transitions from one medium (n_1) to another (n_2) with a different refractive index, even if both mediums are transparent, some of the light scatters at their interface, $\theta 1$and θ_2 represent the angles formed between the incident angle and the refracted angle.

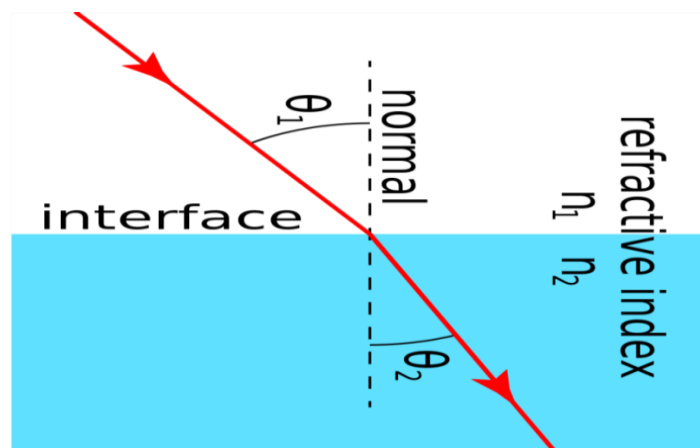

Figure II. 6: Reflected, transmitted and absorbed radiation [36]

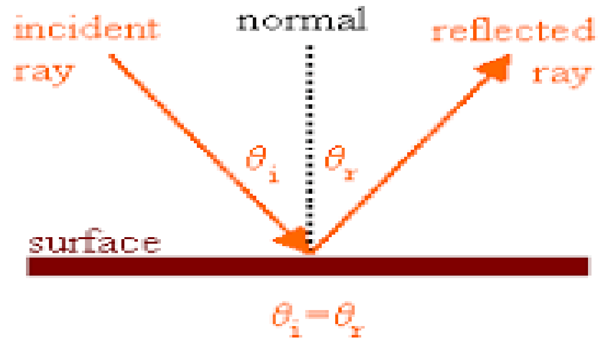

Figure II. 7: Law of reflection

The reflectivity (R) is defined as the fraction of the reflected light reflection I_R on the incident intensity I_i

$$R = \frac{I_R}{I_i}) \qquad \text{(II-3}$$

For normal incidence of light from air into a solid having an index of refraction (n):

$$R = \left(\frac{n_1 - n_2}{n_1 + n_2} \right)^2 \qquad \text{..(II-4)}$$

The transmission coefficient T The term "transmittance" refers to the ratio of the intensity of light or radiation that passes through a medium (It) to the initial intensity of the incident light (Ii).

$$T = \frac{I_T}{I_i} \qquad \text{(II-5)}$$

Ou

$$T = \frac{1 - R}{1 + R} \qquad \text{(II-6)}$$

The relative permittivity of a material or dielectric note explains the response of a material

To a

$$\varepsilon_r = \chi\varepsilon_0 . \quad \text{(II-7)}$$

With χ is the electrical susceptibility of the material and ε_0 is the vacuum permittivity

When the phenomenon of absorption takes place in a material, the refractive index has a complex component and is defined by:

$$\eta(\lambda) = n(\lambda) + ik(\lambda) \quad \text{(II-8)}$$

Where k is the attenuation coefficient also called extinction coefficient

6. Oxide Charges in Silicon Dioxide Thin Films

In general, the Si-SiO2 interface is characterized by four types of charges: fixed oxide charge (Qf), interface trapped charge (Qi), oxide trapped charge (Qot), and mobile oxide charge (Qm). This section provides an explanation of their sources and origins, along with a reference to the charge location diagram and energy band structure for the Si-SiO2 interface.

6.1. Fixed oxide charge (Q_f):

The fixed oxide charge, denoted as Qf, represents a concentration of immobile positive charges situated at or near the interface. Qf remains unaffected by voltage bias-induced c-Si surface band bending, as it is electrically isolated from the underlying silicon. Typically, it remains positive and unresponsive to changes in the Fermi level position [35]

6.2. Interface trapped charge (Q_i):

Interface trapped charge (Q_i) refers to the density of those traps located at the oxide-silicon interface ($Si\text{-}SiO_2$) and the density of charges trapped by those traps. Interface traps are also known as interface defects, interface states, or fast interface states, and they are caused by the existence of non-saturated silicon bonds (dangling bonds). By altering the silicon surface potential, these traps can be either charged or discharged, and they can directly exchange charges with the interface.

6.3. Ionic mobile charges:

Ionic mobile charges are due to the contamination of the oxide by ionic impurities (Metals alkalis: K+, Li+, Na+...). The mobile oxide charge (Qm) is caused by positively charged alkali ions, such as sodium (Na+), potassium (K+), and lithium (Li), Modifying the silicon surface potential has the capability to change the charge state of interface traps,

Sodium ions (Na+) hold paramount significance in Qm due to their prevalence in both the environment and the human body, making them the most abundant alkali ions, and it has the highest mobility in SiO2. Li and K, on the other hand, are considered less significant because they are less abundant and have lower mobility [37].

6.4. Oxide trapped charge (Qt):

Broken Si-O bonds in the bulk of the oxide can create imperfections that behave like trap centers. Imperfections of this nature can stem from ionizing radiation, plasma etching, or ion implantation, and they exist within the device at extremely low concentrations.

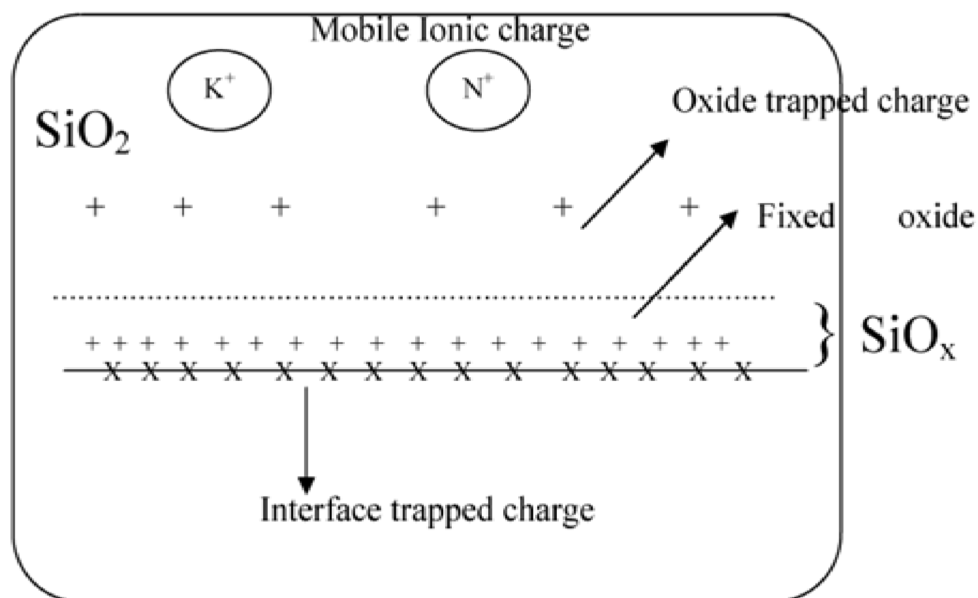

Figure II. 8: Various charge varieties within the oxide

7. Different types of conduction in the oxide

During the injection of charge carriers into the oxide, three main processes of conduction are to be considered:

7.1. Thermionic conduction

This conduction takes place when the electron's energy surpasses the height of the potential barrier (insulator/semiconductor), so the electron enters the oxide in overcoming the energy barrier of the insulation (Figure II-4)

7.2. Conduction by direct tunnel effect

If the voltage applied to the oxide is lower than the height of this potential barrier, and the thickness of the oxide is sufficiently low, the electron can directly cross this layer of oxide even subjected to a mild external electric field. This mechanism is called direct-type tunneling effect (Figure II4).

7.3. Fowler-Nordheim type tunneling conduction

For thicker oxides, the tunnel effect is only observable if a strong electric field is applied (>100 kV/mm)[36]. This will modify the shape of the barrier potential, allowing the electron to cross the deformed part of the barrier. This transport mechanism is called type tunneling effect Fowler-Nordheim conduction

7.4. Hopping Conduction:

Conductance occurs by the transfer of localized electrons from an occupied atomic site to an empty site by tunnel jump, only if the electron's energy falls below the maximum height of the energy barrier between two traps.

7.5. Poole-Frenkel effect conduction

Finally, the Poole-Frenkel effect, analogous to thermionic conduction in the volume References, occurs when the electron's energy surpasses the depth of the trap. In this case, the electron passes from one trap to another by local thermionic conduction [37].

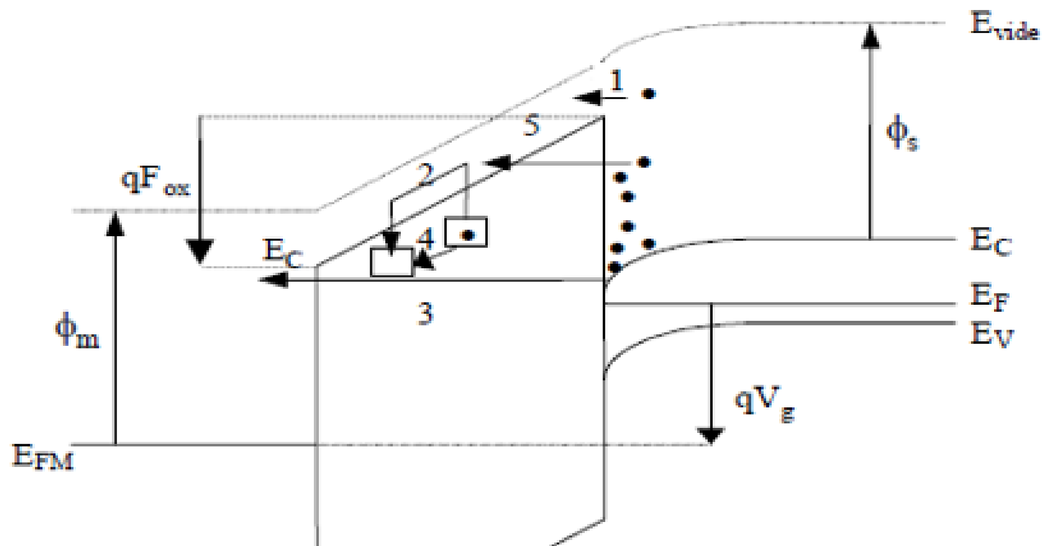

Figure II. 9: Schematic representation of the different types of conduction in the oxide. [37]

1: thermoïonique, 2:Poole- Frebkel; 3:Tunnel directe, 4:Par saut ou «hopping», 5:tunnel Fowler-Nordheim

Conclusion

A comprehensive analysis has been conducted on a wide range of materials for solar cells using a variety of techniques. This investigation encompasses both theoretical assessments involving device simulations of metal-insulator-semiconductor (MIS) structures. Notably, significant attention has been given to c-Si-based solar cells and those composed of (a-Si:H) amorphous silicon.

As miniaturization advances in MIS technology, there is a growing need to replace SiO2 with gate dielectric materials that have higher dielectric constant values (high-k). Consequently, the integration of high-k dielectrics into MIS structures proves to be crucial in enhancing the electrical performance of the design.

References

[1]-König D, Ebest G Novel thin film solar cell model with two antipolar MIS structures. Sol Energy Mater Sol Cells 56:67–74. https://doi.org/10.1016/S0927-0248 (98)00126-3(1998)

[2]-Marouf Y, Dehimi L, Bouzid F, Pezzimenti F, Della Corte FG (2018) Theoretical design and performance of InxGa1-xN single junction solar cell. Optic. 163:22–32. https://doi.org/10.1016/j.ijleo.2018.02.106

[3]-Shousha AHM, El-Kosheiry MA (1997) Computer simulation of amorphous MIS solar cells. Renew Energy 11:409–420. https://doi. org/10.1016/S0960-1481 (97)00013-X

[4]- Navneet Gupta 'Material selection for thin-film solar cells using multiple attribute decision making approach Materials and Design 32 1667–1671(2011)

[5]- March 2009 Issue of Photon International.

[6]-Renaud VARACHE Development, characterization and modeling ofinterfaces for high efficiency silicon heterojunction solar cells UNIVERSITE PARIS-SUD(2012).

[7]-Denis Pascual Sánchez. Crystalline silicon Heterojunction solar cells Universitat Politècnica de Catalunya Barcelona Juny (2015)

[8]- Y. Hamakawa (Ed.), Thin-Film Solar Cells: Next Generation Photovoltaic's and its Applications, Springer, Berlin, (2004).

[9]-V. Avrutin, N. Izyumskaya, H. Morkoç Semiconductor solar cells: Recent progress in terrestrial applications United States (2011)

[10]-Adegbenro Ayodeji Comparison of Novel AND State of the Art Solar Cells Kassel University, Germany June (2016)

[11]-Reusch, Markus: "Analyse von Full faktor limitierenden Mechanismen von Silizium-

Heterosolarzellen", Albert-Ludwigs-Universiy at Freiburg, Master thesis,(2013)

[12]-Christoph Messmer Numerical Simulation and Analysis of Metal Oxide Contact Properties for Silicon Heterojunction Solar Cells DOI: 10.13140/RG.2.2.19788.10886/1 (2017).

[13]- SALIHA Modélisation et simulation des propriétés électriques d'une structure Métal-ZELLAG Isolant-Semi-conducteur MIS Thèse de Doctorat Université Biskra (2018).

[14]-N. SAHOUANE, Elaboration, Modélisation et Caractérisation des Cellules Solaires de

Type IIIème Génération dotées de Couches Antireflets à Indice Graduel, Université Abou Bekr Belkaïd: Thèse de Doctorat, (2016).

[15]-Mireille LONTSI FOMENA, Etude Theorique De La Diffusion De L'oxygène Dans Des Oxydes Diélectriques, Université Bordeaux 1, Thèse de Doctorat, (2008)

[16]- W. Yang, J. Marino, A. Monson, C.A. Wolden, An investigation of annealing on the dielectric performance of TiO2 thin films Semicond. Sci. Technol. 21(12), 1573–1579 (2006)

[17]- L. Truong, Y.G. Fedorenko, V.Afanasev, A.Stesmans, Admittance spectroscopy of traps at the interfaces of (100)Si with Al2O3, ZrO2, and HfO2. Microelectron .Reliab. 45(5–6), 823–826 (2005)

[18-]Jahani Bahnamiri, Fatemeh Synthetic strategies for modifying dielectric properties and the electron mobility of fullerene derivatives University of Groningen (2016)

[19]- Francis Lévy, Traité des Matériaux Physique et technologie des semi-conducteurs, presses polytechniques et universitaires Romandes, (1995)

[20]-Taki Eddine TAOURIRIT Etude des Transistors couches minces (TFTs) à base d'alliages des oxydes amorphes d'In, Sn et Zn. Study of thin film transistors (TFTs) based on In, Sn and Zn amorphous oxides alloys Doctorat en physique Université Biskra (2018).

[21]-John Pointet, Elaboration et caractérisation de structures métal-isolant-métal à base de TiO2 déposé par Atomic Layer Deposition, Thèse de doctorat de l'université de Grenoble Alpes, (2006)

[22]-G.D Wilk, R.M Wallace, and J.M Anthony, High-κ gate dielectrics: Current status and materials properties considerations J. Appl. Phys. 89, 5243 (2001).

[23]- M. Houssa, High-k Gate Dielectrics, Institute of Physics Publishing, Bristol, UK (2004).

[24]-T. Hori, Gate Dielectrics and MOS ULSIs: Principles, Technologies, and Applications, Springer, Berlin, Germany (1997).

[25]-Mohammad Mojammel Al Hakim Modeling of direct tunneling gate current and gate capacitance in deep submicron MOSFETs with high-K dielectric. Master of science Bangladesh University (2002)

[26]-Mme Benabadji née Benyelles Batoul Dimensionnement des émetteurs enterrés EWT des cellules solaires industrielles à base de silicium multicristallin Doctorat En SCiences Tlemcen (2018)

[27]-Prerna Future MOSFET Devices using high-k (TiO2) dielectric Vol. 1 Issue II, ISSN: 2321-9653. (2013)

[28]-Luis V. Rodriguez- Marcos, 1, 2 Juan I. Larruquert, 1,* José A.Méndez,1 And José A. Aznarez Self-consistent optical constants of SiO2 andTa2O5 films Vol. 6, No. 11 | 1 Nov (2016)

[29]-J.M. Reyes, B.M. Perez Ramos, C.Z. Islas, W.C. Arriaga, P.R. Quintero, a. T.Jacome, Chemical and Morphological Characteristics of ALD Al2O3 Thin-Film Surfaces after Immersionin pHBufferSolutions,J.Electrochem.Soc.60 B201–B206. doi:10.1149/2.060310jes. (2013)

[30]-G. He, Z. Sun, High-k Gate Dielectrics for CMOS Technology, Wiley-VCHVerlag & Co. KGaA, Weinheim, Germany, (2012)

[31]--J.C. Ranuárez, M.J. Deen, C.H. Chen, A review of gate tunneling current in MOS devicesMicroelectron.Reliab.46(2006)19391956.doi:10.1016/j.microrel.2005.12.006.H.Nicollian, and J. R. Brews, MOS (Metal Oxide Semiconductor) Physics and Technology, New York: Wiley & Sons, Inc, (1982).

[32]. B. E. Deal. "Standardized terminology for oxide charges associated with thermally oxidized silicon, "Journal of the Electrochemical Society, vol. 127, no. 4, pp. 979-981, (1980).

[33]. D. M. Fleetwood. ""Border traps" in MOS devices," IEEE Transactions on Nuclear Science, vol. 39, no.2, pp. 269-271, (1992).

[34] D. K. Schroder, Electrical Characterization of Defects in Gate Dielectrics: CRC Press, Taylor &Francis Group, Boca Raton, (2009).

[35]. H. Nagel, C. Berge, and A. G. Aberle, "Generalized analysis of quasi-steady-state and quasi-transient measurements of carrier lifetimes in semiconductors," Journal of Applied Physics, vol. 86, no. 11, pp.

[36].Olivier Fruchier, Etude du comportement de la charge d'espace dans les structures MOS, Université Montpellier II - Sciences et Techniques du Languedoc, (2006).

[37].Yves Maneglia, Analyse en profondeur des défauts de l'interface Si-SiO2 par la technique du pompage de charges, Physics. Institut National Polytechnique de Grenoble - INPG, (1998)

Chapter III
Physics model and method

1. Introduction:

Building experimental cells is still the most accurate way to measure PV cell efficiency, but it is too expensive and time-consuming for widespread use. Numerical modeling and simulation can be used to optimize the structure of solar cells, improve understanding of important physical processes, and speed up the development process. A crucial step in achieving maximum performance in solar cell design is to investigate various combinations of geometric parameters through simulation. However, determining the ideal values of these parameters often depends on a variety of challenging considerations [1].

In this study, we share the results of 2D numerical simulation conducted using the SILVACO ATLAS software to improve the design of the MIS silicon solar cell by adjusting layer geometries. We also provide insights into Silvaco TCAD, an extensive TCAD tool for semiconductor device simulations. The discussion will emphasize the rationale behind selecting specific geometrical parameters, in alignment with solar cell manufacturing techniques.

2. Device simulator: Atlas module

For most simulations using the ATLAS simulator, the text file contains executable commands, while the structure file defines the simulated structure. The integrated structure and mesh editor (input1) in the Atlas simulator allows you to design any desired device. The commands file (input2) contains input statements that describe the models and numerical techniques used to simulate the system, as well as the boundary conditions after the device has been designed. The device simulator then uses the chosen numerical methods to solve the model equations, taking into account the boundary conditions and the device's structure (considering the device's geometry, material properties, and interfaces). Electrical parameters including current, voltage, and capacitance are produced as outputs by the simulator. Furthermore to the physical characteristics of every device mode, such as mobility, carrier lifetimes, and electric fields

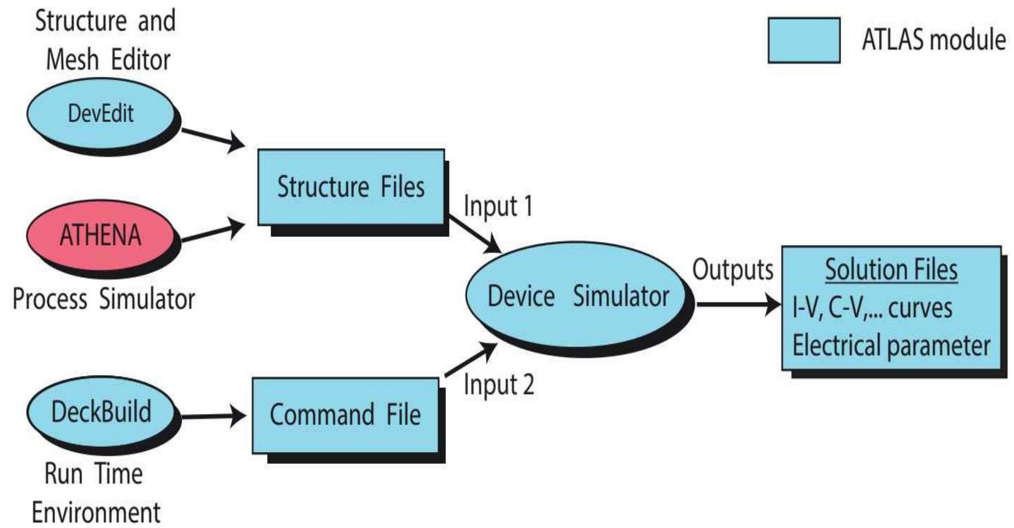

Figure III. 1: Device simulator's low-level simulation and scheme for sub-modules [2]

2-1.Structure of the reference cell used

The figure below represents the structure as given by Atlas where the regions (material) are specified knowing that the specific materials are then defined in the input file (program).

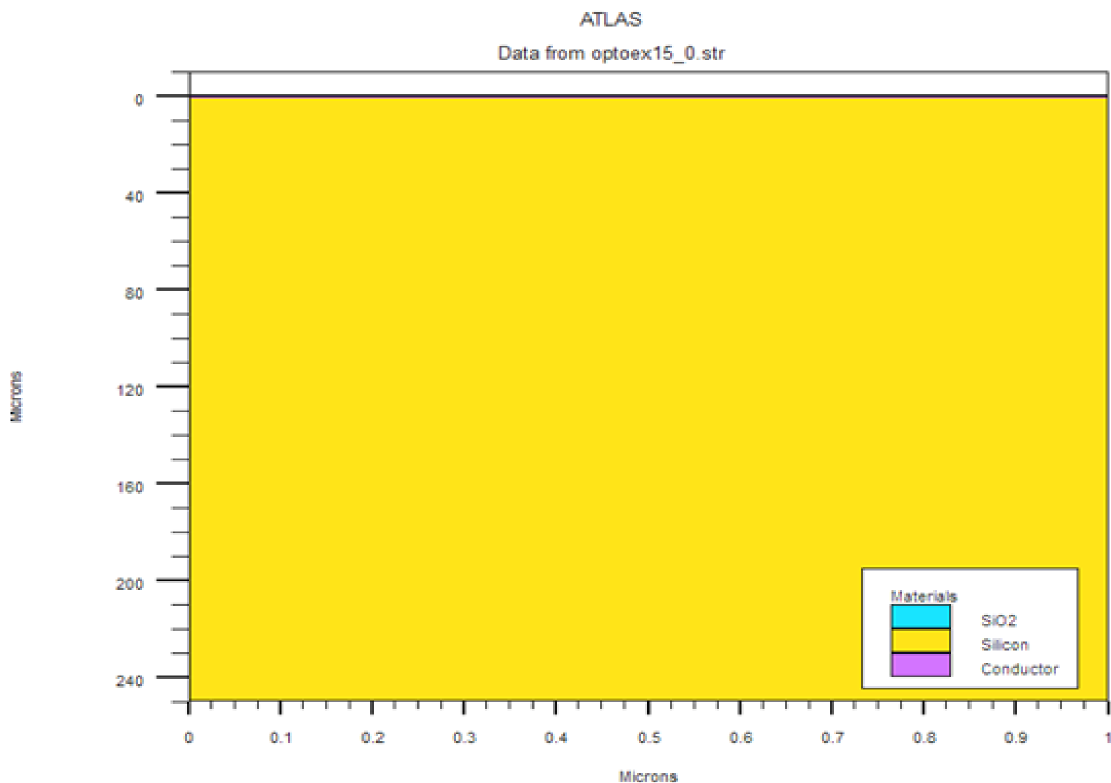

Figure III. 2: Metal- Insulator- Semiconductor (MIS) cell two-dimensional structure.

2.2. Structure and Mesh Editor:

The simulator library incorporates these parameters into its functionality. The editor also provides auto-meshing software that allows the definition of a specified regular mesh. To solve the partial differential equation numerically, a mesh of nodes (N) is used. The solver encompasses a collection of differential equations, including the Poisson equation and the continuity equations for electrons and holes, which are the basic transport equations for charges in semiconductors. The simulator then solves these equations numerically at each mesh node using Boltzmann's statistics to calculate the carrier concentration. A fine mesh must be used for accurate and precise results, but if the mesh is too fine, the computation time increases. Therefore, it is important to strike a balance between computational time and accuracy. To ensure accuracy and convergence of the equations, the mesh must be refined near areas of interest, such as heavily doped regions and contacts. The mesh quality is critical to the simulation because It has a direct impact on the precision of the results.

Later in this chapter, the effects of various factors are examined using the ATLAS tool in Silvaco. Both MIS diode and simulation results are analyzed.

We took a number a number of steps to fully understand how to construct the structure and run a Silvaco Atlas simulation of a MIS (Metal-Insulator-Semiconductor) structure. Starting with the design of simple semiconductor devices, we made observations about The I-V curves of the semiconductor devices were obtained under forward and reverse bias, as well as how they behaved in the enhancement and depletion modes, and how they compared to other examples. The collected I-V data is presented on a Tony-plot and recorded in the log file for further investigation.

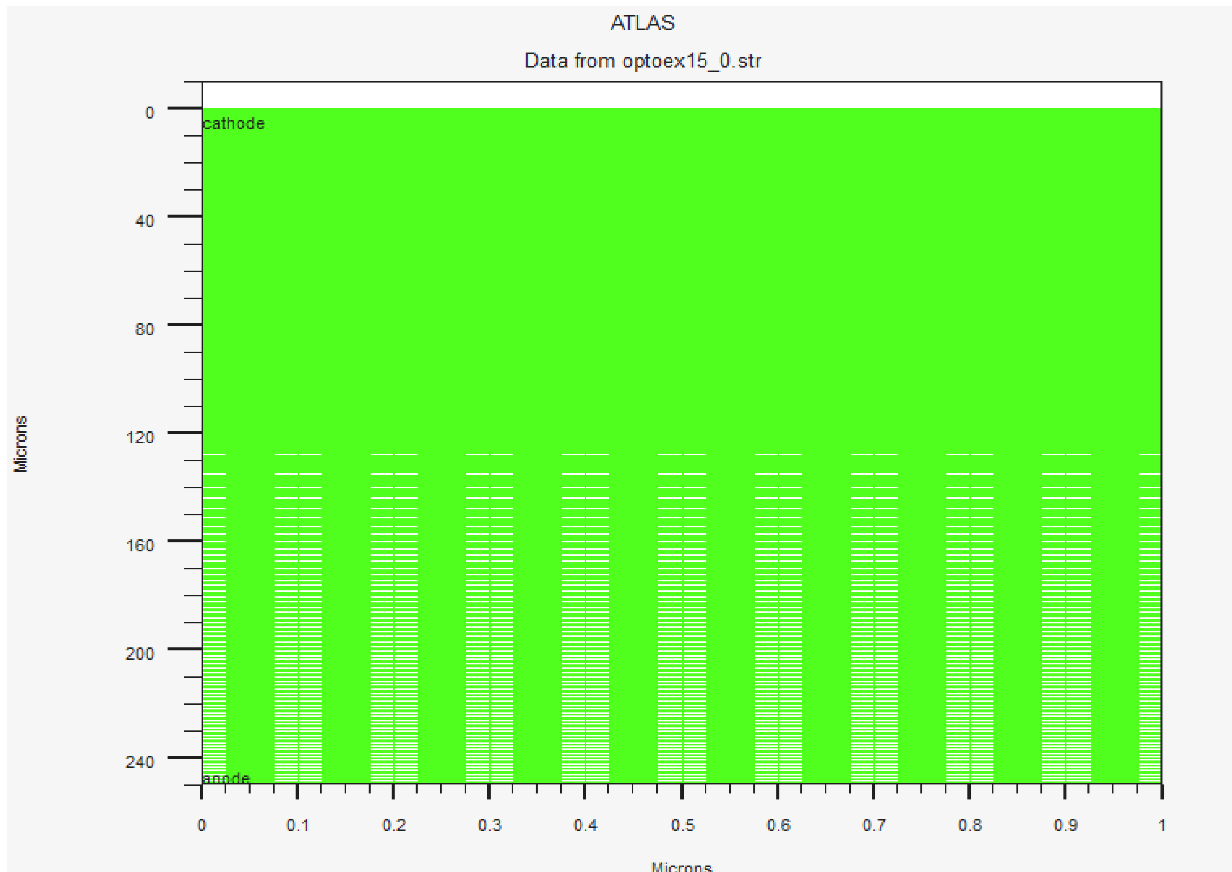

Figure III. 3: Mesh example for MIS solar cell based on Silicon (p-type)

2.3. Numerical Methods:

The computations use the Newton method as their numerical approach, with a default temperature of 300 K. It is possible to calculate the current-voltage relationship for individual electrodes, along with assessing the carrier density, electric field, and electric potential profiles within the device.

Poisson's equation, which accounts this account for the influence of both mobile and stationary charges, along with ionization traps. Carrier continuity equations for electrons and holes, and transport equations using the drift-diffusion model, are some of the fundamental equations that need to be solved. In this study, illumination is provided by AM 1.5 radiation with an incidence power density of 100 mW/cm^2 [4].

It is essential to establish and describe the material characteristics that will be used throughout the modeling of the physical structure of a solar cell using the ATLAS Silvaco simulation program [2].

- The methods used for simulation under ATLAS/SILVACO:

The methods used in this work include the GUMMEL method (decoupled equations), the NEWTON method (coupled equations), and the BLOCK method.

-The Newton method solves the entire system by considering all the unknowns simultaneously. The Gummel method solves the system by varying each unknown one at a time, while keeping the While maintaining the other unknown factors at a constant level, and iterating the procedure until a stable solution is obtained. This involves decoupling the global system into three subsystems, and the three equations are solved iteratively one after the other until reaching total convergence of the solutions. The potential advantage of this method compared to the Newton method is the reduction of the dimensions of the matrix systems to be solved, which may reduce the calculation time.

-The Block method employs the Newton method to solve particular coupled equations, while simultaneously decoupling and solving others using the Gummel method.

The choice of method in this investigation is explicitly the "NEWTON METHOD," signifying the specific utilization of the Newton method. The Gummel method is generally employed for weakly coupled systems offering linear convergence, while the Newton method is preferred for strongly coupled systems, providing quadratic convergence [4].

4. The physical models used for the simulation under ATLAS/SILVACO

In this work, the models used to optimize the MIS structure underwent thorough meshing and was analyzed using the Atlas Silvaco numerical simulator, with a focus on achieving a finer mesh resolution In the vicinity of the insulator/semiconductor interface.

The essential physical models considered encompass the temperature-dependent material band gap, the apparent narrowing effect of the band gap, incomplete activation of doping, impact ionization, and the expressions for carrier lifetime and mobility, rely on both temperature and doping concentrations, all considered within the modeling framework., we took into account various recombination phenomena, including monomolecular, bimolecular, and trimolecular mechanisms. These recombination processes operate concurrently, but the semiconductor nature of the material influences the prevalence of one or more of these mechanisms. Monomolecular recombination mechanisms can have a significant impact in indirect band gap materials. These mechanisms rely on the recombination of electrons and holes through traps possessing energy levels within the energy gap.In materials characterized

by low mobility; the bimolecular recombination rate takes precedence. This phenomenon is defined by the modified Langevin model.

Lastly, the tri-molecular recombination rate, commonly associated with Auger recombination, tends to assume dominance as the concentration of free carriers increases [7]

This study includes a thorough analysis of the density of states within the amorphous layer to understand how traps affect the performance of semiconductor devices by examining the likelihood of these states being occupied by charge carriers.

To ensure an accurate simulation of a specific structure, it is essential to incorporate physical models specifically tailored to that particular structure. The selection of appropriate parameters in the physical models is critical, as it determines the functioning and performance of the simulated structure. Therefore, it is important to incorporate the relevant parameters in the chosen physical models to account for all the mechanisms at play in the operation of the studied structure. Each model has its own statistics and rates, and careful consideration is required to determine the dominant mechanism or mechanisms.

In our study, we employed various models, including those for calculating charge carrier mobility, Auger recombination, Shockley-Read-Hall (SRH) generation-recombination mechanisms, and the tunneling effect. We will now provide a detailed explanation of the most dominant models utilized in our specific case

4.1. Mobility models

Carrier mobility is a physical concept that relates the velocity of the charge carrier to the electric field it experiences. There are various mobility models available in Atlas, with "CONMOB" and "FLDMOB" being the ones used in our work. However, it's worth mentioning that these are not the only models available in Atlas, as there are other options as well. In our work, we used the “CONMOB” and “FLDMOB” models

Physical model	Description
Conmob	Explains how to use a mobility model that depends on silicon concentration. presented as a doping-mobility table applicable solely at 300K temperature.
Fldmob	The mobility model reliant on the lateral electric field's influence, described as a function of mobility
Consrh	Shockley-Read-Hall recombination is described using concentration-dependent lifetimes.
qtnlsc.	Enables self-consistent direct quantum tunneling with electron participation.
qtnlsc.ho	Permits the self-consistent behavior of the direct quantum tunneling model for holes.
qtnl.derivs	As a result, more terms will be included in the Jacobian matrix, enhancing convergence in the self-consistent direct quantum tunnelling models.

Table III. 1: Some of Atlas's mobility models

4.2. Recombination models used for simulation under ATLAS/SILVACO

The total rate of recombination in a semiconductor is the sum of all possible rates, and various recombination processes may occur simultaneously depending on their likelihood. However, some processes may predominate due to the way the semiconductor functions and its properties. For example, the tunneling model must be used to accurately depict the tunneling of gate electrons under negative gate bias conditions. Additionally, a novel differential rate equation has been formulated to encompass Transient trap simulations encompass both emission and capture processes.

4.2.1. Shockley-Read-Hall (SRH) recombination

The Shockley-Read-Hall (SRH) recombination mechanism entails the recombination of both electrons and holes. through traps situated within the band gap. These traps can serve as catalysts for the recombination process, which takes place in two steps: the first phase involves an electron being captured by the trap, and the second involves the electron being released from the trap and recombining with a hole located in the valence band. The SRH recombination rate can be determined by taking into account the four processes responsible for the population or depopulation of an energy state trapped inside the forbidden band (E_t), as illustrated in Fig. III.3, the SRH recombination rate may be determined.

$$R_{RSH} = \frac{np - n_i^2}{\tau_p \left[n + n_i \exp\left(-\left(\frac{E_t - E_i}{KT} \right) \right) \right] + \tau_n \left[p + n_i \exp\left(\frac{E_i - E_t}{KT} \right) \right]} \quad \text{(III.1)}$$

Where E_t is the energetic position of the trap states, E_i is the Fermi level in the intrinsic semiconductor, and τ_n and τ_p are the electron and hole lifetime parameters. k is the Boltzmann constant and T the temperature in Kelvin.[2.9]

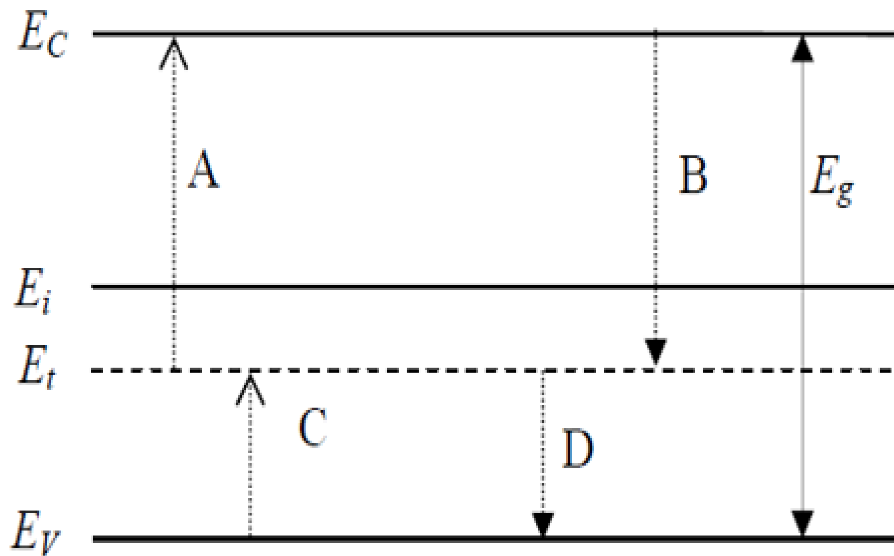

Figure III. 4: Transitions through a level inside the band gap of a semiconductor [11].

4.2.2. Auger recombination

The Auger model is employed for managing minority carrier recombination, while the Shockley-Read-Hall (SRH) model addresses generation and recombination processes. Model is favored in silicon-based solar cells due to its capability to closely replicate experimental data. Notably, the dominant influence of SRH and Auger recombination models in silicon-based solar cells significantly affects material longevity and overall solar cell performance.

Combining these models for enhanced accuracy is advisable, but careful attention should be paid if convergence issues arise during the solution. [10].

During the Auger recombination process, the surplus energy produced when an electron-hole pair recombines is transferred to a third particle. This process involves three particles and can encompass either a hole in the valence band or an electron in the conduction band, [12]. As described by the following equation:

$$R_{AUGER} = AUGN\left(pn^2 - nnie^2\right) + AUGP\left(np^2 - pnie^2\right) \tag{III.2}$$

Where n_{ie}: the effective intrinsic concentration is denoted as such, with AUGN and AUGP being user-defined parameters contingent upon the material in use. Default values are listed in Table [2.9].

Parameter	Default value
AUGN (cm6/s)	2.8x10-31
AUGP (cm6/s)	9.9x10-32

Table III. 2: The default values used for the simulation of Auger recombination.

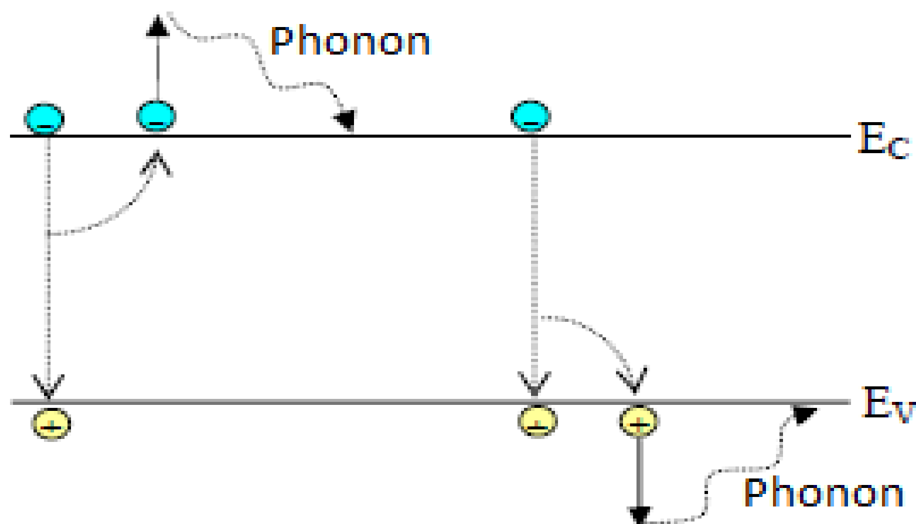

Figure III. 5: Diagram illustrating Auger recombination [10].

4.2.3. Langevin recombination

Langevin's hypothesis, put forward in 1903, is a straightforward yet successful approach to describe This refers to the immediate recombination of unbound charge carriers, where their average travel distance is shorter than their capture radius. According to Langevin's theory, when an electron and a hole are closer than the Coulomb radius, their mutual attraction is stronger than the thermal energy, allowing them to bind and recombine. Langevin's ingenious assumption is that only electron-hole pairs with a radius less than rc experience recombination. The Langevin prefactor is used to calculate the recombination current and recombination rate when this assumption is extended to account for the carrier concentrations.

In organic semiconductors, holes are more likely to capture a neighboring electron than in conditions where their mobility is higher because of the slower movement of electrons and holes. Organic semiconductors are known for their poor mobility. This is explained by the Langevin theory.

In metallic semiconductors, there exists a recombination mechanism resembling direct band-to-band recombination, wherein the recombination rate is inversely linked to the product of the hole concentration (p) and the electron concentration (n) [13-14]. According to Langevin's hypotheses, two charge carriers that are attracted to each other will eventually recombine when the Coulomb attraction energy (E_{cb}) between them exceeds the thermal energy (E_{th}) dictating their Brownian motion. The Coulomb radius (r_c) signifies the point at which the forces of attraction and thermal motion reach equilibrium. As a result:

$$\frac{q^2}{4\pi\varepsilon_0\varepsilon_r r_c} = KT \quad \text{(III.4)}$$

.Expressed in terms of r_c, this establishes the minimum separation between two charges, ensuring they won't spontaneously recombine beyond this distance.

$$\frac{q^2}{4\pi\varepsilon_0\varepsilon_r KT} = r_c \quad \text{(III.5)}$$

4.3. The tunnel effect

Tunneling current is the movement of electrons through a potential barrier, and the local generation rate, (r), quantifies the electron generation per unit volume at a specific point r within the barrier.. It is related to the density of the local tunnel current, $JTun$, by the following expression: [15]:

$$G_{Tun}(r) = \frac{1}{q}\nabla J_{Tun} \tag{III.6}$$

$$J_{Tun}(r) = \frac{A^{*}T}{K_B}\vec{E}\Gamma(r)\mathbf{ln}\left[\frac{1+\exp(-q(\psi-\phi_n)/K_BT}{1+\exp(-q(\psi-\phi_m)/K_BT}\right] \tag{III.7}$$

Where T is temperature, A^{*} is Richardson's constant, $\vec{E} = -\nabla\psi$ is potential Electrostatic, $\Gamma(r)$ is the tunnel probability given by eq (III-10), $E_{Fm} = q\emptyset_m$ is the, Fermi level of the metal, $\varepsilon = -q\psi$, it is the energy level, $E_{Fn} = q\emptyset_n$ is the quasi Fermi level in the semiconductor.

$$\Gamma(r) = \exp\left(\frac{-2}{h}\int_{2}^{r}\sqrt{2m\left(\frac{\phi_b}{q}+\phi_m-\Psi(x)\right)}dx\right) \tag{III-8}$$

However, we would like to point out that in addition to the models seen above; we have also introduced in the simulation program the instruction (in trap acceptor) for a better simulation.

In fact the “in trap” instruction activates the existence of interface faults “the traps” to

4.4 - Models of the Density of States (DOS) used in simulation

For precise simulations of metal-insulator-semiconductor (MIS) solar cells involving crystalline silicon (c-Si) and hydrogenated amorphous silicon (a-Si:H), it's crucial to employ software that can accurately model the density of states within the band gap. Silvaco TCAD is widely adopted in the solar industry to faithfully replicate c-Si characteristics, but when working with a-Si:H, it's vital to consider the unique state distribution

To accurately describe the electrical properties of materials like a-Si:H and the devices employing them, it's essential to consider the substantial presence of defect states within the band gap, especially in disordered materials such as amorphous substances [17]. Within the Atlas software, one can create an energy distribution for continuous defect states situated within the band gap of amorphous semiconductor materials and seamlessly integrate them into the simulation process [16]. For precise modeling of devices made from amorphous materials, a continuous density of states is utilized. This incorporates band tail states that decay exponentially and Gaussian distributions of mid-gap states [18].Additionally, incorporating interface models like a thermionic field emission boundary might be essential. A notable feature of the software is its capacity to generate custom-defined materials for simulations. Any material may be used to define a structure, and its properties can be changed to match those of the chosen material. The material will function similarly to any other material in the simulation, despite having the name of the selected material [19].

The solar cell is constructed using a crystalline silicon wafer that has a thickness of 250 microns, while the amorphous silicon layer is only 2 microns thick. One of the models offered by ATLAS, a program commonly used to simulate crystalline silicon, is one that deals with mobility and temperature-dependent band gap fluctuations.

A more specific model is required because the structure of amorphous silicon is more complicated than that of crystalline silicon. According to the proposed method, a modified density of states can be created by adding new elements to the crystalline silicon density of states. This involves adding two mid-gap states with Gaussian distributions and exponentially decaying band tails to the standard bands of the crystalline silicon density of states. (III-9)

$$g(E) = g_D^e(E) + g_A^e(E) + g_D^g(E) + g_A^g(E) \qquad \text{(III-9)}$$

This includes the donor band tail $g_D^e(E)$, acceptor band tail $g_A^e(E)$, characteristic decay energies associated with donors and acceptors, and g_0 represents the maximum number of states within this tail.

The existence of donor and the acceptor band tails act as an indicator of the level of disorder existing within the material atomic structure, increased disorder in the atomic arrangement leads to a greater the number of energy levels located between the valence and conduction bands [19] Carriers occupying these energy levels become trapped since they cannot effectively transition between states with matching energy levels, thus their contribution to the system's current remains minimal. This distribution applies to both donor-like and acceptor-like states, as expressed in Equation (III.10) and Equation (insert appropriate equation number). Here, E_m represents the minimum energy of the tail states, while E_D and E_A signify the characteristic decay energies for donors and acceptors in the band tails. Additionally, g_0 stands for the maximum number of states within these tails.

$$g_D^e(E) = g_0 / 2\exp(-\frac{E - E_m}{E_D}) \quad \text{(III-10)}$$

$$g_A^e(E) = g_0 / 2\exp(\frac{E - E_m}{E_A}) \quad \text{(III-11)}$$

Amorphous silicon (a-Si:H) Contains trap centers located in the middle of the band gap, in addition to the band tails. These mid-gap states can be further divided into two categories: Dangling bond states follow a Gaussian distribution and represent electrons without a paired partner, known as dangling bonds, found in amorphous materials. These unpaired electrons are not bonded to any other atoms. They can trap either electrons or holes, depending on their energy level.

Donor-like traps bear an electron charge while remaining neutral for holes. They are created when a dangling bond captures an electron. Acceptor-like traps hold a charge for holes but stay neutral for electrons. They are created when a dangling bond captures a hole. Equations III.12 and III.13 give a description of these two Gaussian distributions.

$$g_D^g(E) = N_D^g / \delta_D \exp[-(\frac{E - E_D^g}{2\delta_D})^2]$$ (III-12)

$$g_A^g(E) = N_A^g / \delta_A \exp\left[-(\frac{E - E_A^g}{2\delta_A})^2\right].$$ (III-13)

For Eq. III.12 and Eq.III.13, E_D^g and E_A^g represent the energy positions of Gaussian peaks for donor-like and acceptor-like states, respectively, while σ_D and σ_A define the standard deviations of these Gaussian distributions, and N_D^g and N_A^g signify the peak number of states within these distributions.

All the parameters employed in this study were derived from existing literature. Equations III.13 to III.12 were utilized to construct the density of states (DOS) diagrams for a-Si:H, as illustrated in the figure. (III-6)

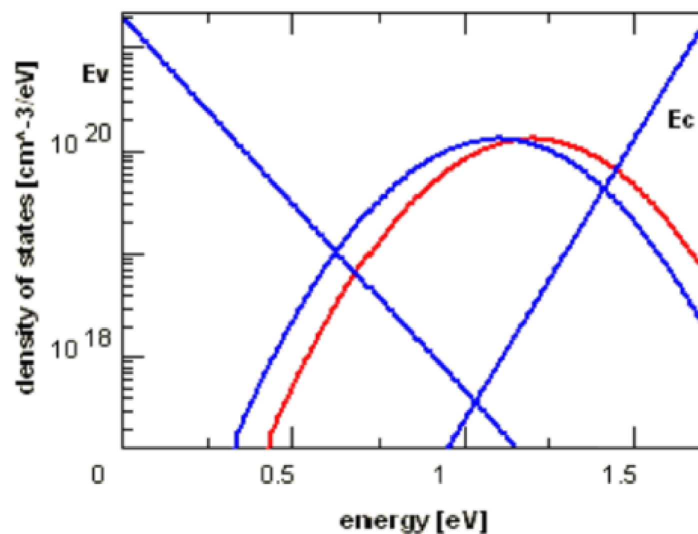

Figure III. 6: (DOS) of hydrogenated amorphous silicon doped: p

5.1. Model for Silicon based MIS junction Diode

The studied MIS (Metal-Insulator-Semiconductor) silicon solar cell was modeled using Silvaco in DeckBuild. An MIS diode was built by following the basics outlined in the Atlas manual and analyzing examples available through DeckBuild. An MIS diode is a two-terminal semiconductor device with a metal-insulator-semiconductor junction that conducts current in only one direction.

The device structure was delineated by creating mesh regions in Atlas along both the x and y directions. After completing the mesh statements for the entire device area, the physical structure was imported into Atlas as input and subsequently simulated. Runtime environment to predict the electrical properties were analyzed while applying specific bias condition. The material, model, and method specifications were set to accurately represent the physics of the modeled semiconductor device, which was a p-type silicon diode.

Solve statements were used to obtain solutions. An initial run simulated the diode forward characteristic under room temperature conditions. A second Atlas run was performed to simulate the reverse and breakdown the device's properties were analyzed under room temperature conditions. By deriving internal parameter distributions from these simulations, it became possible to compute the current density of electrons and holes, enabling the subsequent calculation of the current density-voltage (J-V) characteristics of the cell, both in the absence of illumination and when exposed to light.

The presence of minority carriers plays a crucial role. in influencing the photocurrent (J_{SC}) in a MIS solar cell. In cases where the insulator (oxide) layer dividing the anode and the p-type silicon layer is extremely thin, the primary mechanism governing photocurrent involves direct tunneling through the potential barrier created by the oxide layer. As a result, the (J-V) characteristics of an MIS solar cell can be described in this manner.

$$J(V) = J_{sc} - J_s(\exp(qV / K_B T - 1) \quad \text{. (III-14)}$$

In the following equation, "J_s" represents the dark saturation current

$$J_s = A^* T^2 \exp(-q\Phi_{b0} / K_B T) \exp(-q\phi_{mi})^{\frac{1}{2}}.d). \quad \text{(III-15)}$$

In Eq.(III.15), A* represents the effective Richardson constant, T is the absolute temperature in Kelvin, q signifies the electronic charge, K_B stands for the Boltzmann constant,. ϕ_{mi}: is insulator–semiconductor barrier height ϕ_{b0} is the metal–semiconductor barrier height, and "d" stands for the insulating layer thickness.

Following the direct tunnelling mechanism, the current density, J_{Tun} through the potential barrier formed by the insulating layer is given by

$$J_{Tun}(r) = \frac{A^* T}{K_B} \vec{E}\Gamma(r) \mathbf{ln}\left[\frac{1+\exp(-q(\psi-\phi_n)/K_B T}{1+\exp(-q(\psi-\phi_m)/K_B T}\right] \quad \text{(III-16)}$$

The simulation's output of (J-V) data is recorded in a log file and plotted using Tony. The use of appropriate physical models designed particularly to simulate the MIS (Metal-Insulator-Semiconductor) structure is required to provide a realistic simulation of this structure. This decision affects how the simulated structure behaves, which in turn affects how well it performs. The physical models under consideration must have the proper parameters to account for all the mechanisms, including mass and tunneling effects that are involved in the operation of the structure under study. In the general Schottky tunneling model, "me tunnel" and "mh tunnel" represent the effective masses for electron and hole tunneling, while "tunnel" specifies the effective mass for band-to-band tunneling. To establish a Schottky barrier at the interface between the oxide and semiconductor (SiO2/c-Si, P-type), it is essential that the work function of the anode exceeds the electron affinities of silicon. Both of the examined MIS silicon solar cells fulfill this criterion.

5.2. Input parameters:

The "MATERIAL" statement is employed to outline fundamental material characteristics, and when modeling semiconductor materials, it's necessary to specify the following properties:

Electronic band gap (E_g), Relative permittivity, Electron affinity (χ),Effective density of states in the conduction band (N_C), Effective density of states in the valence band (N_V), Electron and

hole mobility, The recombination of particular band gap states is influenced by the material properties. being studied and the existence of particular state distributions within the band gap.

Simulations for both types of MIS cells are performed at low voltages and compared to actual measurements taken at room temperature (T=300 K).

6. Conclusion

In this chapter, we've presented the fundamental physical model that serves as the basis for designing and modeling both crystalline silicon (c-Si) and amorphous silicon (a-Si) solar cells. This model is rooted in five partial differential equations, comprising the Poisson equation, two continuity equations, and two transport equations. We've also provided an overview of the simulation methods and physical models utilized in Atlas/Silvaco.

References

[1]-Fotis, Konstantinos Modeling and simulation of a dual-junction CIGS solar cell using Silvaco ATLAS the NPS Institutional Archive (2012).

[2]-SILVACO Data Systems Inc Silvaco ATLAS User's manual, (2016)

[3]-C.K.Maiti, Introducing Technology Computer-Aided Desingn (TCAD): Fundamentals Simulations and Applications. Pan Stan ford, (2017)

[4]-Zeghdar K, Dehimi L, Pezzimenti F, Rao S, Della Corte FG Simulation and analysis of the current–voltage–temperature characteristics of Al/Ti/4H-SiC Schottky barrier diodes. Jpn J Appl Phys 58:014002. https://doi.org/10.7567/1347-4065/aaf3ab/meta (2019)

[5]-Fossum JG, Lee DS A physical model for the dependence of carrier lifetime on doping density in non degenerate silicon. Solid State Electron 25:741–747. https://doi.org/10.1016/0038-1101(82) 90203-9 (1982)

[6]-Groves C, Green ham NC Bimolecular recombination in polymer electronic devices. Phys Rev B 78(15):155205. https:// doi.org/10.1103/Phys RevB.78.155205(2008)

[7]- Lu, M. et al. Optimization of in terdigitated back contact silicon heterojunction solar cells by two-dimensional numerical simulation. In: proceedings of 34th IEEE PVSC, Philadelphia, USA. doi:https://doi.org/10.1109/PVSC.2009.5411332 (2009)

[8]- S.E. Swirhun, Electrical Engineering Stanford, 318 (1987).

[9]- J. L. Gray, ―Chapter 3: The Physics of the Solar Cell, ‖ in « Handbook of Photovoltaic Science and Engineering », John Wiley & Sons Inc., pp. 82–12 International, Santa Clara. (2011)

[10]-S. Dubois. "Influence des interactions impureté-défaut et impureté-impureté sur le rendement de conversion des cellules photovoltaïques au silicium cristallin". ". Thèse de Doctorat, Université Paul Cézanne Aix-Marseille III, (2007)

[11]-W. Shockley and W.T. Read, Phys. Rev. 87, 835 (1952)

[12]- J.G. Fossum and D.S. Lee, Solid State Electronics 25, 741 (1982)

[13]-Djicknoum DIOUF, Thèse de doctorat, Cellules photovoltaïques silicium à hétérojonctions et à structure interdigitée en face arrière, Laboratoire de Génie Electrique de Paris (2010)

[14]-Alexander Johannes Wagenpfahl Numerical simulations on limitations and optimization strategies of organic solar cells Univ¨atW¨urzburg (2013)

[15]-E.H. Rhoderick, R.H. Williams, Metal-semiconductor contacts, Oxford University Press, Oxford, (1988)

[16]-A. Fantoni, “Simulation of hydrogenated amorphous and microcrystalline silicon optoelectronic devices,” Mathematics and Computers in Simulation, vol. 49, no. 4-5, pp. 381-401, Sep. (1999).

[17]-A.Dasgupta, N. Palit, and S. Ray, “Accelerated degradation in amorphous silicon solar cells by a combination of current injection and light insolation,” Sol. Energy Mater, vol. 55, pp. 395–402, (1998).

[18]-A. Fantoni, “Simulation of hydrogenated amorphous and microcrystalline silicon optoelectronic devices,” Mathematics and Computers in Simulation, vol. 49, no. 4-5, pp. 381-401, Sep. (1999).

[19]-N. Hernández-Como and A. Morales-Acevedo, “Simulation of hetero-junction silicon solar cells with AMPS-1D,” Solar Energy Materials and Solar Cells, vol. 94, no. 1, pp. 62-67, Jan. (2010).

[20]- Wilson W. Wenas, Syarif Riyadi, Carrier transport in high-efficiency ZnO/SiO2/Si solar cells, Solar Energy Materials & Solar Cells 90 3261–3267. (2006)

Chapter IV
RESULTS AND INTERPRETATIONS

1. Introduction:

A new method for enhancing the efficiency of MIS silicon solar cells beyond 21.85% was simulated. This method uses a multi-layered structure with varying band gaps to convert some of the lost energy into heat, which can be used to generate electricity or improve the efficiency of the solar cell.

In this study, we investigated the optical and electrical characteristics of MIS structures using both c-Si and a-Si:H substrates. Our research highlights the efficacy of amorphous silicon as an active region in MIS solar cells when coupled with silicon dioxide (SiO_2), has been shown to enhance current conduction through quantum mechanical tunneling processes. We utilized TCAD for modeling and simulating the MIS structure. [1-2-3]

According to, the mobility of charge carriers may decrease as the oxide layer thickness decreases, which can potentially lower solar cell efficiency [4]. High-k materials, such as aluminum oxide (Al_2O_3), hafnium dioxide (HfO_2), Si_3N_4, Ta_2O_5, and TiO_2, have emerged as promising alternatives to traditional SiO2. The aim of this research is to assess the impact of various high-k materials on the performance of metal-insulator-semiconductor (MIS) structures. Our findings suggest that high-k materials exhibit higher capacitance and lower leakage currents. Electrical performance can be maintained or improved by using thicker components or devices, which allows for larger physical dimensions without sacrificing electrical performance.

The development of efficient solar cells is a complex and challenging task. The performance of solar cells is dependent on a number of factors, including the materials used, the design of the cell, and the conditions under which it is operating. The primary goal in solar cell fabrication is to optimize production while taking costs into account. As a result, there is always a trade-off between cost and efficiency.

2. Device Structure:

In this research, we explore the cross-sectional analysis of an MIS solar cell. As shown in Figure (IV.1), the structure consists of a thin film of high-k material (10 Å thick) on top of a p-type absorber layer, which can be either a 2 µm-thick a-Si:H substrate or a 250 µm-thick c-Si substrate. The cell is contacted with aluminum. Various oxides, such as SiO_2, Al_2O_3, HfO_2, Si_3N_4, Ta_2O_5, and TiO_2, are proposed as alternatives to current technology to optimize the tunneling of charge carriers in solar cells. [5]

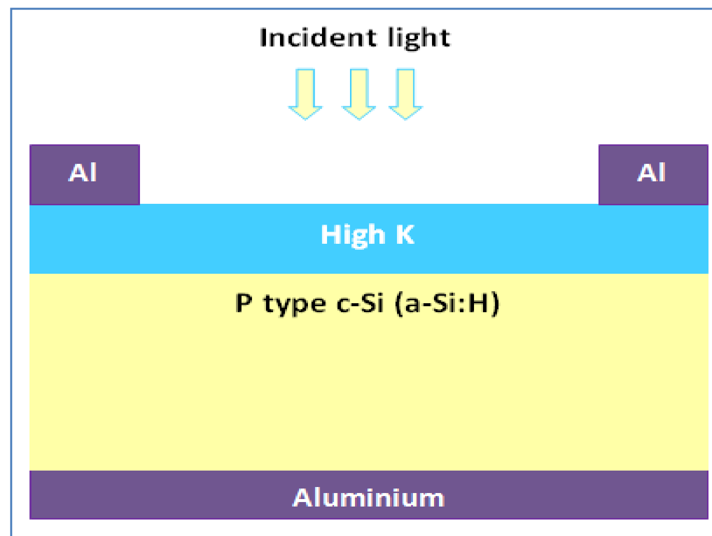

Figure IV. 1: Cross-Sectional Illustration of a 2D MIS Solar Cell Structure

In more detail, complete simulation of dielectric materials has been performed using the Silvaco Atlas software, incorporating multiple simulation parameters such as band gap, absorption coefficient, diffusion length, and recombination velocity. The key electrical properties of the solar cell, including spectral response, open circuit voltage (V_{oc}), short circuit current density (J_{sc}), fill-factor, and conversion efficiency, have been accurately calculated by considering the standard global solar spectrum (AM1.5G) irradiation. It is crucial to define the material properties to accurately simulate the physical structure of a solar cell using the ATLAS simulator. These material properties can be found in Table 1 of the material reference data set, and Table 2 provides further details.

Material	(c-Si)	(a-Si:H)
Band gap (eV) 300K	1.12	1.72
Affinity (eV)	4.1	3.9
Electron mobility ($cm^2/V*S$)	1300	20
Hole mobility ($cm^2/V*S$)	450	1.5
Conduction band density of state, N_C (cm^{-3})	2.8×10^{19}	2×10^{20}
Valence band density of state, N_V (cm^{-3})	1.04×10^{19}	2×10^{20}
Electron capture cross section σ_n(cm^2)	1×10^{-15}	1×10^{-15}
Hole capture cross section σ_p(cm^2)	1×10^{-15}	1×10^{-15}
Intrinsic concentration, n_i (cm^{-3})	6.68×10^{9}	7.14×10^{5}

Table IV. 1: MIS references parameters [6]

parameters	Value
Band edges intercept density, *NTD* (A)	1×10^{21}
Characteristic energy, *WTA* **(eV)**	0.033
Characteristic energy, *WTD* **(eV)**	0.049
Acceptor Gaussian distribution density *NGA*	1.5×10^{15}
Donor Gaussian distribution density *NGD*	1.5×10^{15}
Peak energy distributions, EGA (eV)	0.62
***EGD* (eV)**	0.78
***WGA* (eV)**	0.15

Table IV. 2: Defects parameters for (a-Si:H) [8]

Parameters	Unit	SiO_2	TiO_2	Si_3N_4	Ta_2O_5
Thickness	A°	10	10	10	10
Eg	eV	9	3.5	5.3	4.4
χ	eV	0.9	3.8	2.15	2.95
ε_r	/	3.9	80	7.5	25
ΔE_c	eV	3.5	1.1	2.2	1.5
ΔE_v	eV	4.4	1.3	1.8	3.4

Table IV. 3: Input data of the proposed dielectrics materials [10].

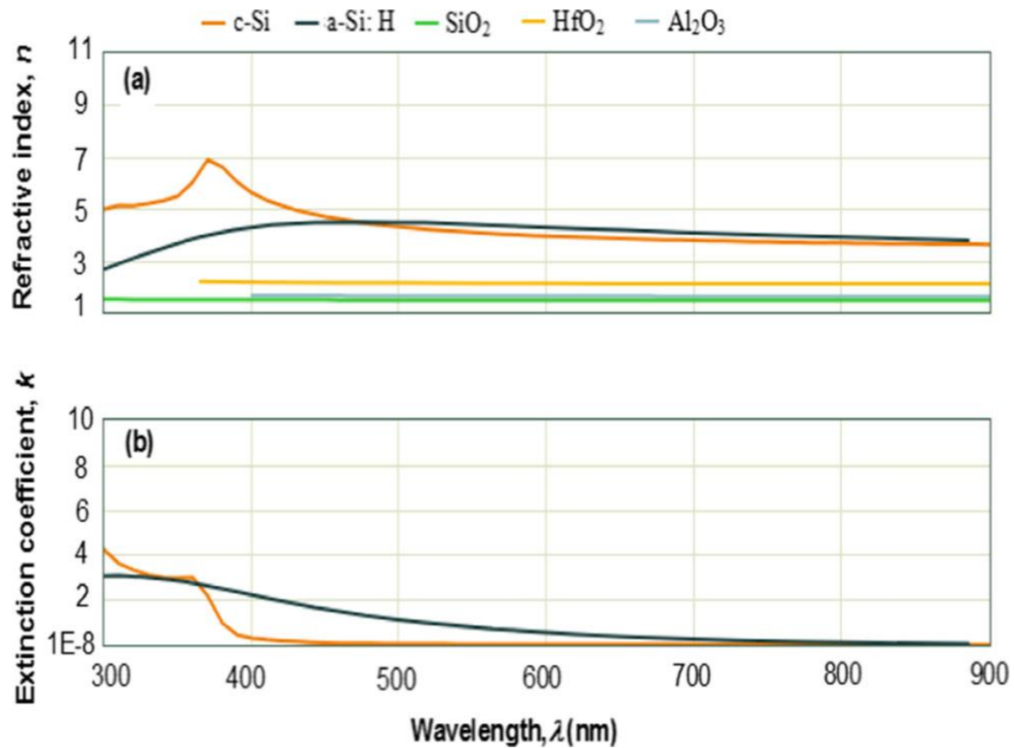

Figure IV. 2 Optical parameters of (c-Si), (a-Si:H), SiO_2, HfO_2 and Al_2O_3 (a) refractive index n(b) Extension coefficient k

Furthermore, the simulation framework should include optical files that provide information about the refractive index n and the extinction coefficient k. Accurate optical data is necessary to create a precise simulation of the performance of a solar cell, taking into account the transmission. and attenuation of light through the device structure. Accurate modeling of the electron-hole pair generation phenomenon is of significant importance when simulating a solar cell, as it involves plotting the behaviors of n and k for the materials under consideration. (Figure.VI.2). a and b

In the simulation framework, photo-generation is achieved by conducting dual concurrent simulations at each mesh point of the structure through the LUMINOUS optoelectronic module. Luminous utilizes the refractive index, 'n,' to simulate the propagation of light through its device. The variation in 'n' values at layer boundaries determines how light is transmitted and reflected at these boundaries. By tracing the path of light from the source to a specific point on the mesh, Luminous can accurately calculate the optical intensity at that point. [7] At each individual point on the mesh, the extinction coefficient, 'k,' is used to measure and quantify the rates of absorption and photo-generation corresponding to the observed optical intensity.

3. Simulation Models and Parameters

The Atlas Silvaco software was used to extensively discretize the MIS structure for the purposes of numerical simulation, with a particular focus on finely dividing the regions around the insulator/semiconductor interface. The simulation includes fundamental physical models such as the temperature-dependent band gap of the material, the apparent band gap narrowing effect, incomplete doping activation, impact ionization, as well as carrier lifetime and carrier mobility expressions. [9] A preliminary simulation was conducted to study the effect of varying oxide layer thicknesses on the electrical characteristics of the solar cell. The findings are as follows:

4. Results and Discussion

4.1. Effect of the Insulator Thickness

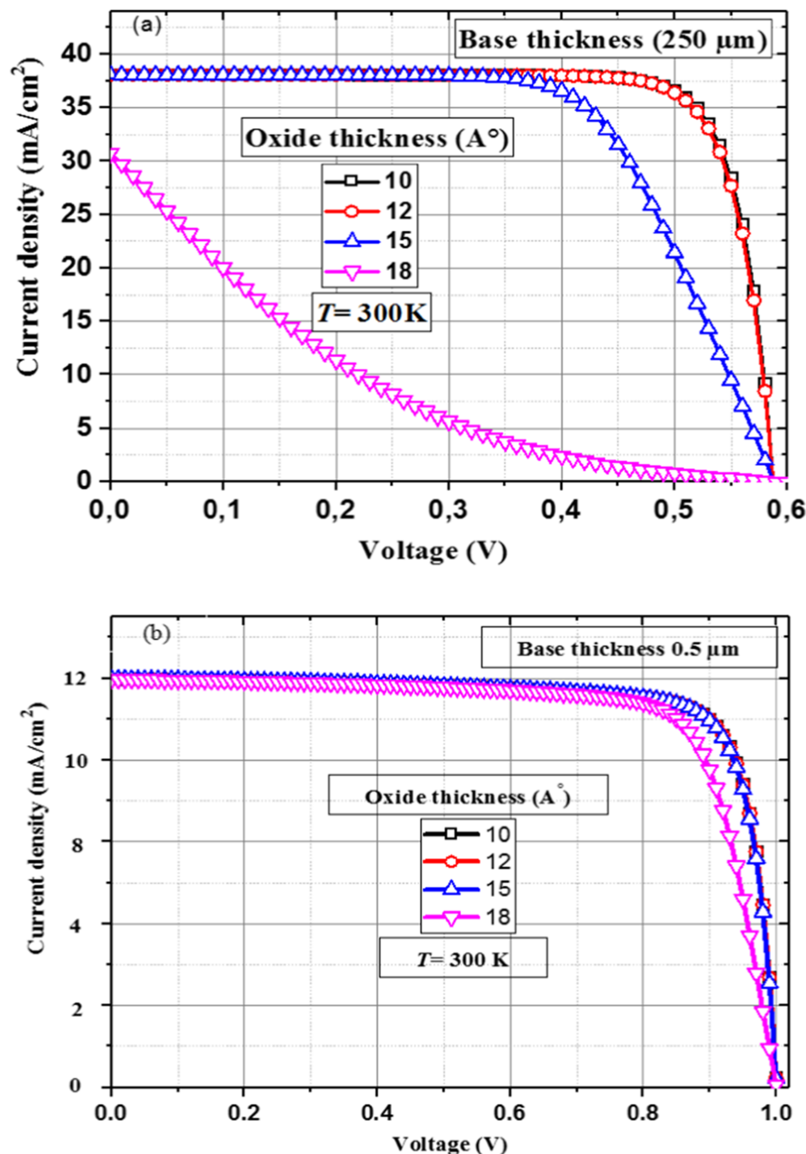

Figure IV. 3: Variation of (J-V) Characteristics with Al-SiO2-p Oxide Thickness in c-Si and a-Si:H-Based MIS Solar Cell Structures

The oxide layer thickness is a major factor affecting the performance of MIS solar cells, making it a crucial element to consider. Its impact depends on the other parameters chosen. We initially investigated the impact of this parameter on the J-V characteristics of both c-Si and a-Si:H-based devices to optimize the solar cell's performance, as shown in Figure IV.3. The carrier transport mechanisms in an MIS solar cell are largely determined by the oxide thickness, highlighting its crucial role in the overall system.

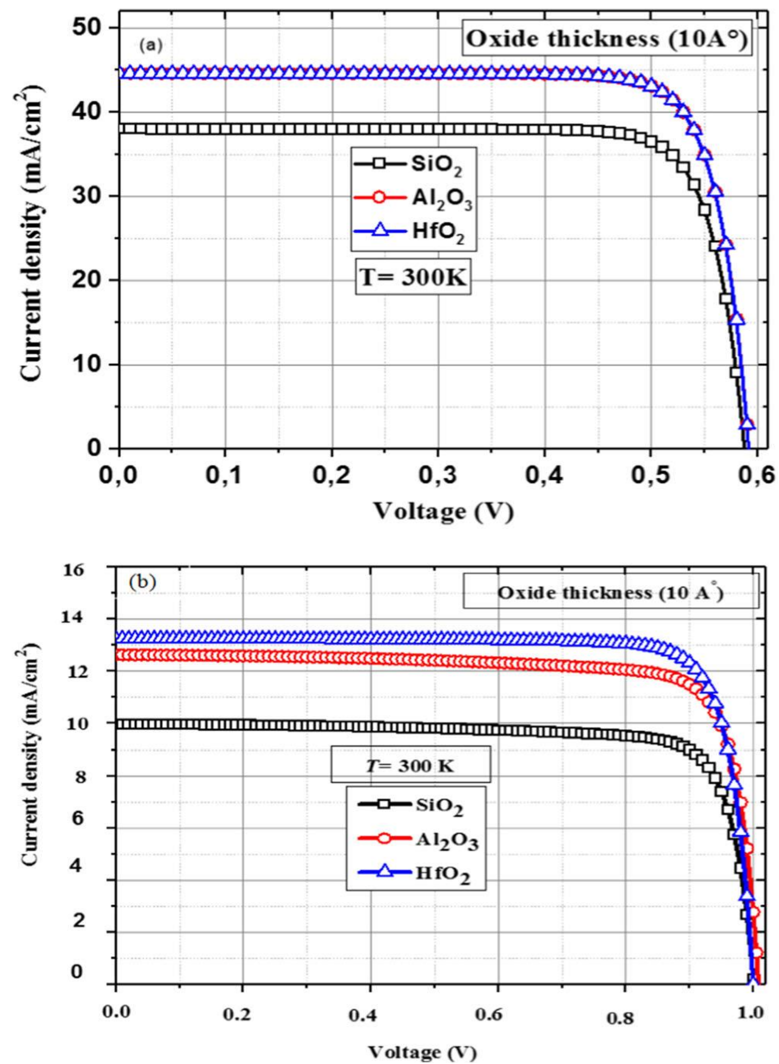

Figure IV. 4: J-V characteristics of the device for different oxide materials (a) c- Si- (b) a-Si:H-based structure

Specifically, the oxide thickness was varied from 10 Å to 18 Å under AM1.5 illumination at a temperature of 300 K. It can be observed that for thinner oxides, the short-circuit current (Jsc) undergoes minimal changes. However, as the oxide thickness approaches a critical value near 15 Å, Jsc starts to decrease, accompanied by a significant decline in the fill factor

.

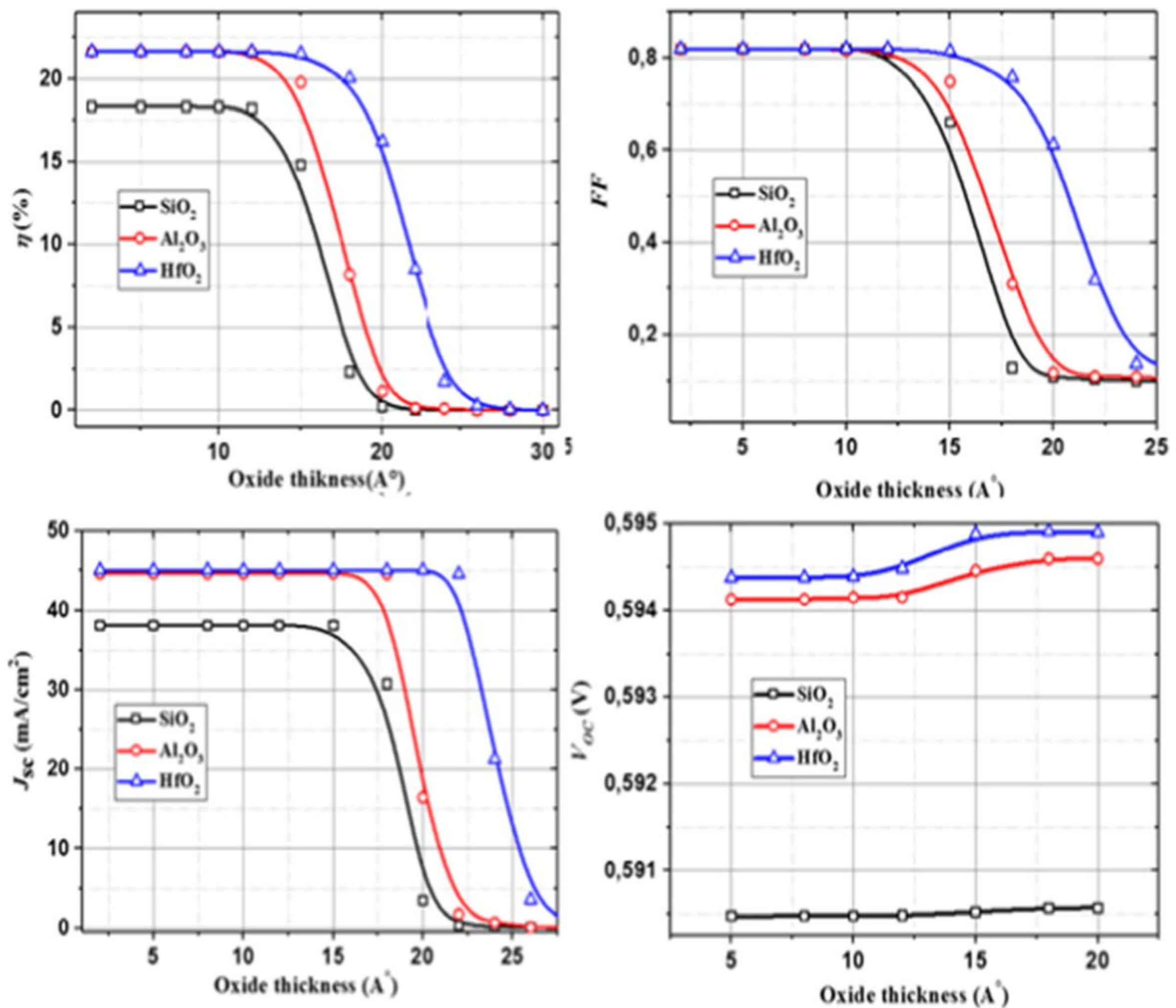

Figure IV. 5: Performance Analysis: Conversion Efficiency, Fill Factor, Short-Circuit Current Density, and Open-Circuit Voltage Behavior in Various Designs of c-Si-Based MIS Solar Cell

This outcome can be linked to the decrease in hole tunneling through the insulator layer as the oxide thickness increases. This provides an explanation for the observed trend. Furthermore, as the oxide thickness increases, it leads to a reduction in photo-generated current and induces band bending within the absorber region. Moreover, there is a tendency for a greater voltage drop across the insulator layer with increasing oxide thickness [11-12].

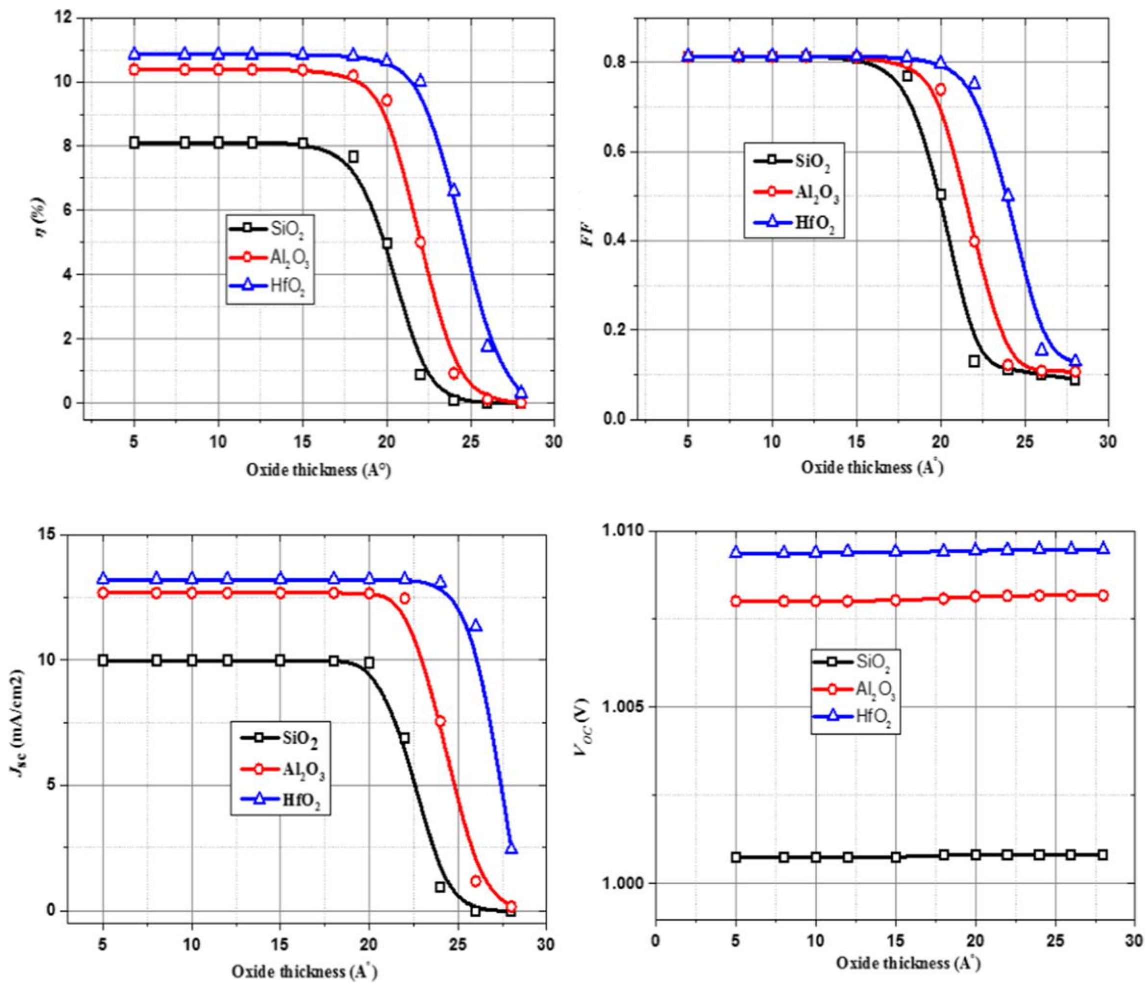

Figure IV. 6: Performance Analysis: Conversion Efficiency, Fill Factor, Short-Circuit Current Density, and Open-Circuit Voltage Behavior in Various Designs of (a-Si:H)-Based MIS Solar Cells

To elucidate the impact of high-k dielectrics on enhancing the performance of an MIS solar cell, Figure IV.5 illustrates variations in conversion efficiency (η), fill factor (FF), open-circuit voltage (Voc), and short-circuit current (Jsc) with different oxide material thicknesses ranging from 5 to 25. In other words, a smaller current can tunnel through a thicker oxide, leading to poor cell efficiency. For insulating thicknesses below 15 Å, efficiency rapidly increases as the insulating thickness decreases until it saturates at around 21.85% for c-Si and 13.1% for a-Si:H.

The utilization of high-k dielectrics significantly enhances the output J-V characteristics of an MIS solar cell, emphasizing the pivotal importance of high-k dielectrics in enhancing the overall device performance [13].

The open-circuit voltage remains unaffected by the oxide thickness due to its extremely thin nature, which has minimal impact on the doping densities, as shown in the equation below.

$$V_{OC} = \frac{nKT}{q} \ln\left(\frac{J_{LIGHT}}{A^{**}T^2} + \frac{q\phi_{bp}}{KT} + \sqrt{q\phi_{bp}}\, d_{OX} \right) \quad \text{(IV-1)}$$

V_{OC} is mostly constant. Through our investigation, we have determined that the illumination characteristics of the device, in relation to the insulator thickness, define the range of insulator thicknesses in which the device exhibits efficient solar cell behavior. This range may extend from 10 to 15Å.for the c-Si, and from 10 to 20Å for the a-Si:H Below 10Å, the device behaves like a Schottky-diode, As the insulator thickness increases, the device gradually transitions to operating as an equilibrium tunnel diode [14].

This is mainly due to the counterbalanced effect between the increased J_{SC} and the reduced V_{OC} of the proposed MIS cell. It is worth noting that the obtained results align with the existing literature data on MIS solar cells, confirming the consistency of our findings with previously reported studies [15-16]. It is also worth noting that MIS solar cells with a high insulator dielectric constant show improved minority carrier tunneling. The obtained results are significant as they validate the consistency of our findings with the existing literature data on MIS solar cells, reinforcing the agreement between our study and previously reported studies [5].

4.2. Effect of the Base Thickness:

The characteristics of two different MIS structures using $(c-Si)$and $(a-Si:H)$as active area can be compared to give a relatively closer look. FigureIV.7 demonstrates the impact of the base thickness on the J-V characteristics of an alternative MIS structure. By examining the figure, it becomes evident that the increase in cell thickness results in a rise in photo-generated carriers, subsequently leading to an improved output photocurrent density. Furthermore, the various recombination rates within the device structure subsequently impact the open-circuit voltage values [15].

To analyze the impact of cell thickness on the MIS solar cell figure of merit, Figures (IV.8) and Figures (IV.9) were examined. These figures were employed to examine how changes in the absorption layer thickness impact the electrical characteristics of the cell,

achieved through the alteration of cell thickness of 1 to 300 μm, It is observed that the short circuit current (J_{sc}) exhibits an increase as the thickness of the c-Si layer, which serves as the absorber layer for incident photons, increases. The observed increase in J_{sc} is attributed to higher carrier accumulation and improved light absorption, leading to an increased generation of charge carriers. This rise in J_{SC} directly impacts efficiency (η), resulting in an overall enhancement.

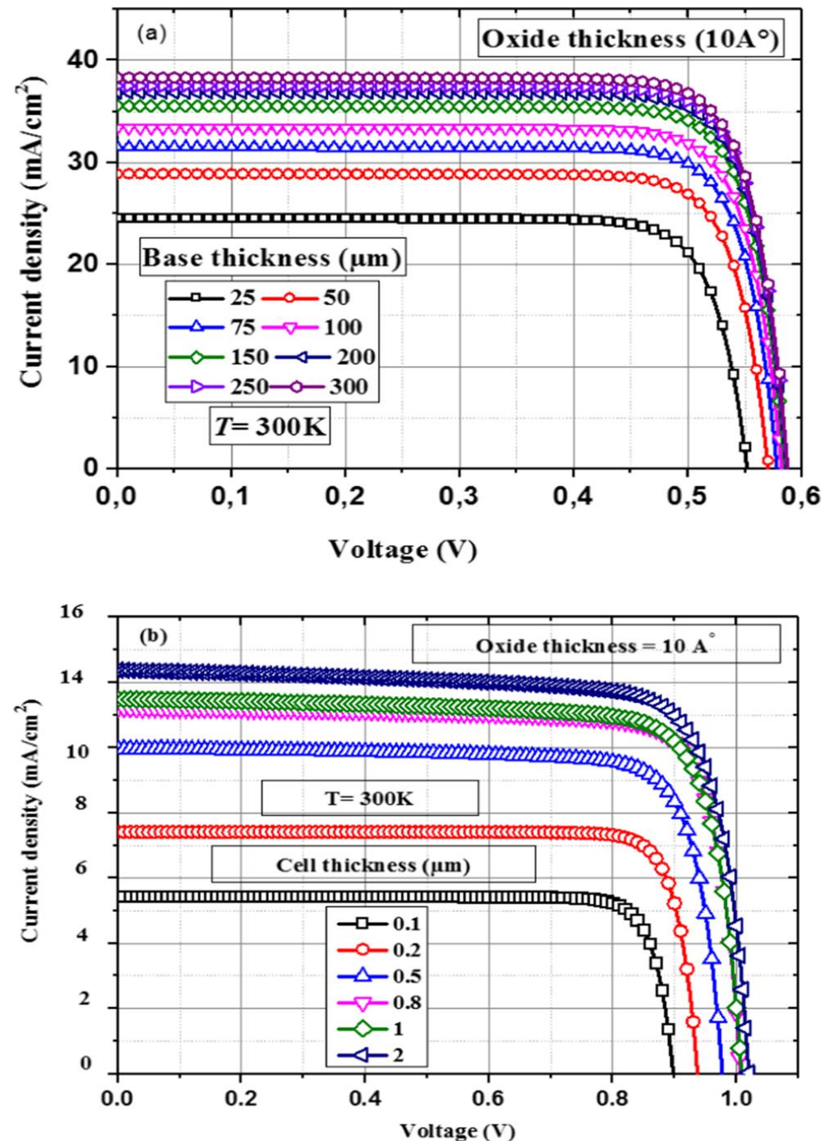

Figure IV. 7: Variations in (J-V) Characteristics of Different MIS Solar Cell Designs with Changing Cell Thickness; (a) Al-SiO2/c-Si structure, (b) Al-SiO2-a-Si:H structure.

Furthermore, it is noteworthy that the behavior of V_{oc} follows a similar trend as that of J_{sc}, which is influenced by the recombination rates within the cell [17].As the cell thickness decreases; there is a reduction in photocurrent due to reduced absorption of longer wavelength photons, resulting in a decrease in conversion efficiency. Therefore, it can be concluded that the optimum thickness for the c-Si layer is approximately 300 µm. When considering the a-Si:H-based design illustrated in Figure (IV.9), it is noted that both J_{SC} and Voc of the solar cell tend to increase with a base thickness exceeding 1 µm. This increase is attributed to the thicker a-Si:H layer's ability to absorb more photons, leading to a higher generation Efficiency, Fill Factor, J_{sc}, and Voc Behavior Across Varied Base Thicknesses

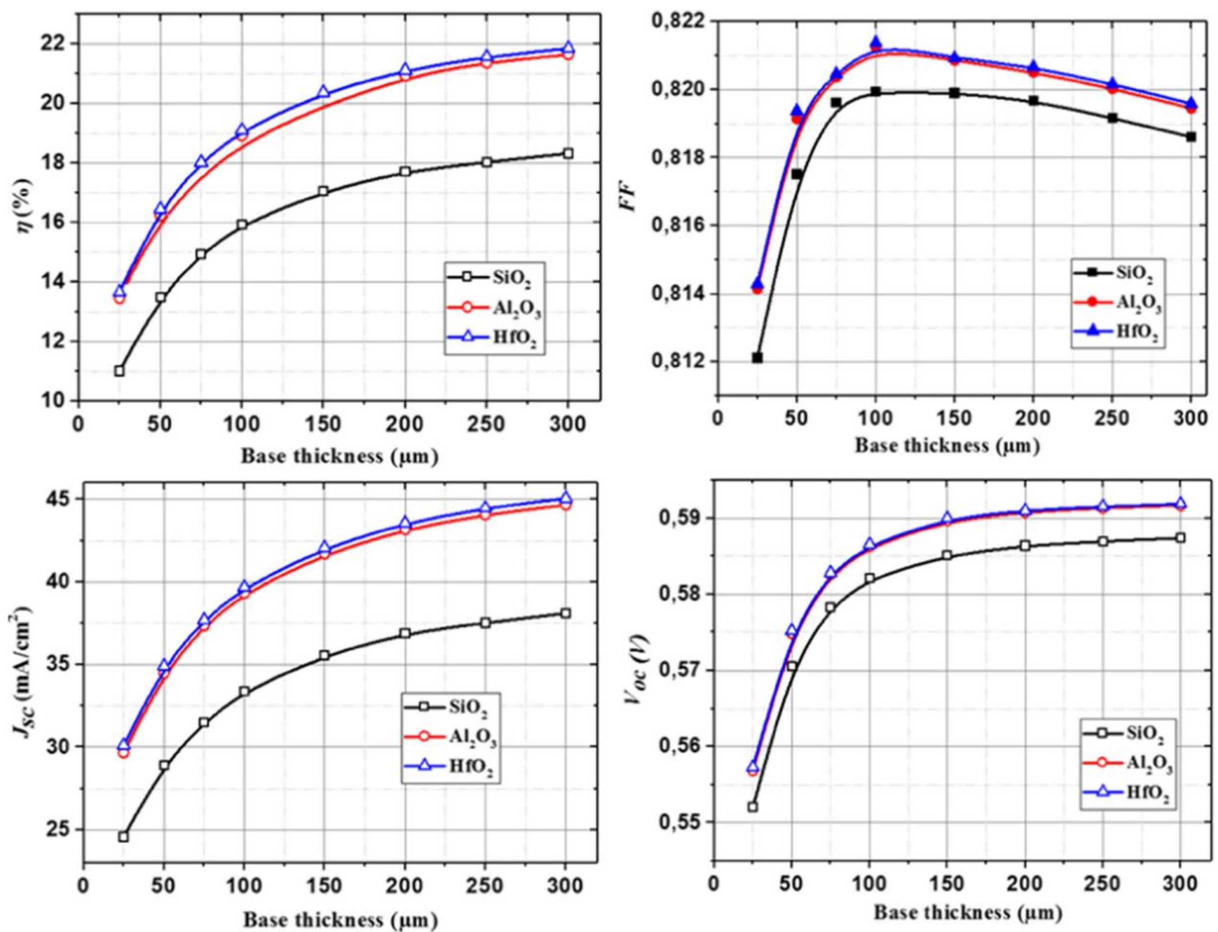

Figure IV. 8: Performance Analyses of c-Si-Based MIS Solar Cell Designs: Conversion Efficiency, Fill Factor, J_{sc}, and Voc Behavior across Varied Base Thicknesses

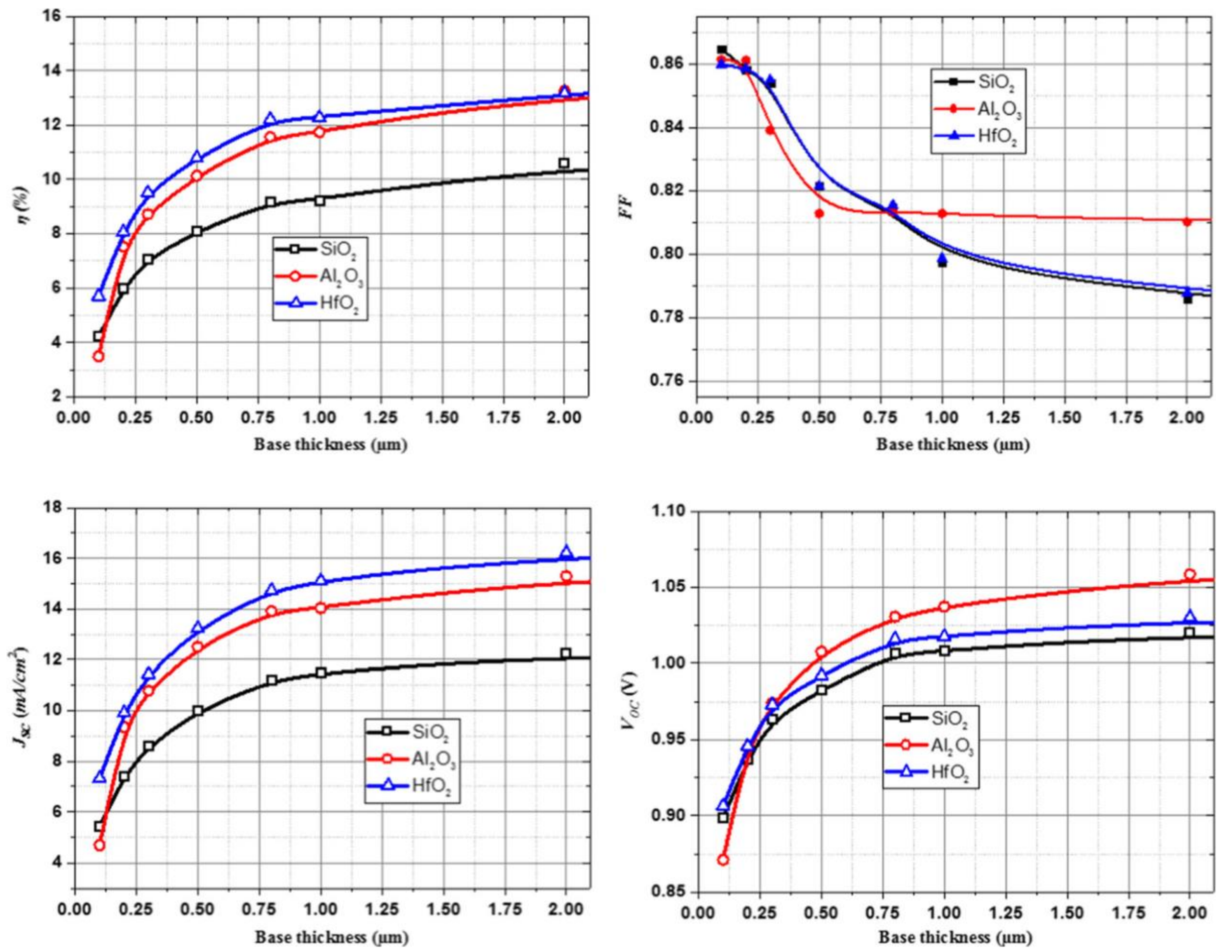

Figure IV. 9: Performance Analyses of (a-Si:H)-Based MIS Solar Cell Designs: Conversion Efficiency, Fill Factor, J_{sc}, and Voc Behavior across Varied Base Thicknesses

The conversion efficiency of the solar cell increases with the increasing base thickness, reaching a peak before eventually saturating. This saturation is attributed to the reduction in the fill factor, which is a measure of how efficiently the solar cell converts light into electricity. [18]. A more detailed analysis of the results reveals that an optimal thickness of approximately 2 µm for the a-Si:H substrate achieves maximum photon absorption and enhances the photo-generated current density of the solar cell. This is due to the thicker a-Si:H layer's increased photon absorption capability, leading to a higher generation of charge carriers. The increased photocurrent density directly enhances the effectiveness of the solar cell.

The base thickness is a critical factor that significantly impacts the overall cost of the proposed structures. The thicker the substrate, the more material is required, resulting in an

increase in the solar cell's cost. The results of the study also confirm the effectiveness of using HfO_2 as an insulator to enhance MIS solar cell efficiency through improved light absorption. The highest recorded cell efficiency reached 21.85% in Figure (IV.8) and 13.1% in Figure (IV.9), highlighting the positive impact of HfO_2 insulation on overall performance.

4.3. Influence of Doping Concentration

The doping concentration in various regions of the device plays a vital role as it induces a variation in the depletion layer, consequently affecting the current capabilities of the device (Figure.IV 10) chows, the influence of substrate doping density is evident in the J-V characteristics of both c-Si- and a-Si:H-based devices with conventional SiO2-based structures under illumination, spanning a wide range of doping concentrations in the substrate (10^{14}, 10^{18} cm^{-3}) .

Figure (IV. 10). Across all samples, the compromise between open-circuit voltage and short-circuit current represents a fundamental property of semiconductor materials. Elevating the doping level will tilt the equilibrium towards favoring open-circuit voltage, but at the expense of short-circuit current, due to the narrowing of the depletion region caused by higher doping density

Doping can diminish the quantity of charge carriers available for photo excitation, and also reduce the mobility of the charge carriers that are present, resulting in significant recombination effects. The observed improvement in open circuit voltage primarily stems from a reduction in saturation current [19]. This investigation focuses on the detailed analysis of how doping affects the electrical results of the suggested solar cell, considering various dielectric materials with a thickness of (10 angstroms) thick, as shown in Figure IV.11.

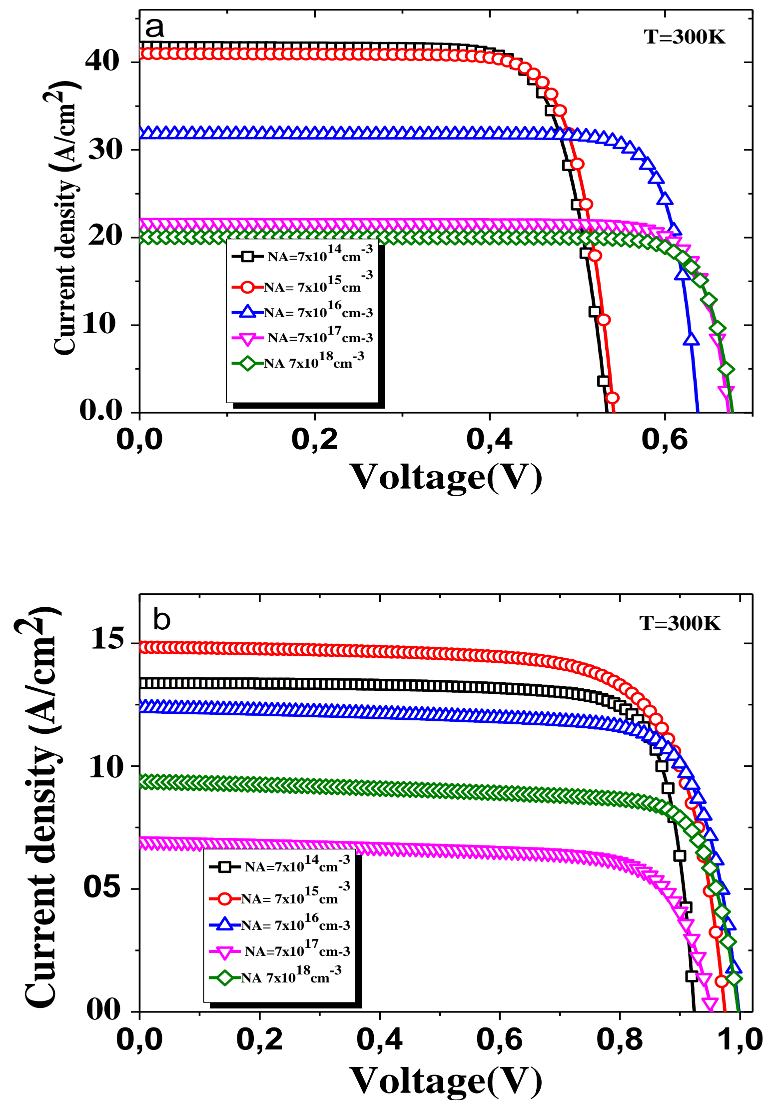

Figure IV. 9: J-V characteristics of theSiO2-based MIS solar cell as a function of the substrate doping. a)- Al-SiO₂-p(c-Si), b)- Al-SiO₂-p (a-Si: H).

Figures (IV.11) and (IV.12) illustrate the dependence of the obtained efficiency (η), short-circuit current density (J_{SC}), open-circuit voltage (V_{OC}), and fill factor (FF) on the absorber doping concentration (N_A) of both the c-Si and the (a-Si:H)-based MIS solar cell. The findings indicate a positive correlation between doping density and efficiency, with the efficiency increasing until reaching a specific threshold, beyond which it starts to decline. This can be primarily attributed to the enhanced light absorption and improved electrical mobility of both electrons and holes.

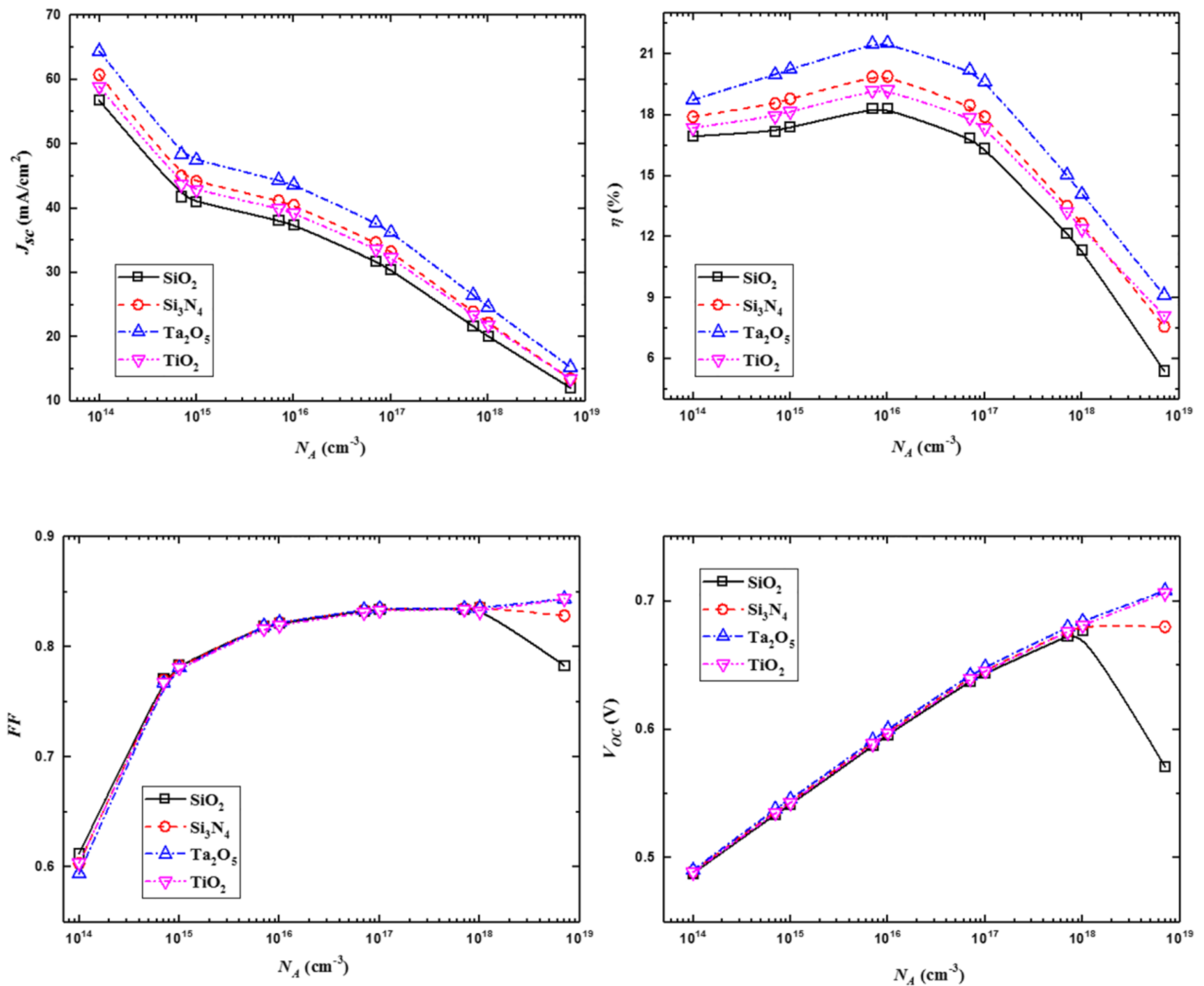

Figure IV. 10: the output characteristics of the suggested MIS solar cell, utilizing various high-k materials, in relation to the substrate doping levelsfor $(c-Si)$.

The a-Si:H-based MIS solar cell exhibits a performance that is comparable to that of the c-Si-based MIS solar cell. The fill factor and open-circuit voltage of a MIS solar cell are inversely proportional to the doping concentration. The increased doping levels also lead to an increase in the number of recombination centers, which reduces the carrier lifetime; the increase in interface state density causes more photo-generated carriers to recombine at the interface, which reduces the number of carriers that can flow through the solar cell.

This leads to a decrease in the short-circuit current, which is a measure of the amount of current that the solar cell can produce under ideal conditions. The decrease in short-circuit current also leads to a decrease in efficiency. [20-21].

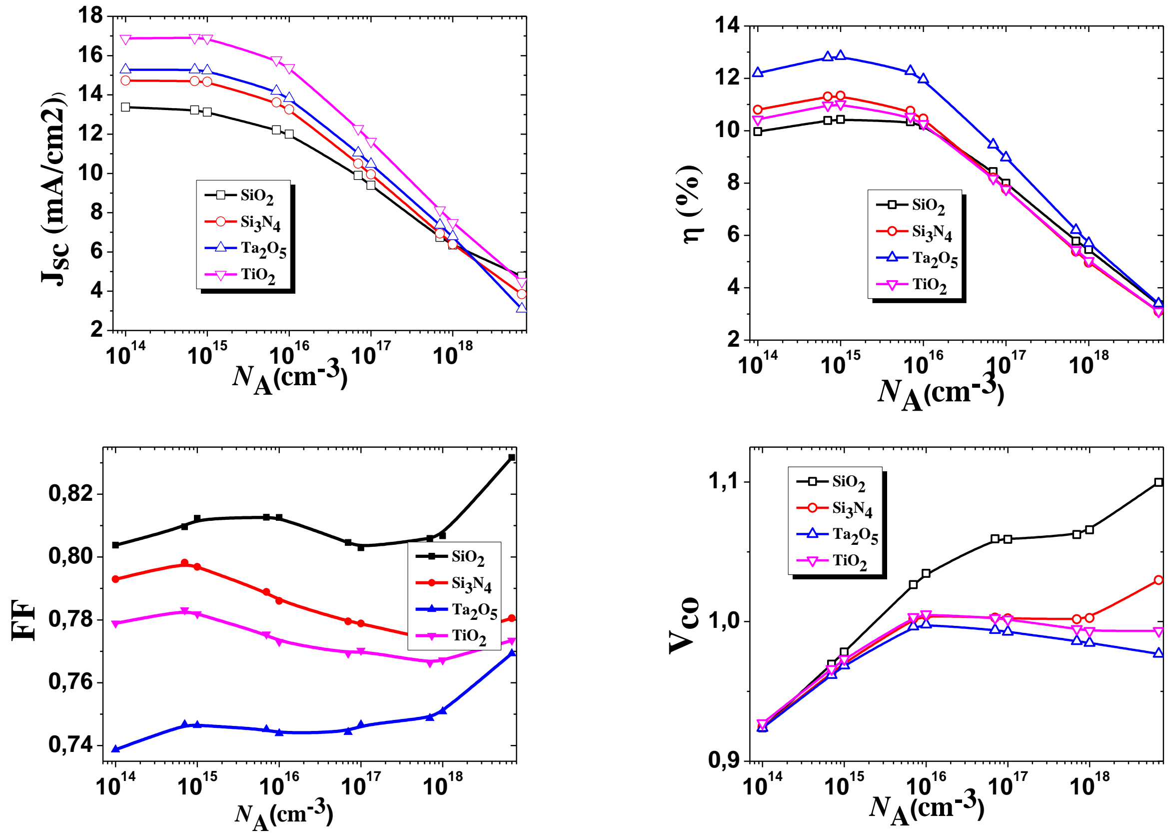

Figure IV. 11: the output characteristics of the suggested MIS solar cell, utilizing various high-k materials, in relation to the substrate doping levelsfor (a-Si: H).

Meanwhile, the relationship between these parameters can be expressed as follows:

$$\tau_p = \frac{\tau_{P_0}}{1 + \left(\frac{NA}{N0B}\right)} \qquad \text{(VI. 2)}$$

$$\mu = \mu_{\min} + \left(\frac{\mu_{\min} + \mu_{\max}}{\left(1 + \frac{NA}{N0B}\right)^{\alpha}}\right) \qquad \text{(VI. 3)}$$

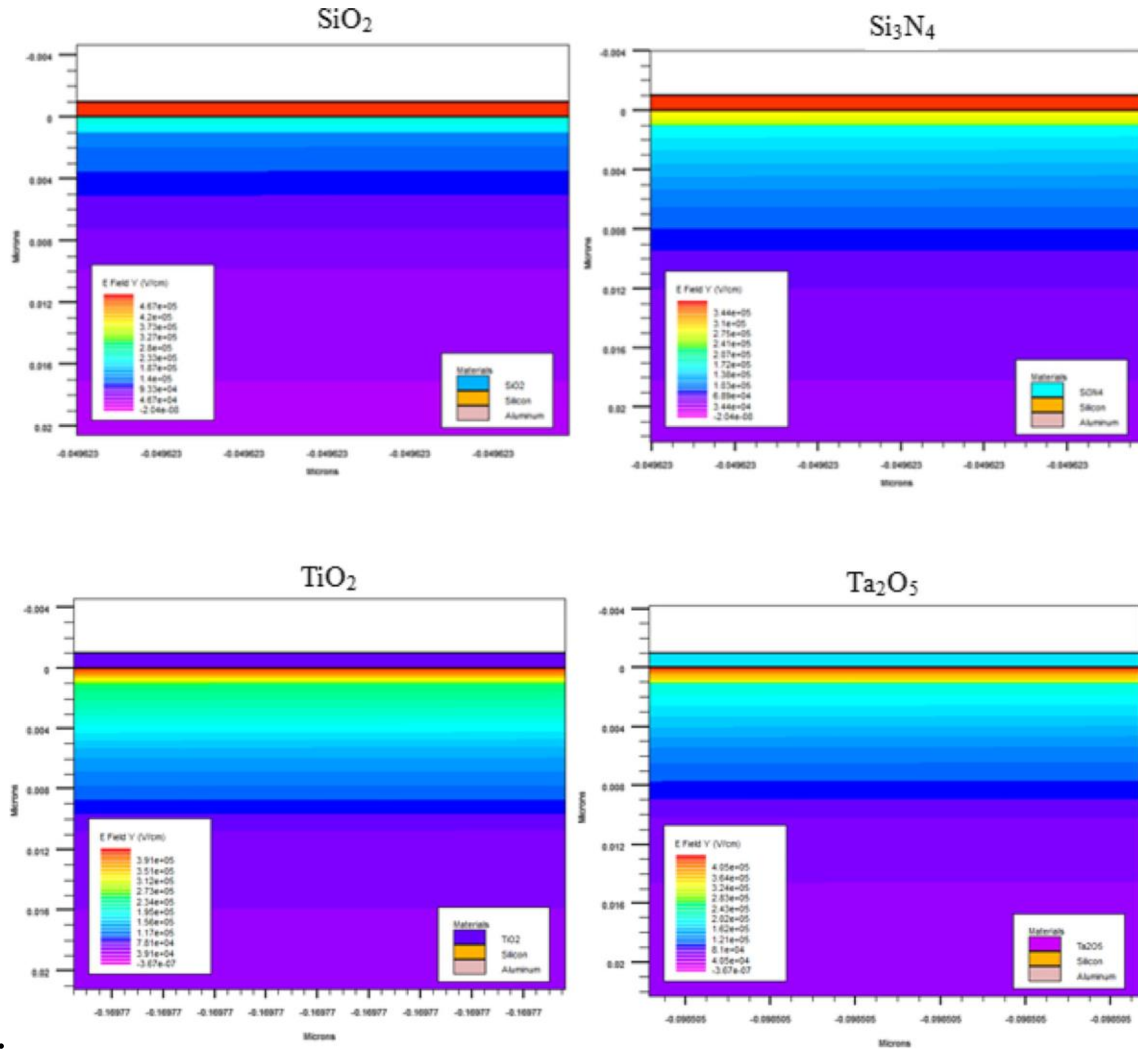

•

Figure IV. 12: demonstrates the distribution of electric fields within the device for various materials. $(c-Si)$

This parameter is defined as $L_P = (D_P \tau_P)^{1/2}$ and $D_p = \mu\left(\frac{KT}{q}\right)$ where μ represents the hole mobility. [21-22]

Observing the solar cell configurations, it becomes evident that the one utilizing Ta_2O_5 as the oxide film achieves the highest efficiency. This outcome is attributed to the improved short-circuit current, primarily attributed to Ta_2O_5 high transparency (Eg = 4.4 eV) and its favorable conduction band alignment with silicon (ΔEC = 1.5 eV). The average efficiency of MIS solar cells increased from 18.30% for SiO_2 to 21.54% for Ta_2O_5. The efficiency of TiO_2 and Ta_2O_5-based solar cells did not decrease because of their elevated conductivity.

The separation of photo-generated charge carriers is intricately linked to the electric field which is created across the p-n junction in thermodynamic equilibrium. Specifically, under illumination, the electric field acts to drive free electrons into the n-type region and holes into the p-type region. This is how the solar cell converts light energy into electrical energy.

Figures (IV.13) and figure (IV.14) illustrate the distribution of the electric field in c-Si and a-Si:H solar cells using various dielectric materials (SiO_2, Si_3N_4, TiO_2, and Ta_2O_5). The figures show that the electric field is strongest at the p-n junction and decreases as you move away from the junction. This is because the p-n junction is where the majority carriers (electrons in the n-type region and holes in the p-type region) are separated.

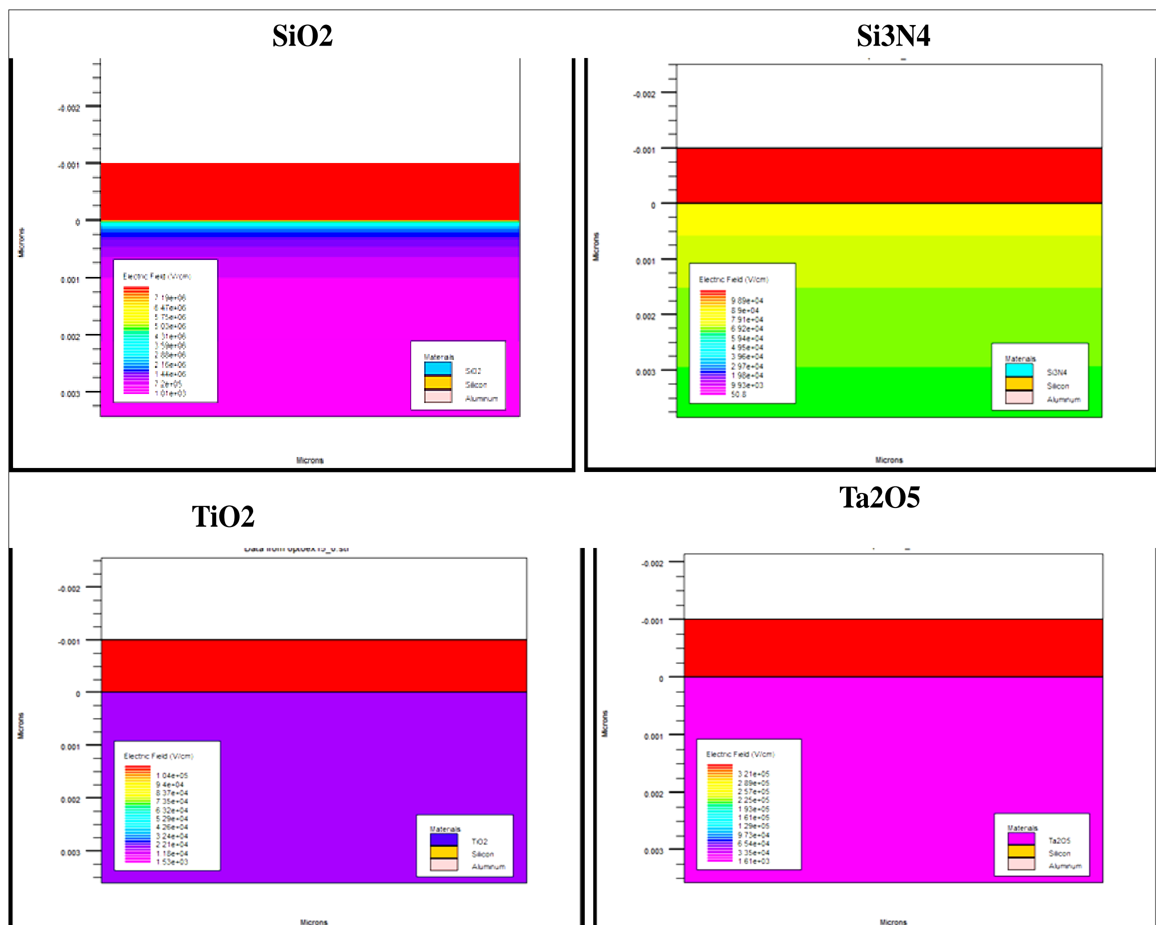

Figure IV. 13: demonstrates the distribution of electric fields within the device for various materials. (a-Si: H)

4.4. Interface States Effects

The transport properties of the proposed solar cell are significantly influenced by the density of interface states (D_{it}) at the dielectric/semiconductor interface. D_{it} is a measure of the number of defects at the interface. These defects can trap electrons and holes, which can lead to a decrease in the efficiency of the solar cell.

Through further research and development of these thin insulator diodes, it is anticipated that significant reductions in D_{it} can be achieved, similar to the observed trend in conventional MIS devices over the past decade. These surface states, which represent defects, can be effectively minimized with continued efforts.

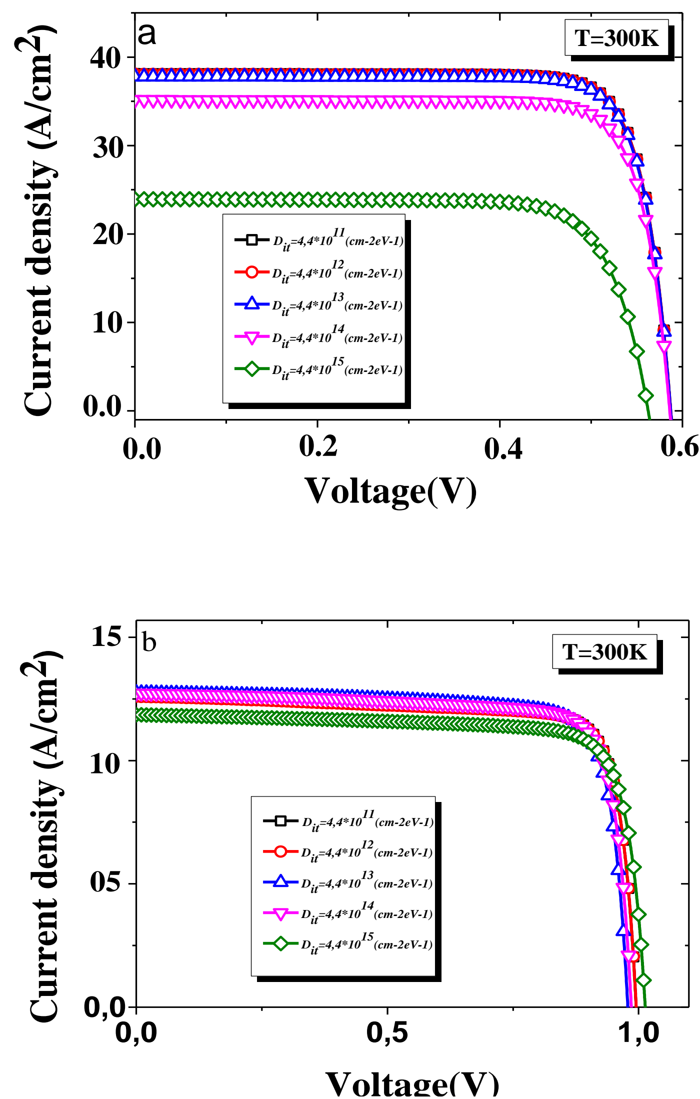

Figure IV. 14: J-V characteristics of the SiO2-based MIS solar cell for different interface state densities. a)- Al-SiO_2-p(c-Si), b)- Al-SiO_2-p (a-Si: H).

FigureIV 15 depicts the device J-V characteristics of the conventional solar cell (SiO_2-based) for an interface trap density D_{it} of both the c-Si- and a-Si:H-based ranging from 10^{10} cm^{-2} eV−1 to 10^{18} cm^{-2} eV^{-1}. From this figure, it is remarkable that for interface state densities in the limit of 10^{14} cm^{-2} eV^{-1}, Jsc and Voc are not influenced, whereas for D_{it}> 10^{14} cm^{-2} eV^{-1} Jsc is reduced harshly.

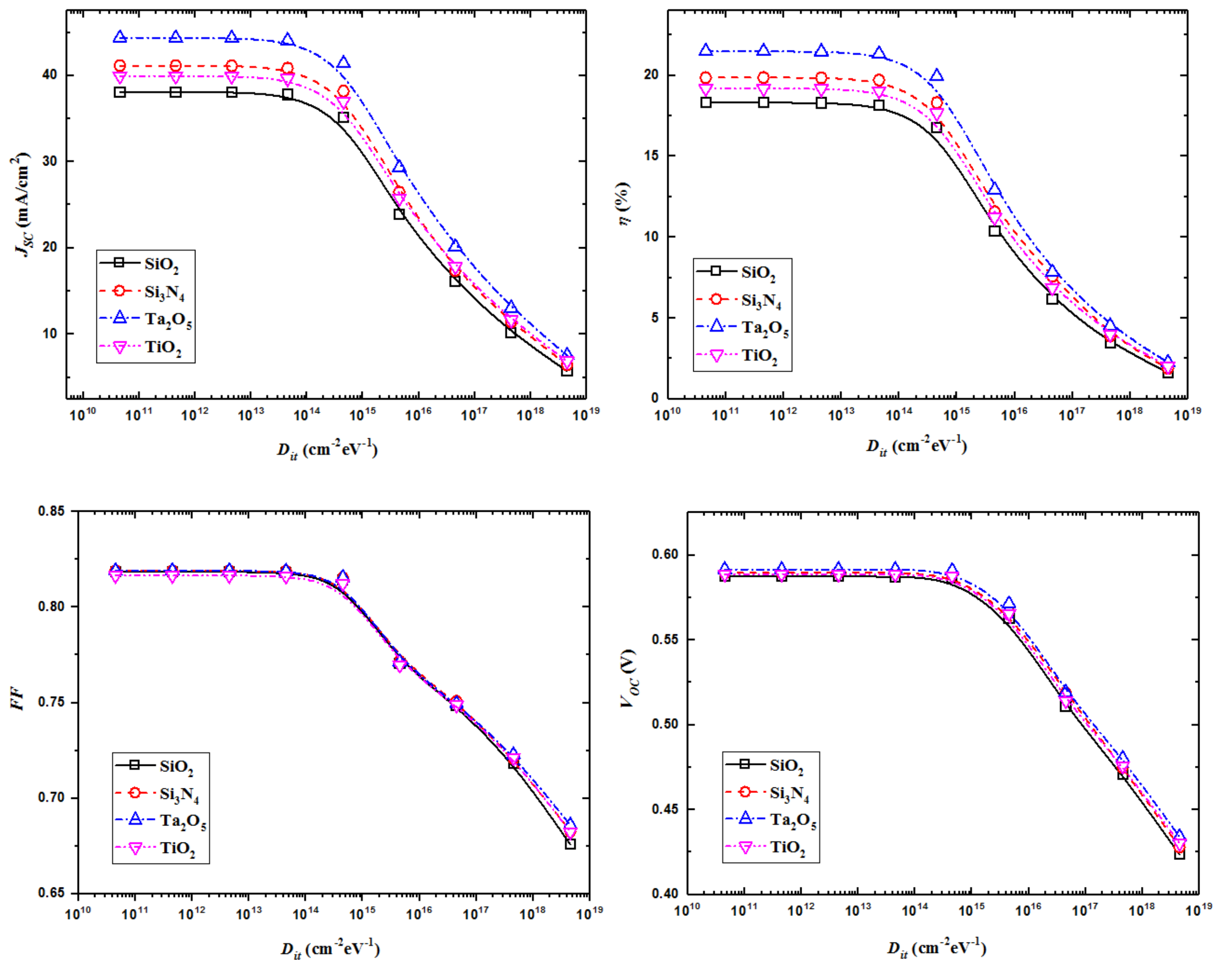

Figure IV. 15: the output characteristics of the suggested MIS solar cell, utilizing various high-k materials, in relation to the interface state density for (c-Si).

The observed outcome can be attributed to heightened recombination effects occurring at the interface. Consequently, the open-circuit voltage (V_{OC}) is impacted, primarily due to the rise in dark current resulting from the improved transport of majority carriers, attributed to the interface states functioning as generation-recombination centers. Notably, in a-Si:H, this effect is intensified due to an increased rate of recombination at defect sites caused by dangling bonds within the intrinsic layer. These defects disrupt the electric field within the

intrinsic layer, ultimately causing a reduction in the photo-generated current produced by the solar cell [22].

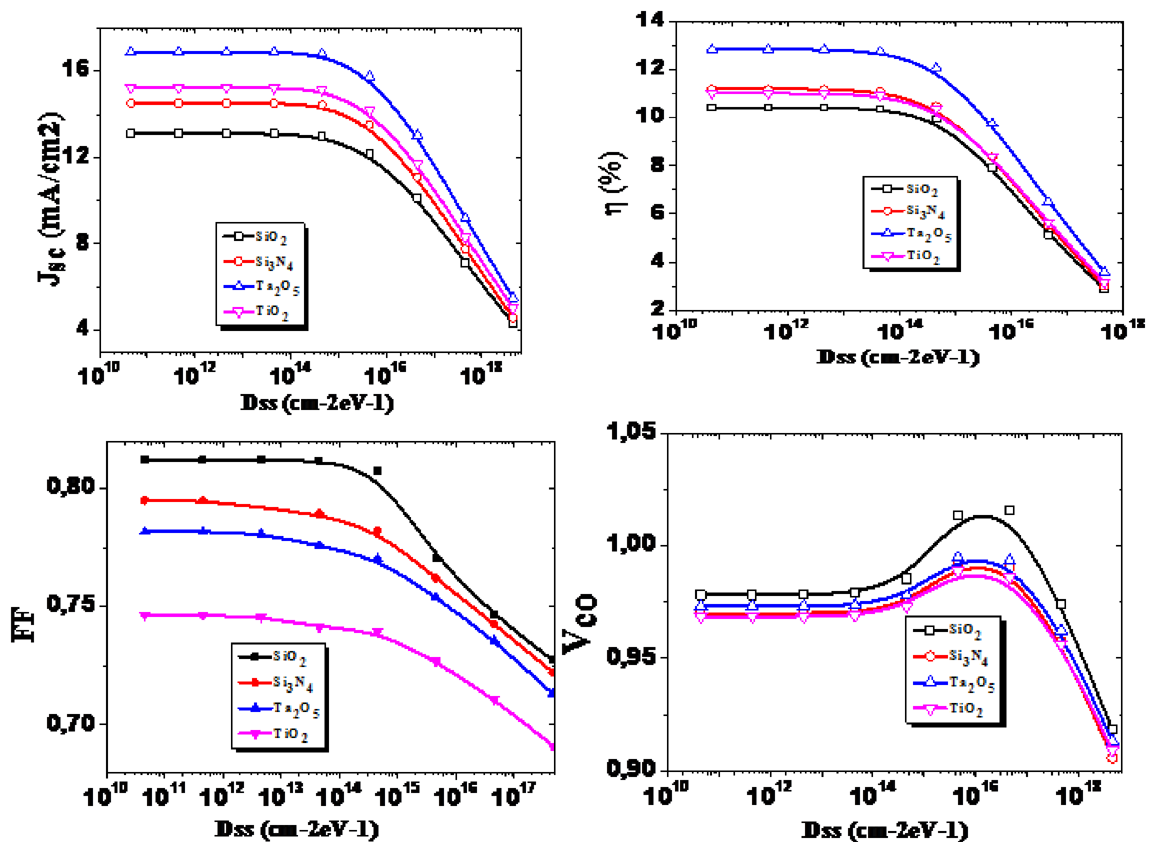

Figure IV. 16: the output characteristics of the suggested MIS solar cell, utilizing various high-k materials, in relation to the interface state density for (a-Si:H).

Figure (IV.16) the figure presented illustrates the electrical performance of the envisaged solar cell can vary when employing different dielectric materials, such as SiO_2, Si_3N_4, Ta_2O_5, and TiO_2. It is noteworthy a significant impact on the device's performance metrics is observed with an increase in trap density. The efficiency decreases for the traditional solar cell from 21, 54% for D_{it} = 10 ^{14} cm^{-2} eV^{-1} to 2.6% for D_{it}=5 × 10 ^{18} cm^{-2} eV^{-1}. D_{it} The increase in D_{it} density leads to a significant increase in dark current, which in turn causes a decrease in efficiency, fill factor, and open-circuit voltage, as depicted in Figure IV.16. This degradation in performance can be primarily attributed to the heightened recombination rate, which adversely affects the electrical outputs of the device. Furthermore, Figure IV.17 provides additional insights based on the obtained results.

The efficiency of Si-based solar cells may be greatly increased when Ta_2O_5 is used as the high-k dielectric material instead of SiO_2, which is the industry standard. Ta_2O_5 is recognized for its high conductivity and transparency. By using Ta_2O_5, it is possible to increase the short-circuit current (J_{SC}) from 39 mA/cm^2 to 44.35 mA/cm^2, resulting in a conversion efficiency of 21.547%. Along with these significant advancements, the solar cells fill factor (FF) and open-circuit voltage (V_{OC}) also saw significant increases.

4.5. Impact of Fixed Oxide Charges

The electrical characteristics of p-Si MIS solar cells utilizing SiO_2 as the insulator are influenced by the quality of the Si/SiO_2 interface. This interface can be characterized by the fixed oxide charge density (N_{fix}), which is determined by factors such as the oxidation process and silicon orientation [21].

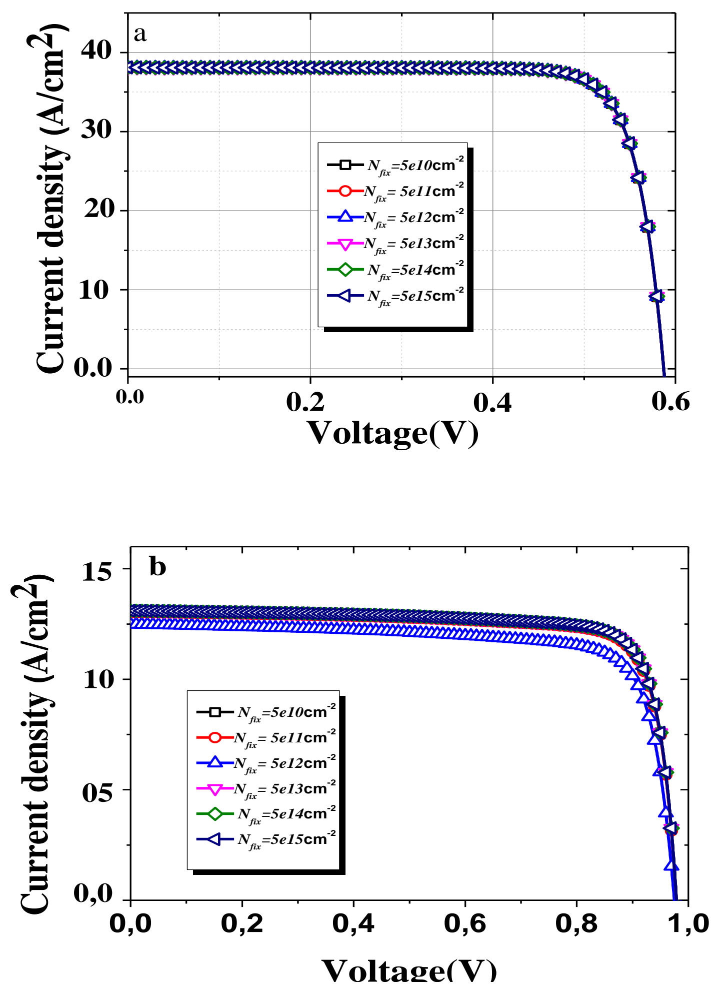

Figure IV. 17: J-V characteristics of the conventional MIS solar cells for different oxide charge: a- Al-SiO_2-p(c-Si), b- Al-SiO_2-p(a-Si:H)

. In this part, the performance of the proposed solar cells of both the c-Si- and a-Si:H-based devices is examined in relation to the effective fixed charge. (Nf_{ix}), Figure (IV. 20) the presented figure displays the current-voltage (J-V) characteristics for various fixed oxide charge densities. It is evident from the figure that the short circuit current (Jsc) and open-circuit voltage (Voc) remain constant; with no significant variation in the fill factor (FF). This lack of substantial change in FF can be attributed to the negligible alteration in the surface potential.

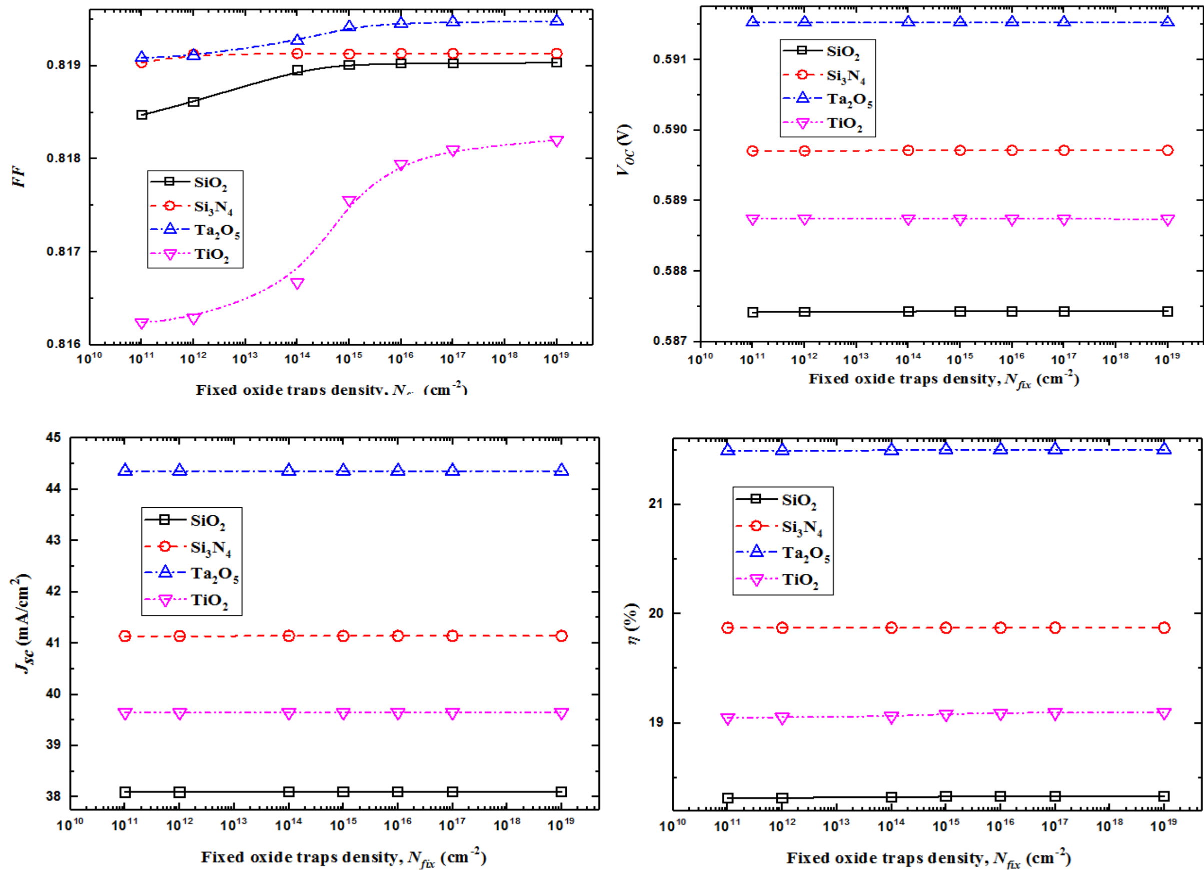

Figure IV. 18: Effect of Oxide Fixed Traps Density on the Output Characteristics of MIS Solar Cells Utilizing Different High-k Materials Compared to c-Si -Based MIS Solar Cell

The evolution of the solar cell efficiency with the dielectric fixed charged density (N_{fix}) of the samples is plotted in Figure (IV.18).and figure (IV.19) This figure shows the conversion efficiency (η), fill factor (FF), open circuit voltage (Voc), and short circuit current (Jsc) of SiO_2 of a 10 A° thickness replaced by different dielectrics in terms of Ta_2O_5, Si_3N_4 and TiO_2 and changing the fixed charged (N_{fix}) from 10^{10} to 10^{15} cm^{-2}. The results obtained from both c-Si and a-Si:H samples clearly indicate that incorporating high-k dielectric

materials leads to improved device performance, with Ta_2O_5 demonstrating the highest performance among the simulated dielectric materials [24].

Incorporating high-k dielectric materials into a-Si:H solar cells can enhance their open-circuit voltage and overall efficiency by mitigating charge carrier losses, as illustrated in Figure (IV.20). However, the existence of a fixed oxide charge density (N_{fix}) is unlikely to significantly affect the performance of solar cells, since it does not substantially disrupt the near-equilibrium conditions at the semiconductor-oxide interface.

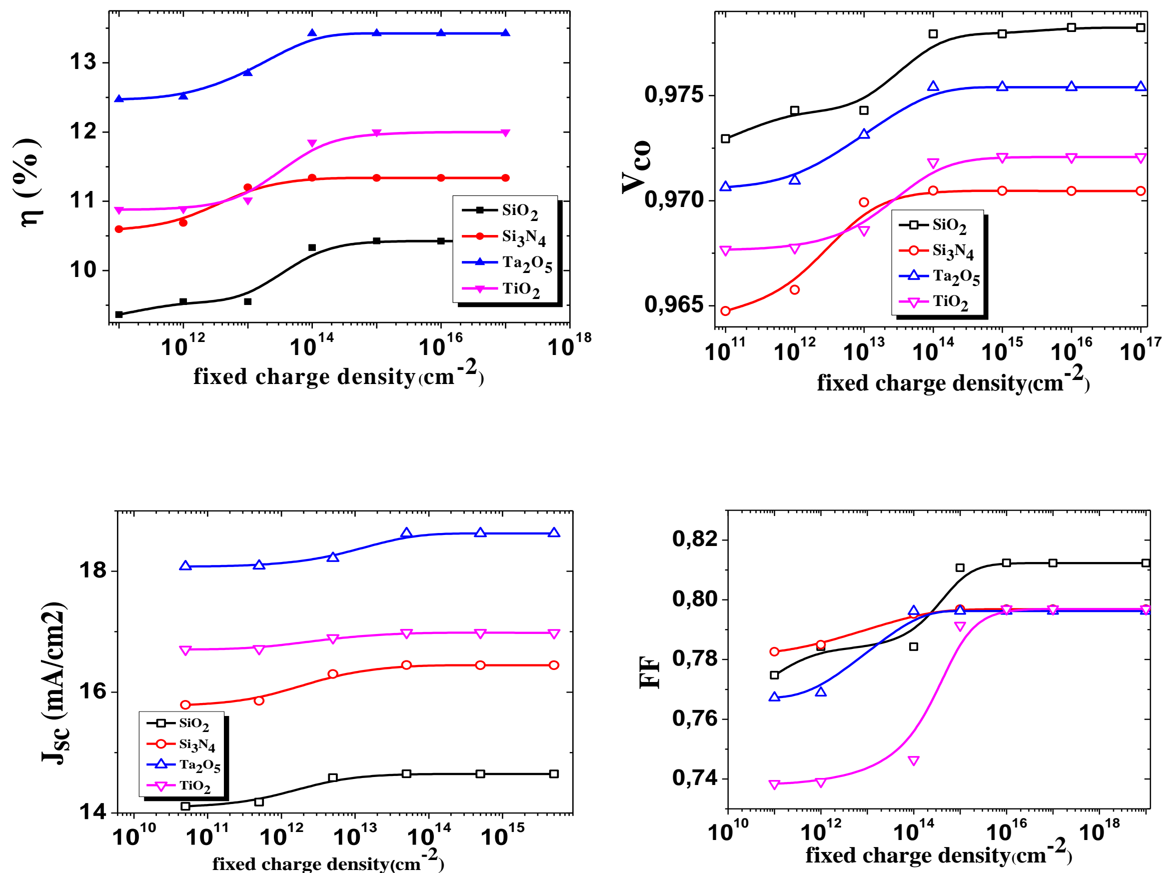

Figure IV. 19: J-V characteristics of the conventional MIS solar cells: a- Al-SiO_2-p(c-Si), b- Al-SiO_2-p(a-Si:H)

4.6. Effect of Metal Work Function

The metal work function in MIS solar cells is known to be a crucial parameter that affects the device's figures of merit. The influence of the metal work function on the J-V

characteristics of the investigated solar cells, which employ SiO2 as an oxide in both the c-Si- and a-Si:H-based devices, is plotted in Figure (IV. 21). The metal work function varies from 4.1 eV to 4.6 eV for a fixed configuration of insulator thickness (10 A°). It is noted from figure 23 that V_{OC} and FF drop significantly. When the value of the work function exceeds 4.4 for c-Si and 4.2 for a-Si:H .

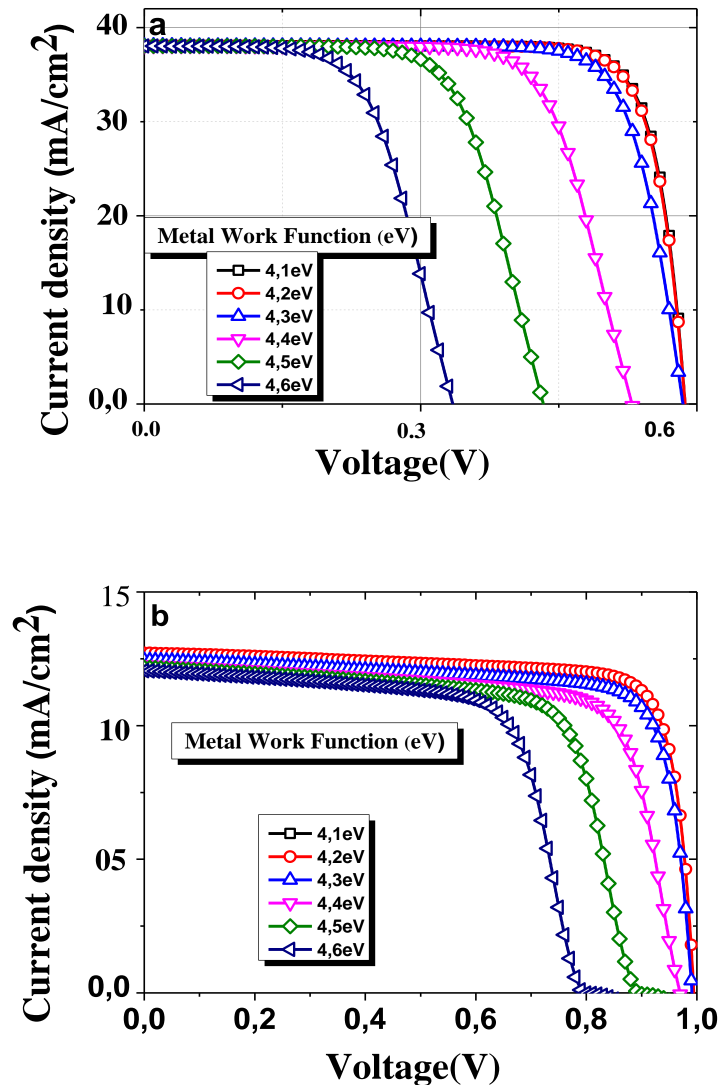

Figure IV. 20: I-V Characteristics of SiO_2-Based MIS Solar Cell Across Various Work Functions a- Al-SiO_2-p(c-Si), b- Al-SiO_2-p(a-Si:H)

Figures IV.22 and IV.23 illustrate how the open-circuit voltage (Voc), short-circuit current density (Jsc), fill factor (FF), and efficiency (η) change with various work functions under the AM1.5G solar spectrum using dielectric materials TiO_2, Si_3N_4, and Ta_2O_5. The metal work functions (Φ_m) considered in this research are less than 4.4 eV. Under

illumination, the dark current density (J_{dark}) can be neglected ($J_{sc} \approx J_{Light}$). The selective energy barriers at the contact layers ensure that the photo-generated carriers are collected efficiently, which leads to improved solar cell

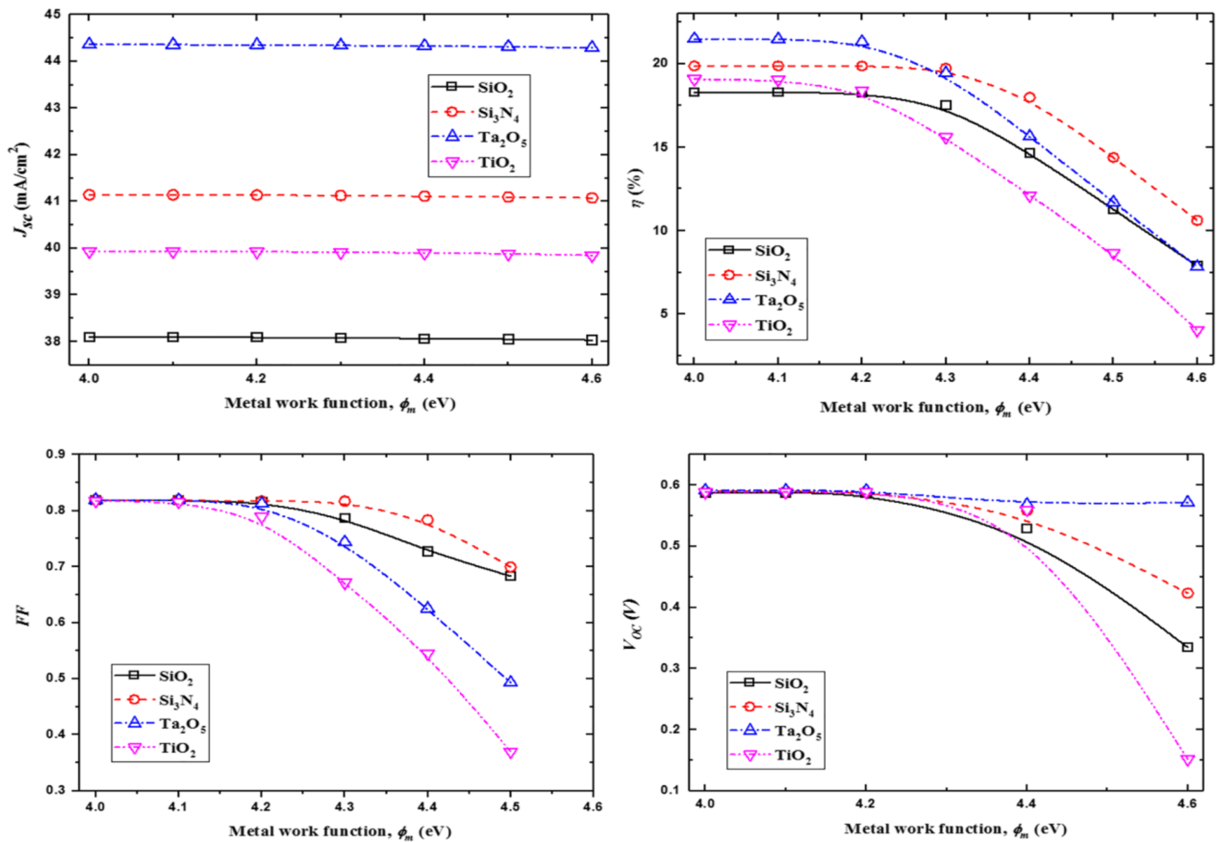

Figure IV. 21: Comparison of Output Characteristics of MIS Solar Cells Utilizing Different High-k Materials with the Metal Work Function Value of (c-Si) -Based MIS Solar Cel

When the work function of the metal electrode is in the range of 4.4 to 4.6 eV, the open-circuit voltage (Voc), fill factor (FF), and conversion efficiency all decrease. This is because the barrier height between the metal electrode and the semiconductor increases in this range, which hinders the flow of electrons from the metal electrode to the semiconductor. However, the short-circuit current density (Jsc) is a measure of the number of photo-generated carriers, and the work function of the metal electrode does not affect the number of photo-generated carriers.

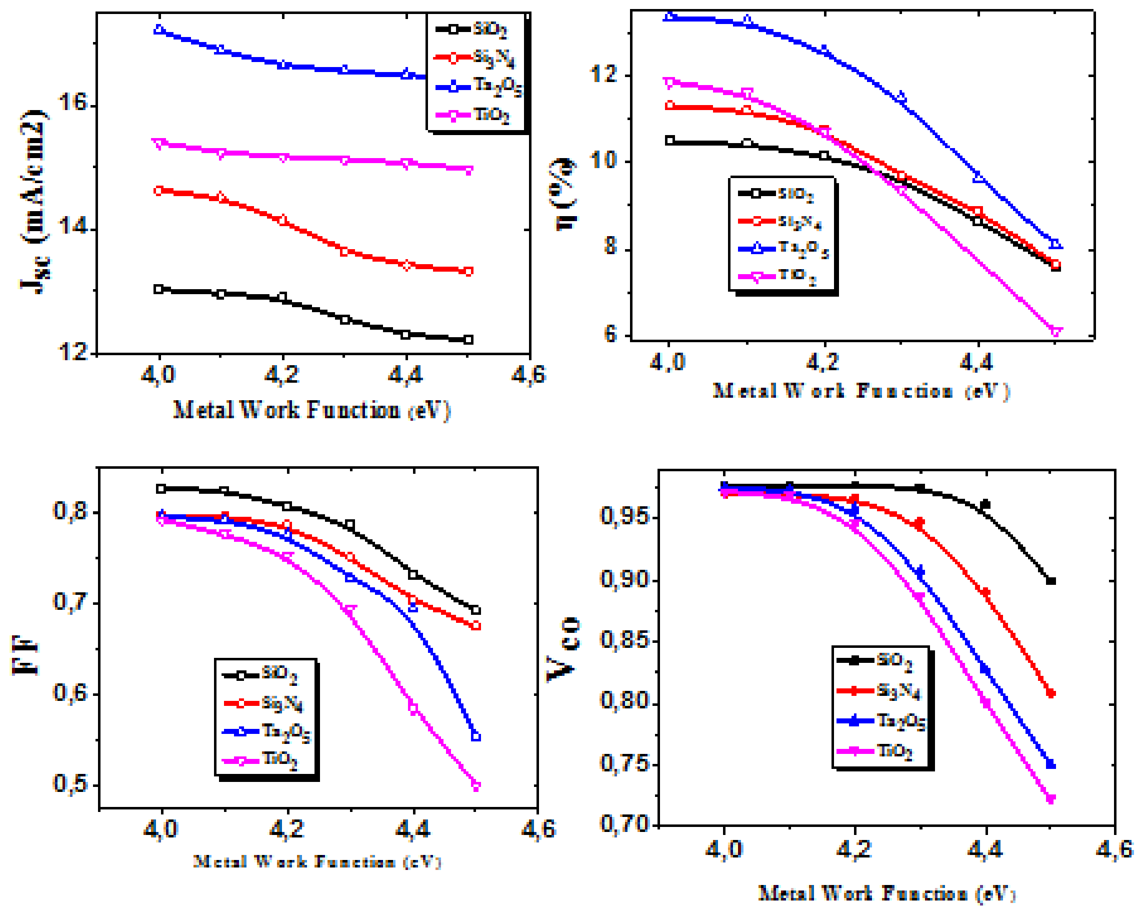

Figure IV. 22: Comparison of Output Characteristics of MIS Solar Cells Utilizing Different High-k Materials with the Metal Work Function Value of a-Si:H-Based MIS Solar Cell

Under illumination, the presence of photo-generated electrons in the silicon cell causes an inversion layer to form at the front surface. The inversion layer creates a potential barrier that prevents electrons from flowing from the metal electrode to the semiconductor, which results in an increase in the dark current density (J_{dark}).

Although the barrier height increases, due to enhanced carrier recombination, the semiconductor surface remains inverted, which ensures that Jsc is still relatively high even when the work function is high. This is because the inversion layer is still able to generate a large number of photo-generated carriers.

Ta_2O_5 scores the highest efficiency at 21.54%, followed by Si_3N_4, TiO_2, and SiO_2. This means that all the high-k candidates show excellent device performance, with low-work-function

Ta_2O_5 being the best material to be utilized compared to SiO_2. This is because Ta_2O_5 has a lower work function than SiO_2, which means that the barrier height between the metal electrode and the semiconductor is lower. This results in a higher Voc, FF, and efficiency.

The research findings emphasize the need to carefully consider the work function and dielectric constant, and the structural design of materials in order to effectively enhance the charge density. This is because the work function and dielectric constant of the material play a role in determining the barrier height between the metal electrode and the semiconductor. The structural design of the material can also affect the charge density by influencing the way in which the electrons and holes are transported through the material.

The observation reveals that for a-Si:H, there is a significant degradation in efficiency when the energy of the photons exceeds 4.2 eV. This is because the bandgap of a-Si:H is 1.7 eV, which means that it can only absorb photons with energies of 1.7 eV or higher. When photons with energies of 4.2 eV or higher strike the a-Si:H cell, they are not absorbed and instead pass through the cell, resulting in a loss of efficiency.

The change in the efficiency degradation slope can be attributed to the changes in the effective barrier height that the charge carriers experience. When the energy of the photons exceeds the band gap of the semiconductor, the effective barrier height increases, this results in a larger number of electrons and holes being reflected back into the semiconductor, which reduces the efficiency of the cell

5. Solar cells spectral response

The spectral response quantifies the ratio of collected carriers to the incoming photon flux at a specific wavelength, expressed as follows [25]: where $J_{SC}(\lambda)$ stands for short-circuit current density, $SR(\lambda)$ denotes spectral response, $R(\lambda)$ represents the reflection coefficient, and $P(\lambda)$ signifies incident power. The external quantum efficiency (QE) was determined using the given relationship:

$$SR_{in}(\lambda) = \frac{J_{sc}(\lambda)}{p_g(\lambda)(1 - R(\lambda))} \quad \text{(VI.4)}$$

λg is the wavelength corresponding to the energy band gap h is Planck's constant, c is the speed of light, q is the electronic charge, In other words, the band gap energy is equal to the energy of a photon with a wavelength of λ_g.

In Figure (IV, 24), the two proposed cell structures have distinct spectral responses in the 0.2-1.2 µm wavelength range, which can affect their performance. For the c-Si-based design, the spectral response experiences an initial increase as the wavelength extends up to 0.5 µm, followed by a decline toward zero for λ around 1 µm. On the other hand, for the a-Si:H-based design, the peak spectral response is observed around 0.7 µm, with a steeper decrease beyond this point.

As is commonly understood, the peak spectral response corresponds to the lowest reflection value. This decrease in reflection is primarily attributed to the optical alignment at the interface separating the oxide layer and the semiconductor, causing the light's electric field to redirect and concentrate within the solar cell's active layer. Consequently, this reduction in reflection results in an elevation of the short circuit current (J_{SC}) [26]. Based on the findings from the initial part of the study, it can be inferred that integrating a slender insulating layer (with a thickness of 10-15 angstroms) enhances both the open-circuit voltage and the short-circuit current of the solar cell. This result in an enhanced spectral response for the device configurations examined.

However, when a thicker insulator is used, it disrupts the tunneling current, preventing a gradual reduction in the short-circuit current. This ultimately leads to a significant decline in the spectral response across the entire range of wavelengths investigated [27].

Additionally, the MIS solar cell based on a-Si:H exhibits reduced quantum efficiency owing to the presence of defects, which further contributes to the deterioration of the short circuit current density.. [28- 29].

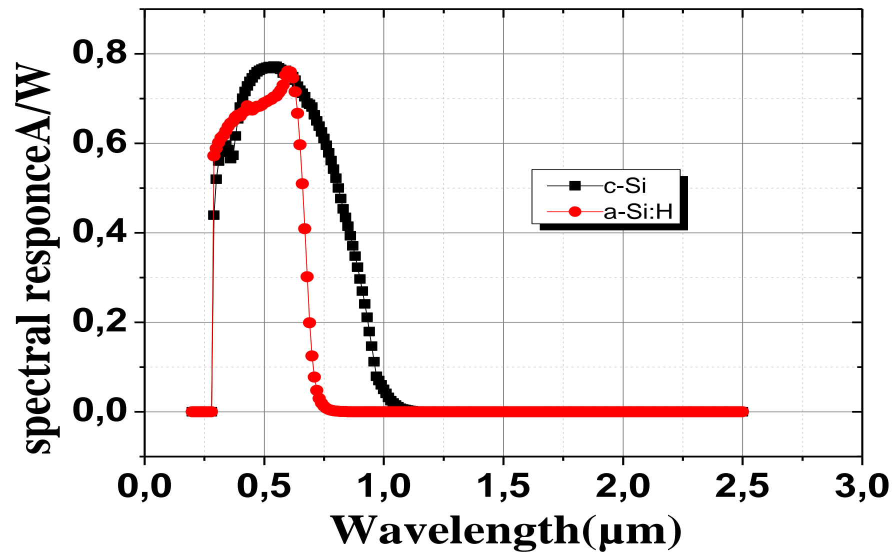

Figure IV. 23: Spectral Response of MIS Solar Cell as a Function of Wavelength

Conclusion

The performance of two MIS solar cell samples was evaluated using both c-Si and a-Si:H materials in the active region through the Atlas Silvaco 2D numerical simulator. Our findings indicate that the performance remains consistent even with a thin layer of a-Si:H.

Our study reveals that a-Si:H with a thickness of only 2 μm absorbs the highest amount of incident light. On the other hand, the c-Si equivalent requires a thicker active region due to the amplified reflection degradation effect. Furthermore, novel materials like Al_2O_3, Si_3N_4, TiO_2, Ta_2O_5, and HfO_2, which are high-k dielectrics, have been proposed for use to advance the carrier transport mechanism in MIS solar cells. Through meticulous simulation research, the impacts of different physical parameters have been explored. A comprehensive evaluation of the effects of doping, carrier trapping, and metal work function has been undertaken.

When compared to SiO_2, HfO_2 stands out as a suitable candidate for MIS solar cell structures. The broad band gap and strong dielectric properties of hafnium oxide films make it very attractive for improving dielectric isolation. HfO_2 achieves the best efficiency, up to 22.71% for c-Si and 13.6% for a-Si:H. A significantly enhanced output characteristic of the device can be observed with the use of an oxide characterized by a high relative permittivity. Among the tested oxides, Ta_2O_5 demonstrates the greatest resilience against interfacial traps and achieves a notable performance efficiency of $\eta = 21\%$.

References

[1]-Esposito DV Enhanced performance of Si MIS photocathode’s containing oxide-coated nanoparticle electrocatalysts. Nano Lett 16:6452–6459.https://doi.org/10.1021/acs.nanolett.6b02909 (2016)

[2]-Chang TY, Chang CL, Lee HY, Lee PT Characteristics of MIS solar cells using sputtering SiO2 insulating layers.In 2010 35th IEEE photovoltaic specialists conference.IEEE. 001318-001321 https://doi.org/10.1109/PVSC.2010. 5614304(2010, June)

[3]-Sze SM, Ng KK Physics of Semiconductor Devices, John Wiley & Sons Inc. (2006)

[4]- Saeed Mohsenifar, M. H. ShahrokhabadiGate Stack High-κ Materials for Si-Based MOSFETs Past, Present, and Futures, Microelectronics and Solid State Electronics, 4(1): 12-24 DOI: 10.5923/j.msse.20150401.03 (2015).

[5]-Robertson J (2005) High dielectric constant gate oxides for metal oxide Si transistors. Rep Prog Phys. https://doi.org/10.1088/0034- 4885/69/2/R02/meta

[6]- Hlali S, Hizem N, Kalboussi A Electrical characteristics of metal–insulator–semiconductor and metal–insulator–semiconductor– insulator–metal capacitors under different high-k gate dielectrics investigated in the semi-classical and quantum mechanical models. Bull Mater Sci 40:67–78. https://doi.org/10.1007/s12034- 016-1341-5 (2017)

[7]-Bencherif H, Dehimi L, Pezzimenti F, Della Corte FG Temperature and SiO2/4H-SiC interface trap effects on the electrical characteristics of low breakdown voltage MOSFETs. Appl Phys A. https://doi.org/10.1007/s00339-019-2606-9 (2019)

[8]- SILVACO Data Systems Silvaco ATLAS User’s manual. Inc2016

[9]-Doghish MY, Ho FD A comprehensive analytical model for metal-insulator-semiconductor (MIS) devices: a solar cell application. IEEE Trans Electron devices 39:2771–2780. https://doi.org/10. 1109/16.168723(1993)

[10]Optical properties of coating materials from Sopra S.A., website: http://www.soprasa.com, (2006)

[11]-Green MA Crystalline and thin-film silicon solar cells: state of the art and future potential. Sol Energy 74:181–192. https://doi. org/10.1016/S0038-092X (03)00187-7(2003)

[12]-Chang TY, Chang CL, Lee HY, Lee PT Characteristics of MIS solar cells using sputtering SiO2 insulating layers.In 2010 35th IEEE photovoltaic specialists conference.IEEE. 001318-001321 https://doi.org/10.1109/PVSC.2010. 5614304 (2010, June)

[13]- J. Sheng, W. Wang, Q. Ye, J. Ding, N. Yuan, C. Zhang, "MACE texture optimization for mass production of high-efficiency multi-crystalline cell and module," IEEE Journal of Photovoltaics, vol. 9, no. 3, pp. 918-925, (2019).

[14]-M.A. Green, F.D. King and Shewchun, Minority carrier MIS tunnel diodes and their application to electronics and photovoltaic energy conversion –I theory, Solid-State Electron., 17 551–561(1974)

[15]- R. Chauhan, P. Chakrabarti, "Influence of ionizing radiation on the performance of MIS solar cells: a theoretical model," International Journal of Electronics, vol. 89, no. 7, pp. 525-535, (2002)

[16]- DoghishMY, Ho FD A comprehensive analytical model for metal-insulator semiconductor (MIS) devices: a solar cell application. IEEE Trans Electron devices 39:2771–2780. https://doi.org/10. 1109/16.168723(1993)

[17] -Mohamed Yehya Doghish and Fat Duen Ho A Comprehensive Analytical Model for Metal-Insulator-Semiconductor (MIS) Devices: A Solar Cell Application IEEE TRANSACTIONS ON ELECTRON DEVICES, VOL. 40, NO. 8, (1993)

[18]- Shousha AHM, El-Kosheiry MA Computer simulation of amorphous MIS solar cells. Renew Energy 11:409–420. https://doi. org/10.1016/S0960-1481 (97)00013-X. (1997)

[19]- V. Yerokhov, I. Melnyk, A. Korovin, "External biasing as the factor of efficiency increase of silicon MIS/IL solar cells," Solar Energy Materials and Solar Cells, vol. 58, no. 2, pp. 225-236, (1999).

[20]- Shewchun J, Dubow R, Myszkowski A, et al. The operation of the semiconductor-insulator-semiconductor (SIS) solar cell: theory. J Appl Phys. ; 49:855–864. 1978

[21]- Fatimah A. Noora, Fandi Oktasendra b, Euis Sustinia and Khairurrijal Khairurrijal, The effects of insulator thickness and substrate doping density on the performance of ZnO/SiO2/n-Si solar cells 2018, VOL. 33, NO. 14, 865–871 Materials Technology, Institut Teknologi Bandung, Bandung, Indonesia

[22]-The effects of insulator thickness and substrate doping density on the performance of ZnO/SiO2/n-Si solar cells Materials Technology, VOL. 33, NO. 14, 865–871 https://doi.org/10.1080/10667857..15209562018(2018)

[23]-T. Azizi1, A. Torchani1, M. Ben Karoui1,2, R. Gharbi1, M. Fathallah1, E. Tresso Effect of defects on the efficiency of a-SiC:H p-i-n based solar cells.2013

[24]- Clima S, Pourtois G, Van Elshocht S, De Gendt S, Heyns MM, Wouters DJ, Kittl JA ECS Trans 19(2):729. (2009).

[25]- Bencherif H,Dehimi L,Pezzimenti F,DellaCorte FG AppliedPhysics A 125(5):294(2019)

[26]- Sze SM, Ng KK Physics of Semiconductor Devices, John Wiley & Sons Inc (2006)

[75]-Bencherif H, Dehimi L, Pezzimenti F, Yousfi A, Abdi M A, Saidi L, Della Corte F G Improved InxGa1_xP/GaAs /Ge tandem solar cell using light trapping engineering and multi-objective optimization approach. Optik https://doi.org/10.1016/j.ijleo.2020.16534611-(2020),

[28]- Green MA The short-wavelength response of MIS solar cells. J Appl Phys 50:1116–1122. https://doi.org/10.1063/1.326090 (1979)

[29]-. Gupta N Material selection for thin-film solar cells using multiple attribute decision making approach. Mater Des 32:1667 1671.https://doi.org/10.1016/j.matdes.2010.10.002 (2011)

GENERAL CONCLUSION

The thesis work centered on creating and electrically evaluating MIS structures using c-Si and a-Si:H as absorber layers, all conducted at room temperature, As a cost-effective substitute for p-n junctions and Schottky devices, the research aimed to explore MIS structures for efficient photovoltaic energy conversion.

The incorporation of an interfacial dielectric layer with good morphological characteristics and a wide band gap is an effective way to reduce the defects at the semiconductor/dielectric interface. Substituting the dielectric layer with another high-k material that possesses properties similar to SiO_2, such as a wide band gap, high interface quality, low oxide trap density, and excellent thermal stability, can result in a diminished trapping rate of free carriers at the interface, subsequently enhancing current flow and the overall device performance.

We used the Silvaco ATLAS simulator to simulate the performance of crystalline silicon (c-Si) and amorphous silicon (a-Si:H) solar cells. The simulator allows the simulation of semiconductor devices from the electrical and optical simulations performed in this thesis, providing valuable insights into the relevant physical mechanisms that crucially affect the efficiency of p-type silicon MIS solar cells. The developed program enabled the optimization of the physical and geometrical parameters of the cell to maximize its performance and minimize losses. Based on the obtained results, the thinner active area of a-Si:H solar cells allows for maximum light absorption, while the thicker active area of c-Si solar cells is necessary to reduce reflection losses.

. A meticulous simulation study revealed that the performance limitations of the MIS solar cell are primarily attributed to interface states and the metal Fermi level pinning position. This configuration introduces a novel tri-terminal multi-material solar cell. The reliability of the oxide dielectric in an MIS solar cell has been assessed under the influence of various physical parameters. Additionally, new high-k dielectric materials, including Al_2O_3, Si_3N_4, TiO_2, Ta_2O_5, and HfO_2, are being suggested as alternatives to conventional SiO_2 technology for further improvement of the MIS solar cell carrier transport mechanisms. Notably, HfO_2 exhibits a remarkable improvement in the main device figure of merits. This oxide has a high relative permittivity, a large band gap, and a high dielectric constant, which significantly enhances the device's output. In contrast, Ta_2O_5 demonstrates the highest resistance to interfacial traps, resulting in superior performance. Opting for a metal electrode with a low work function would be a favorable choice to further improve the device's

performance metrics. The proposed device (Al/Ta_2O_5/Si) appears particularly well-suited for enhancing the production of high-performance silicon solar cells.

Currently, HfO_2 and Ta_2O_5 are the dielectric materials that can simultaneously meet the criteria of high performance, high reliability, and good stability. These choices become ideal due to double-layer dielectrics, which have a substantial physical thickness and a very small electrical thickness. Double-layer dielectrics are the hope for the next generation of devices that rely on dielectrics in combination with semiconductors. This is because double-layer dielectrics have the potential to combine the best of both worlds: the reliability of thick dielectrics and the performance and stability of thin dielectrics. This makes them ideal for use in future devices that rely on dielectrics in combination with semiconductors.

Appendix

Atlas statements syntax

Simulated Structure:

We began by selecting a reference cell from the literature with fixed parameters. Then, we systematically varied one parameter at a time while keeping others constant to examine their impact on the MIS cell's characteristics. The MIS configuration, which incorporated a tunneling oxide, was simulated using the Silvaco Atlas TCAD software. The structure file was generated using Deckbuild. The model utilized p-type Si with a doping concentration of approximately 10^15. Silicon dioxide (SiO_2) was used as the oxide material. Refer to Figure for the depiction of the reference cell used in the simulation.

Mesh

In order to continue the numerical simulation, it becomes essential to establish the structure's mesh. This task is facilitated by the DecKbuild tool, which permits the specification of structural dimensions, parameters for doped regions (including location, type, level, and doping profile), positioning of electrical contacts, and definition of the mesh itself. The meshing process involves dividing the simulated structure into smaller cells, enabling the solution of equations within the model.

For accurate simulation results, using the finest mesh available is essential. However, it's important to consider that an extremely fine mesh can lead to extended calculation times due to the larger number of elements to process. Conversely, a coarser mesh speeds up the simulation process at the potential cost of precision However; this approach sacrifices some precision in the results. Thus, it becomes crucial to strike a balance between computation time and precision. The finite element method serves as the digital technique for solving physical equations. In our case, we utilized the subsequent mesh: After initializing the device with the "go atlas" declaration, the first crucial step involves mesh definition.

MESH SPACE.MULT=<VALUE>

The mesh constitutes a network of intersecting horizontal and vertical lines that span the physical region where the device is constructed and tested. This arrangement is succeeded by X.MESH establishes the mesh along the x-axis, while Y.MESH sets the mesh along the y-axis.

X.MESH: defines the mesh in the x direction.

and Y.MESH: defines the mesh in the Y direction.

statements.

X.MESH LOCATION=<VALUE> SPACING=<VALUE>;
Y.MESH LOCATION=<VALUE> SPACING=<VALUE>.

Specifying Régions and Materials:

Once the mesh has been established, it becomes imperative to outline the specific areas or regions within it. As depicted in, the code segment responsible for delineating these regions is identifiable. A total of three distinct regions are demarcated. The precise boundaries of each region are explicitly marked along the axes. Subsequently, the reference material name is attributed using the "Region" statement. It is essential to maintain ascending order when defining regions; for instance, defining region 2 before region 3 is not permissible. Regions are generated utilizing the subsequent set of statements:

REGION number=<integer><material_ type> / <position parameters>

Specifying Electrodes

After configuring the regions, the electrodes must be allocated to specific areas for electrical analysis, including designations such as "top" or "bottom," as demonstrated in this study. As indicated, electrode assignment is specified for both the anode and the cathode. Notably, the cathode is designated with Aluminum as the material. The positioning along the x and y coordinates corresponds to the previously established region.

ELECTRODE NAME=<electrode name><position_parameters>

Specifying Doping:

Concluding the structure construction, the remaining aspect is the process of doping. Doping can take the form of either n-type or p-type, allowing for distributions like uniform, Gaussian, and more

The following are their respective syntax

<distribution_type><dopant_type><position_parameters>

Specifying Material properties:

While initially using default parameters for all defined materials, you have the option to specify your own fundamental parameters for solving the model, as demonstrated in the provided example syntax:

MATERIAL MATERIAL=<material name> EG300=<value> MUN=<value>…

Please be aware that the syntax mentioned above allows you to include not only E_G300 and MUN, but also various other material properties such as TAUN, TAUP, N_C300, and more

Specifying Physical Models

The MODELS and IMPACT statements are used to define physical models, which are categorized into five classes: mobility, recombination, carrier statistics, impact ionization, and tunneling. The choice of model statements depends on these classes.

For example, the statements:

MODELS CONMOB FLDMOB SRH FERMIDIRAC
IMPACT SELB

This directive indicates that the simulation will utilize standard concentration-dependent mobility, parallel field mobility, Shockley-Read-Hall recombination using constant carrier lifetimes, Fermi 92 Dirac statistics, and Selberherr impact ionization models.

Specifying Interface Properties

By employing the INTERFACE statement, you can define both the interface charge density and surface recombination velocity, which apply to interfaces situated between semiconductors and insulators. This allows for precise control over these parameters:

INTERFACE QF=<value>

Is used to specify the fixed charge between semiconductors and insulators

Specifying Numerical methods

The subsequent aspect to define is the numerical solution strategy, instructing the program on which numerical methods to employ for computing solutions within the device. Deckbuild offers three distinct methods: Gummel, Block, and Newton, designated within the method statement. Each method adopts a distinct approach to solving the equations. The Gummel method calculates each unknown while maintaining variable constancy, iterating until a stable solution is achieved. The Newton method resolves the complete set of unknowns

as a unit, while the Block method combines elements of both Gummel and Newton approaches. Generally, the Newton method is favored and serves as the default if the method statement is not specified.

METHOD <Method Name>

Obtaining Solutions

To attain solutions for the designed device, users can choose to employ DC, AC, small signal, and transient voltages for calculations. After defining the electrode voltages, Solutions are obtained by ramping the biases on electrodes from this initial equilibrium condition. These obtained results are saved in log files and finally displayed using EXTRACT and TONY-PLOT statements.